Retrieval of Tephra Size Spectra and Mass Flow Rate From C-Band Radar During the 2010 Eyjafjallajökull Eruption, Iceland

Luigi Mereu, Frank S. Marzano, *Senior Member, IEEE*, Mario Montopoli, and Costanza Bonadonna

***Abstract*—The eruption of the Eyjafjallajökull volcano in April–May 2010 was continuously monitored by the Keflavík C-band weather radar. The Keflavík radar is located at a distance of about 156 km from the volcano vent, and it has sensitivity of about −5 dBZ at 2-km range resolution over the volcanic area. The time series of radar volume data, which was available every 5 min, is quantitatively analyzed by using the Volcanic Ash Radar Retrieval (VARR) technique. The latter is a physically based methodology that is applied to estimate ash-fall rate and mass concentration within each radar volume. The VARR methodology is here extended, with respect to the previous formulation, to provide an approximate estimate of both mean particle diameter and airborne tephra particle size distribution under some assumptions. Deposited tephra at ground is also extrapolated together with an estimate of the magma mass flow rate (MFR) at the volcano vent, derived from the implementation of the mass continuity equation in the radar reference system. The VARR-based retrievals are compared with those derived from a direct tephra sampling at the ground, experimentally carried out in terms of ash grain size and loading during the Eyjafjallajökull eruption activity on May 5–7, 2010. VARR-based particle diameter estimates may suggest that a sorting of airborne particles during the downwind transport is taking place together with aggregation processes during the ash fall. VARR-derived daily ash mass loadings in the period between April 14 and May 10 are also evaluated with respect to integrated ground and model-based data in the Eyjafjallajökull area. VARR-retrieved MFRs are finally compared with corresponding values obtained from analytical 1-D eruption models, using radar-estimated plume height and radio-sounding wind fields. A fairly good agreement is obtained, thus opening the exploitation of weather radar retrievals for volcanic eruption quantitative studies and ash dispersion model initialization.**

***Index Terms*—Radar data, tephra, volcanic eruption.**

Manuscript received June 21, 2014; revised December 22, 2014 and March 8, 2015; accepted April 8, 2015. This work was supported in part by the Marie Curie Fellowship within the call FP7-POPLE-2010-IEF under Grant 273666 and in part by the FP7 project FUTUREVOLC "A European volcanological supersite in Iceland: A monitoring system and network for the future" under Grant 308377. The work of C. Bonadonna was supported by a Fond National Suisse project (200020-125024).

L. Mereu, F. S. Marzano, and M. Montopoli are with the Dipartimento di Ingegneria dell'Informazione (DIET), Sapienza Università di Roma, 00184 Rome, Italy, and also with the CETEMPS Center of Excellence, Università dell'Aquila, 67100 L'Aquila, Italy (e-mail: mereu@diet.uniroma1.it; marzano@diet.uniroma1.it; frank.marzano@uniroma1.it; montopoli@diet.uniroma1.it).

C. Bonadonna is with the Section des Sciences de la Terre et de l'Environnement, Université de Genève, 1205 Genève, Switzerland (e-mail: Costanza.Bonadonna@unige.ch).

Color versions of one or more of the figures in this paper are available online at http://ieeexplore.ieee.org.

Digital Object Identifier 10.1109/TGRS.2015.2427032

I. Introduction

THE explosive eruption at the summit of subglacial Eyjafjallajökull volcano in 2010 was of modest size, but ash was widely dispersed over Iceland and Europe [31]. The Eyjafjallajökull pulsating explosive activity started on April 14 and ended on May 22 with a volcanic eruption index of about 3, which was estimated on the basis of the maximum volume discharge, and a total tephra volume of about 0.01–0.1 km^3 [8], [30]. The combination of prolonged and sustained ejection of volcanic ash and persistent northwesterly winds resulted in the dispersal of the volcanic cloud over a large part of Europe [2], [22].

Tephra dispersal from an explosive eruption is a function of multiple factors, including magma mass flow rate (MFR), degree of magma fragmentation, vent geometry, plume height, particle size distribution (PSD), wind direction, and its velocity [4], [25], [26]. Volcanologists are used to characterizing the volume and explosivity of the volcanic eruptions through the analysis of tephra distribution. This is because tephra deposits retain a large amount of important information related to the dynamics and physical parameters of the associated volcanic eruptions [29]. One of the most important geophysical parameters, derivable from the analysis of tephra deposits, is the erupted mass, which is essential for the source characterization and assessment of the associated hazards [5]. MFR can then be derived by dividing the erupted mass by the eruption duration (if known) or based on empirical and analytical relations with plume height (e.g., [7], [21], and [33]).

By combining data from ground surveys and remote sensing measurements, it is possible to gain more insights into tephra dispersal [6]. In particular, multispectral visible and infrared observations from both low-Earth orbit and geosynchronous Earth orbit satellites can provide estimates of dispersed fine ash, particularly over the ocean at hundreds of kilometers far away from the vent [31]. However, contamination by water clouds, water vapor variability, and low sensitivity to particles larger than 10 microns are still open issues for quantitative retrieval [28].

Microwave radars can be exploited to extract tephra spatial–temporal distribution in proximity of the volcano vent [10], [12], [16]. Radar technology is well established and can nowadays provide fast 3-D scanning antennas together with Doppler and dual polarization capabilities [19], [32]. The sensitivity of microwave radar measurements depends on the distance between the radar antenna and the target, the transmitter central wavelength, receiver minimum detachable power, and the

resolution volume [24]. Previous studies have shown that coarse ash grain sizes larger than 100 microns can be detected by C-band radars at few hundreds of kilometers with a spatial resolution of a few kilometers [19]. The quantitative interpretation of the detected ash signal was investigated in [13] and [14], where the Volcanic Ash Radar Retrieval (VARR) physically based technique was introduced.

The aim of this paper is to analyze C-band radar data for the Eyjafjallajökull eruption in April–May 2010 to estimate the airborne tephra characteristics and to compare the radar-based retrievals with those obtained from direct tephra sampling at ground carried out during the Eyjafjallajökull volcanic activity [2], [8]. These ground-based measurements were taken by using conventional *a posteriori* techniques: 1) studying stratigraphic sections and collecting ground samples of the tephra deposit to estimate ash loading in a given set of points [8]); and 2) collecting tephra using dedicated ash trays together with mechanical sieving and laser diffraction for estimating accumulation rate and ash size distribution in a given set of locations [2]. Although satellite-based ash loading estimates are available, the latter cannot be considered *in situ* data and, among other problems, are affected by an inherent saturation in the areas close to the vent, thus limiting the sensitivity to finer ash particles (smaller than about 10 μm) [27].

The radar data we used are those of the Keflavík C-band weather radar with time and range spatial sampling of 5 min and 2 km, respectively, located at a distance of about 156 km from the volcano vent and operated by the Icelandic Meteorological Office (IMO) [17]. The VARR technique has been applied to give an estimation of the tephra particle category, ash-fall rate, and mass concentration together with the airborne PSD, as already applied in a previous detailed intercomparison for the Grimsvötn volcanic eruption observed in 2004 [18]. The objective of this work is to assess the VARR estimates for the 2010 Eyjafjallajökull eruption by providing a further analysis of PSD parametric retrieval close to the eruption source and to provide an evaluation of the MFR from radar-based measurements above the volcanic vent.

This paper is organized as follows. Section II provides an overview of the available data in terms of ground deposits and radar measurements. VARR is briefly summarized in Section III, where an extension to the estimate of PSD, mean diameter, and MFR is proposed. Section IV is dedicated to the intercomparison of available ash measurements at ground in terms of PSD, MFR, and ash loading. Conclusions are drawn in Section V.

II. Available Data

During an explosive volcanic eruption, a mixture of ash and gas (so-called volcanic plume) rises into the atmosphere, first due to momentum and then to buoyancy. If the speed of the surrounding wind is larger to the vertical plume speed, the volcanic plume is bent downwind and starts spreading horizontally when it reaches the neutral buoyancy level [26].

The 2010 eruption of the Icelandic Eyjafjallajökull volcano was characterized by a long-lasting bent-over plume that injected a large amount of ash into the atmosphere [23]. The downwind plume was observed from several satellites, which followed its transport as it crossed the European airspace. The ash reached a maximal altitude of 10 km above sea level due to the strong wind modulating the plume elevation and advecting it eastward [2], [6], [22].

Fig. 1. Ash plume of the Eyjafjallajökull volcano and cloud seen during an observation flight on May 13, 2010. The eruption plume is gray and heading southeast. The height is mainly 6 km but has reached up to ∼9 km. Wind is calm over the eruption site and unstable air south of it, which does affect the height of the ash cloud. Ash fall has been reported since six o'clock this morning from various farms in the vicinity; the ash is somewhat finer today than yesterday. These observations are based on a status report issued collectively by the IMO and the Institute of Earth Sciences at 16:00 UTC. Flight over Eyjafjallajökull 13th May 2010, 19:45 UTC. Credits: Photo by Árni Sigurðsson, http://en.vedur.is/earthquakes-and-volcanism/articles/nr/1884.

The ash plume development in time is typically characterized by a lowering of the cloud top with increasing distance from the volcano, as shown in Fig. 1. The latter shows the ash plume about 30 km southwestward with respect to the Eyjafjallajökull vent, pictured during an observation flight on May 13, 2010 at 19:45 UTC. The plume height at that time was between 5 and 7 km with the plume top hitting a stable layer in the atmosphere. The ash cloud drifted away in spatially stable long waves.

When volcanic plumes develop in strong wind fields, their MFR cannot be determined based only on plume height as their height is significantly affected by entrainment due to wind shear [7], [33]. Direct observations and experimental studies have shown that most particles with a diameter of less than 125 μm fall as aggregates of various types, according to the amount of liquid involved [25]. Particle aggregation has been also observed during the 2010 Eyjafjallajökull eruption [2], [27]. In the following sections, the *in situ* specifications and the radar retrieval methods for the 2010 Eyjafjallajökull events are summarized.

A. In Situ Measurements

Two sets of ash-fall measurements are here considered: 1) proximal sampling, where the tephra samples are collected up to 56 km from the vent [2]; and 2) distal sampling, where the tephra samples are collected by a systematic survey within a wide area comprising Iceland and the North Atlantic [8].

Proximal samplings are described by Bonadonna *et al.* in [2]. Three sampling methodologies are followed: 1) collecting tephra in dedicated trays to determine PSD and accumulation

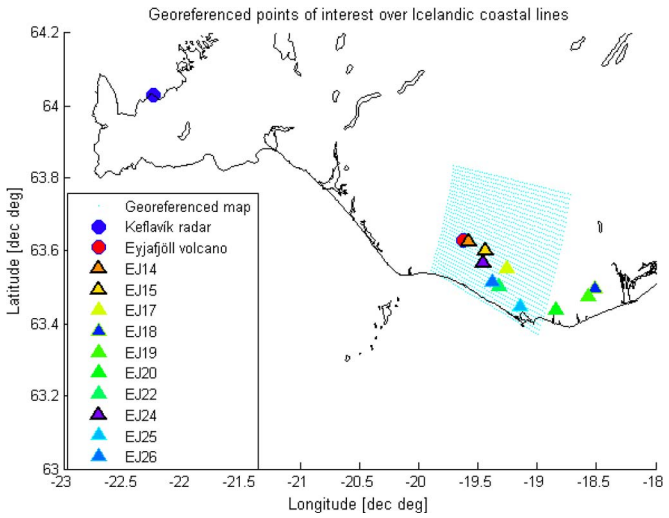

Fig. 2. Ground reference sampling sites are coded as "EJn" for the nth site and indicated by symbols (Δ). Black lines highlight the ground sites used in this study (EJ14, EJ15, and EJ24). Also the site EJ22 was considered in this study, although not providing useful data for our analysis. The georeferenced Keflavík radar grid points, within the ground reference area of experimental sites, are superimposed by cyan dots ($\cdot$). The Eyjafjallajökull volcano and the Keflavík radar location are indicated by (•) and (•), respectively.

rate; 2) collecting volcanic particles and aggregates while they were falling to characterize their properties in terms of size, shape, and surface features; and 3) carrying out vertically pointing X-band Doppler radar measurements of near-surface settling velocities (using the PLUDIX instrument).

Both eruptive and atmospheric conditions were relatively constant during the whole sampling period (i.e. 4-8 May 2010), allowing the direct tephra sampling in ten locations, close to the vent, distributed between 2 and 56 km from it in the east and southeast sectors. Fig. 2 shows the relative positions of the ten experimental sites (hereinafter named "EJn" with n as the site number) with respect to the volcano and the Keflavík radar location. Only three out of ten experimental sites are considered in this study because of their temporal matching with the radar acquisitions and because of their visibility to the lowest radar rays that were not blocked by the surrounding topography.

Table I lists, for each of the three considered experimental sites, the location coordinates, the collection time, and some of the tephra deposit features. In particular, the tephra deposit features [2]. The tephra accumulation over 30 minutes and accumulation rateat the locations within $\sim$ 21km from the vent vary between 0.01 and 1.26 kg $\cdot$ m^{-2} and between $\sim 5 \cdot 10^{-6}$ and $\sim 7 \cdot 10^{-4}$ kg $\cdot$ m$^{-2} \cdot$ s^{-1}, respectively [2]. The highest tephra accumulation rates were recorded close to the vent. Beyond 20 km, accumulation rates were found to range between about 10^{-2} and 10^{-4} kg $\cdot$ m$^{-2} \cdot$ s^{-1}.

In contrast to the proximal sampling data set we just discussed, the data set collected in distal area is referred to as a systematic survey within a wide area comprising Iceland, the Atlantic Ocean, and the European continental regions. Distal sampling was carried out combining data from ground surveys and remote sensing tools, as described by Gudmundsson *et al.* in [8]. As already mentioned, the combination of prolonged and sustained ejection of volcanic ash and persistent northwesterly winds resulted in significant particle dispersion over a large part of Europe, although concentrations were everywhere quite low.

TABLE I
SUMMARY OF COLLECTION AND DEPOSIT CHARACTERISTICS OF ALL SAMPLES ANALYZED, EXTRACTED FROM [2], FOR THE LISTED SITES (EJ14, EJ15, AND EJ24) DURING A SPECIFIC TIME INTERVAL. THE LAST THREE ROWS ARE REFERRED TO ESTIMATES OF TOTAL ASH CONCENTRATION C_a, SURFACE DEPOSIT LOADING L_a, AND FALL RATE R_a FOR THE CORRESPONDING SITE AND INTERVAL AS DERIVED FROM C-BAND VARR ALGORITHM, USING THE KL VELOCITY-DIAMETER MODEL. ($\phi = -\log_2$ D, WHERE D IS THE PARTICLE DIAMETER IN MILLIMETERS)

		Measuring sites		
Features	**Units**	**Sample EJ14**	**Sample EJ15**	**Sample EJ24**
Longitude	[decimal deg]	-19.5811	-19.4376	-19.4536
Latitude	[deg]	63.62738	63.60145	63.56872
Elevation [m]	[m]	1414	835	521
Distance from vent	[km]	2	9.6	10.7
Collection date	[dd/mm/yyyy]	05/05/2010	05/05/2010	07/05/2010
Collection time	[hh/mm]	17:39-17:49	19:00-20:36	15:35-16:20
Total mass/area	[kg/m^2]	0.42	0.68	0.29
Accumulation rate	[kg/m^{2}s]	$6.98 \cdot 10^{-4}$	$1.19 \cdot 10^{-4}$	$1.07 \cdot 10^{-4}$
Median particle diameter	[mm (ϕ)]	1.87 (-0.9)	0.62 (0.7)	0.41 (1.3)
30-min mass/area	[kg/m^2]	1.26	0.21	0.19
***Average C_a* (VARR-KL)**	[kg/m^3]	$2.08 \cdot 10^{-3}$	$6.02 \cdot 10^{-4}$	$3.71 \cdot 10^{-4}$
***Average L_a* (VARR-KL)**	[kg/m^2]	5.78	7.76	1.11
***Average R_a* (VARR-KL)**	[kg/(m$^2 \cdot$s)]	$1.01 \cdot 10^{-2}$	$2.97 \cdot 10^{-3}$	$1.70 \cdot 10^{-3}$

Field observations in the region within 10 km from the vent in the summers of 2010 and 2011 and individual grain size analyses indicate that during the first period, the produced tephra was coarser with a reduced percentage of very fine ash. During the second period of analysis, the tephra was sampled in a systematic manner with a number of traps around the volcano. The results in this second period, in terms of grain size and during the most intense explosive phase of April 2010 at distance of 10–15 km from the vent, indicate that about 35%–50% of the ash was finer than 63 μm, whereas 10%–30% was finer than 30 μm [8].

B. Weather Radar Observations

Meteorological microwave radars can be used to quantitatively estimate the geophysical properties of a volcanic ash cloud, as successfully demonstrated in the last decade [12], [14], [18]. Under the assumption of Rayleigh scattering, the copolar horizontally polarized reflectivity factor Z_H (mm$^6 \cdot$ m^{-3}), very often expressed in decibels (dBZ) and hereinafter also referred to as reflectivity, is related to the size distribution of ash particle polydispersion by [24]

$$Z_H(r,\theta,\varphi) = \int_{D_1}^{D_2} D^6 N_a(D) dD \qquad (1)$$

where D(mm) is the equivolume spherical particle diameter, and $N_a(D)$ is the PSD (m$^{-3} \cdot$ mm^{-1}) with D_1 and D_2 as the expected minimum and maximum particle diameter. The quantity ϕ is defined as $\phi = -\log_2 D$, and it is usually preferred to D in geology.

The Rayleigh approximation (i.e., wavelength $\gg D$) used to derive (1) is not always valid, particularly at wavelengths shorter than the C-band (i.e.,. wavelength less than 5 cm). In these cases, the particle Mie backscattering effects need to be taken into consideration depending on the ash cloud formation and the radar wavelength [13], [15]. However, an equivalent Rayleigh reflectivity Z_H is usually defined. It is a function

of the radar-received power, and it has sensitivity to ash size and concentration, which mainly depends on the transmitted wavelength, receiver minimum detectable signal, range (the received power is inversely proportional to square range), and antenna beamwidth [24].

Previous numerical analyses have shown that intense concentration of fine ash (about 5 g/m^3 of average diameter of 0.01 mm) cannot be detected by a C-band radar [14]. This means that the Keflavík radar measurements can be used to detect light to intense concentration of coarse ash and any lapilli distribution, i.e., particles with average diameters larger than 0.1 and 1 mm, respectively. Thus, microwave radar signatures refer to near-source plume depending on the sedimentation and settling of coarse ash and lapilli. Indeed, fine ash may represent few percentage of the total tephra and can be transported far from the volcano vent [26]. Moreover, the radar observation geometry inevitably produces occluded regions at longer ranges and in the presence of obstacles.

The sampling size along the radial directions (Δr) is proportional to the pulse duration (order of microseconds), whereas its transverse spacing quadratically increases with the target range (r). Thus, for a given antenna elevation angle, the radar sampling volume (ΔV) increases with distance from the radar as $\Delta V \approx (\pi/4) \cdot r^2 \cdot \Delta\theta \cdot \Delta\varphi \cdot \Delta r$. This has a dual-range effect: 1) to increase the probability of intercepting undesired ground targets by the radar sampling volumes; and 2) to have the sampling volumes not uniformly filled producing an ambiguous reduction of Z_H [24]. For example, for the Keflavík radar, at a distance of 155 km from the radar, the transverse section of the sampling volume, i.e., ΔV, is about 4.2 km^3 (i.e., 2 km in range and 2.1 km in azimuth). Another aspect of ash detection is the issue related to the discrimination between ash and hydrometeors and the identification of ash-water aggregates. The former can be theoretically tackled investigating the time evolution of the radar acquisitions, whereas the latter seems, at the current knowledge, beyond the capabilities of single-polarization weather radar, and it should be treated as an ambiguity (uncertainty) affecting the qualitative and quantitative interpretation of the radar imagery of ash clouds [18], [19].

The main specifications of the C-band (5.6 GHz) weather radar in Keflavík are: 5-min time sampling; antenna elevation angles: 0.5°, 0.9°, 1.3°, 2.4°, 3.5°, 4.5°, 6.0°, 8.0°, 10.0°, and 15.0°; azimuth spacing: 0.86°; range spacing 2 km (after a radial averaging) minimum detectable reflectivity signal: -5 dBZ (after radial averaging), at the Eyjafjallajökull position. The radar system is operated by IMO, and a detailed description is found in [12] and [16]. The Eyjafjallajökull eruption was observed by Keflavík radar, 155 km northwest far away from the Eyjafjallajökull volcano from 00:10 UTC on May 5, 2010 until 23:55 UTC on May 10, 2010. The complete radar data set consists of a total of 3730 polar volumes in spherical coordinates, where each volume consists of a matrix having 420 rows (azimuth angles) and 120 columns (range bins).

Being aware of the previous *caveats* when quantitatively interpreting radar data, the three sampling locations, which are identified as EJ14, EJ15, and EJ24, respectively, 2, 9.6, and 10.7 km away from the volcano vent have been analyzed (see Table I and Fig. 2). These sites are those where the beam occlusion effects are almost negligible, and the lowest radar bin is relatively close to the surface. As a matter of fact, by increasing the distance of the EJn site with respect to the Eyjafjallajökull volcano, the radar sampling altitude considerably increases, as shown in Fig. 3. The minimum altitude between the top of the Eyjafjallajökull volcano and the lowest radar ray is 2.5 km when considering radar ray bending in a standard atmosphere [24].

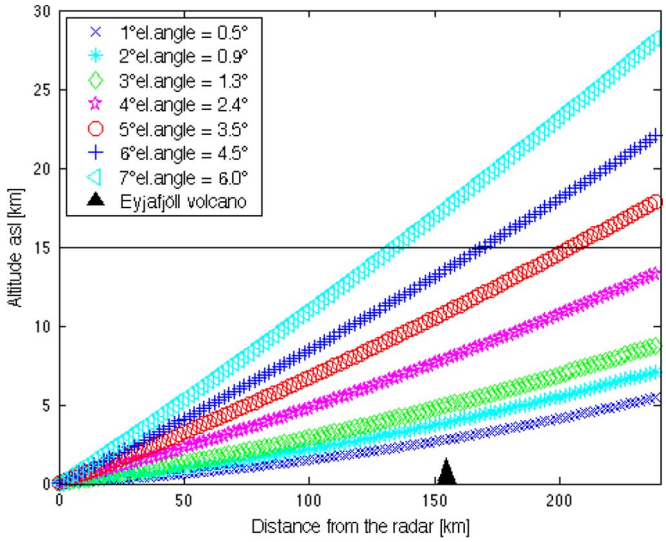

Fig. 3. Altitude of the radar antenna boresight beam simulated within a standard atmosphere for different radar elevation angles, as listed in the figure's legend. The position of the Eyjafjallajökull volcano is shown by a black triangle, whereas the Keflavík radar is set in the origin of the figure.

In the case of the 2010 Eyjafjallajökull event, the observed temporal sequence of radar imagery indicates a distinct ash feature erupted from the volcano vent, which can be effectively detected, as already documented in [17]. An example of the radar vertical profiles [range height indicator (RHI)] of Z_H is shown in Fig. 4 during four instants of the volcanic activity on May 5, as specified in each panel title. The position of the ground sampling sites EJn is also highlighted in each panel by a red box. From this figure, we can derive an average horizontal and vertical extension of the plume on the order of 10 and 6 km, respectively. For the reasons mentioned above, this is a partial three-dimension perspective of the ongoing event. In the same figure, we can note the absence of the radar-detected ash plume in correspondence of EJ22 and EJ24 sites. The latter sites clearly show a measured signature at ground; this discrepancy may probably be due to the radar beam partial occlusion and also to the selected azimuth direction.

To complete the radar standpoint, Fig. 5 shows the ground projection [called the plan position indicator (PPI)] of the radar reflectivity Z_H conical sampled area at the lowest antenna elevation angle. These maps are georeferenced and are enlarged around the volcano vent within an area of about 110 km^2. They clearly show the predominant downwind plume southeast direction with the progressive attenuation of the reflectivity as the end of the sequence is approaching. Fig. 5 confirms that the ash plume is not detected above the site EJ22 at 20.6 km from the vent, but it is present above the site EJ24.

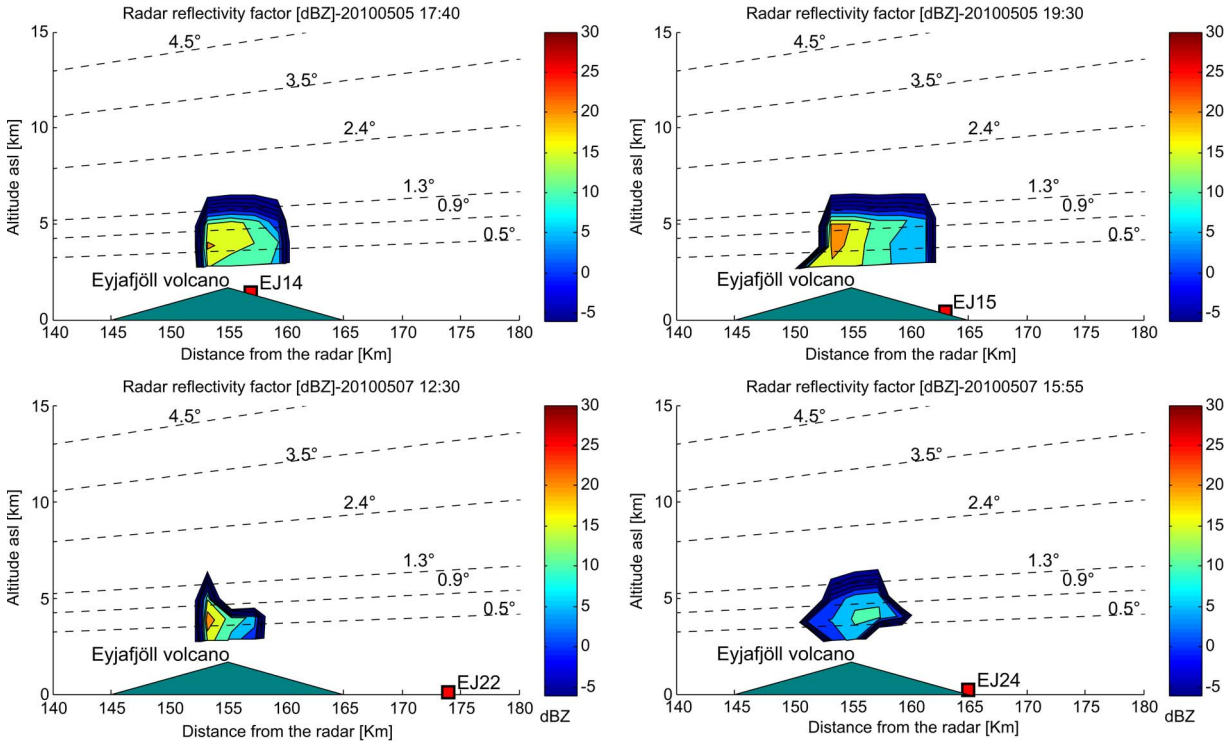

Fig. 4. Radar RHI images of radar reflectivity Z_{H} along the radar-EJn line of sight at 17:40 UTC on May 5, 2010 (EJ14), at 19:30 UTC on May 5, 2010 (EJ15), at 12:30 UTC on May 7, 2010 (EJ22), and at 15:55 UTC on 72010 (EJ24). See Fig. 1 and Table I for details on the EJn sites.

III. VARR

In the following sections, quantitative definitions and a physical parameterization of volcanic ash clouds will be briefly introduced, together with some radar reflectivity modeling issues (details can be found in [13] and [14]). Note that we will limit our attention to the single-polarization amplitude radar observables due to the characteristics of the Keflavík radar, although polarimetric signatures can be included as well when they are available [19], [35].

A. Tephra Particle Parameterization

From (1), which describes the radar reflectivity factor under the Rayleigh assumption, it is clear as it includes the information on the ash particle size and its distribution. In particular, the weighted integrals of the ash size distribution, i.e., N_a, is able to explain all quantities of our interest: ash mass concentration (C_a), ash-fall rate (R_a), and number-weighted mean diameter (D_n). When N_a assumes a form of Gamma or Weibull distribution, the weighted integrals are easily calculated in a closed form as moments of N_a of k-th order [13]. Thus, among others, it is convenient choosing some of these distribution shapes. In addition, past studies have also demonstrated, using experimental data, that their assumption is a reasonable choice [9], [13], [15].

In this paper, the ash particle distribution, i.e., N_a $(\mathrm{mm}^{-1}\mathrm{m}^{-3})$, is assumed to behave as a scaled gamma, which assumes the following form:

$$N_a(D) = N_n \left(\frac{D}{D_n}\right)^{\mu} e^{-(\mu+1)\left(\frac{D}{D_n}\right)} \tag{2}$$

where D_n, N_n, and μ are the number-weighted mean diameter in millimeters, the intercept parameter in $(\mathrm{mm}^{-1}\mathrm{m}^{-3})$, and the unitless shape factor, respectively. Thus, from (2), the ash mass concentration and the ash-fall rate, respectively, indicated by C_a in $(\mathrm{g}\cdot\mathrm{m}^{-3})$ and R_a in $(\mathrm{kg}\cdot\mathrm{m}^{-2}\cdot\mathrm{h}^{-1})$, can be expressed by

$$C_a = 10^{-9}\int_{D_1}^{D_2} m_a(D)N_a(D)dD = \frac{\pi}{6}\rho_a E_3 \tag{3}$$

$$R_a = 3.6\cdot 10^{-9}\int_{D_1}^{D_2} v_a(D)m_a(D)N_a(D)dD = \frac{\pi}{6}v_a\rho_a E_{(3+b_v)}. \tag{4}$$

In (3) and (4), $m_a = \rho_a(\pi/6)\cdot D^3$ is the ash mass of the particle's equivalent sphere, and ρ_a is the ash density in $(\mathrm{g}\cdot\mathrm{m}^{-3})$. In (4), the particle's terminal velocity (v_a) in $(\mathrm{m}\cdot\mathrm{s}^{-1})$ is assumed to follow a power law as $v_a(D) = a_v D^{bv}$ with a_v and b_v empirical coefficients. The coefficients are chosen from a regression analysis of past experiments of previous eruptions (see [2], [10], [11], and [34]). Four different models have been extracted from those proposed in the literature: 1) Wilson's model (1972) [34], which refers to ash plume heights between 5 and 10 km above the ground; 2) Harris and Rose's models, respectively, of 1980 (Mt. St. Helens; May 18, 1980) and 1982 (Mt. St. Helens; March 19, 1982) [10]; and 3) Kunii and Levenspiel's (KL) model (1969), considering an ash density of $1500\cdot\mathrm{kg}\cdot\mathrm{m}^{-3}$ [3], [11] (see Section III-B). The methods in 1) and 2) are derived from a parametric regression analysis [14], whereas the KL model is physically based and depends

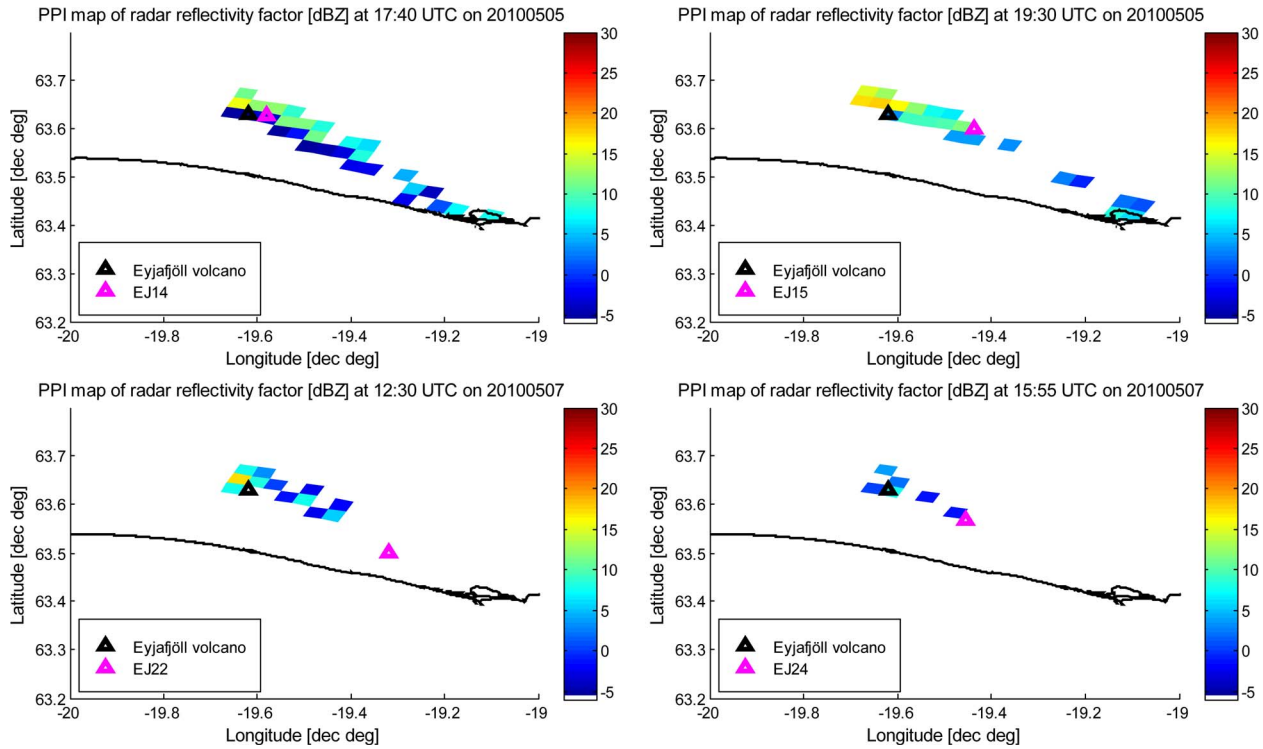

Fig. 5. Radar PPI images of radar reflectivity Z_H, corresponding to RHI and EJ sites of Fig. 4 (EJ14 on the top left, EJ15 on the top right, EJ22 on the bottom left, and EJ24 on the bottom right).

on ambient parameters so that it is taken as a reference in this work.

Fig. 6 shows the modeled curves for $v_a(D)$ for various sets of a_v and b_v parameters, as listed in the legend. The velocity-diameter models may significantly differ for larger diameters, even doubling the velocity itself for a given particle size. In this paper, we have used, as a primary choice, the Kunii–Levenspiel (KL) model parameters, described in [11] and applied to the 2010 Eyjafjallajökull event. It is worth noting that one of the main issues in considering the particle's terminal fall velocity is that the airborne ash-fall velocity cannot be directly measured so that we can take the literature models as a set of possible plume scenarios to take into account the fall velocity uncertainty.

B. VARR Methodology

The VARR attempts to extract some quantitative information from radar data of volcanic clouds, making use of forward model electromagnetic simulations of the radar signal as a function of various possible ash scenarios. The VARR methodology is extensively described in detail in previous works by Marzano *et al.* [14]–[16]. In this paper, we give the elements useful for the VARR implementation without going into the details of the algorithms. VARR outputs, in its default configuration, are estimates of the ash mass concentration C_a $(\mathrm{g}\cdot\mathrm{m}^{-3})$, and the ash-fall rate, R_a $(\mathrm{kg}\cdot\mathrm{m}^{-2}\cdot\mathrm{h}^{-1})$. These quantities are related to the measured radar reflectivity Z_{Hm} $(\mathrm{mm}^6\cdot\mathrm{m}^{-3})$ through power law coefficients c_c, d_c, a_c, and b_c as follows:

$$\begin{cases}\hat{C}_a^{(c)} = a_c Z_{H_m}^{b_c} \\ \hat{R}_a^{(c)} = c_c Z_{H_m}^{d_c}\end{cases} \tag{5}$$

where the symbol "c" is used as the apex, and the subscript in (5) indicates a particular ash scenario also called ash class.

The ash classes are fixed in VARR and stored as lookup tables. They basically include parameter variations of the ash size distribution, N_a, in (2), i.e., D_n, N_n and μ in a prescribed and consistent way. From $N_a(D)$, Z_H, C_a, and R_a are calculated using (1), (3), and (4). Thus, we identified $N_c = 12$ classes of ash scenarios (3 size by 3 mass concentration classes). In each class, D_n and N_n follow a Gaussian random distribution, whereas μ is fixed. The defined classes are labeled as fine, coarse ash, and lapilli further partitioned into light, moderate, and intense mass concentration regimes. Thus, for each of the aforementioned classes, we have average values of particle diameters $\langle D_n\rangle$ equal to 0.01, 0.1, and 1.0 mm for fine, coarse, and lapilli ash classes, respectively, with a standard deviation $\sigma_{Dn} = 0.2\langle D_n\rangle$ and ash mass concentration with mean values $\langle C_a\rangle$ equal to 0.1, 1, and 5 $\mathrm{g}\cdot\mathrm{m}^{-3}$ for light, moderate, and intense concentration regimes, respectively, and a standard deviation $\sigma_{\mathrm{Ca}} = 0.5\langle C_a\rangle$.

The ash density ρ_a is assumed equal to an average value of $1500\cdot\mathrm{kg}\cdot\mathrm{m}^{-3}$, according to the ash particle andesitic density model of Bonadonna and Phillips [3] considering a particle diameter of 0.1 mm, and the PSD shape parameter μ has been set to 0.9, 1.1, and 1.4 for fine ash, coarse ash, and lapilli particles, respectively. Note that the choice of the ash density is consistent with Eyajafjallajokull data and the goal of estimating airborne PSD from radar observations [2], [3].

The ash classes are identified as minimizing the distance between the radar measured quantities (i.e., the radar reflectivity, Z_H, in our case) and the expected radar signatures of

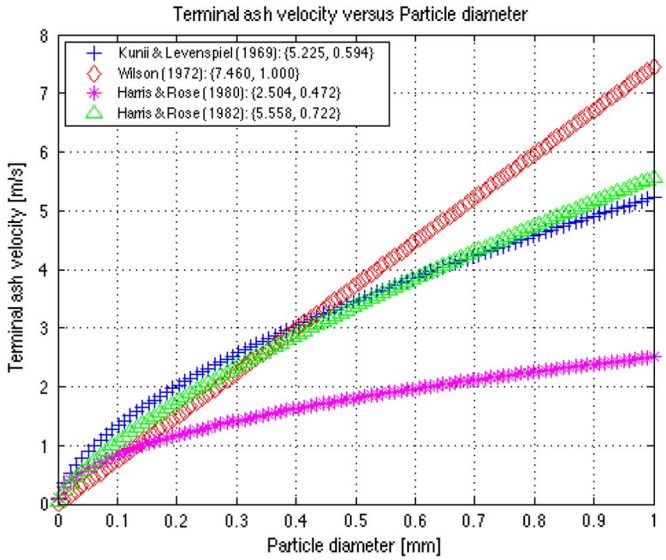

Fig. 6. Parameterized power law models ($v_a(D) = a_v \mathrm{D}^{b_v}$) for the ash terminal velocity [2], [10], [11], [34]. The values a_v and b_v for each model are listed in the panel's legend.

ash for each class. In VARR, this is performed in a probabilistic framework using the maximum *a posteriori* probability criterion. Each ash class is characterized by some members in terms of radar variables, which are distributed with a Gaussian probability density distribution. Thus, the minimization process to assign a class "cth" to the measured reflectivity factor ZHm requires the maximization of the conditional probability $p(c|ZHm)$. It can be demonstrated that this reduces to the minimization of a quadratic form characterized by 1) $m_Z^{(c)}$ and $\sigma_Z^{(c)}$, which are the mean and standard deviation of the simulated reflectivity for class "c," and 2) $p(c)$, which is the *a priori* probability of existence of class c.

C. Estimate of Ash PSD, Loading, and MFR

Here, we wish to extend the VARR outputs including the estimation of the mean diameter, mass loading, and MFR. Within the usual approximation of Rayleigh backscattering and assuming the scaled gamma distribution for N_a as in (2), it can be easily demonstrated as Z_H in (1) can be expressed as

$$Z_{H_m}^{(c)} = f_z(\mu^c)\frac{D_n^3}{\rho_a}\hat{C}_a^{(c)} \tag{6}$$

which yields

$$D_n = \sqrt[3]{\frac{\rho_a Z_{H_m}^{(c)}}{\hat{c}_a^{(c)} f_z\left(\mu^{(c)}\right)}}. \tag{7}$$

In (6) and (7), D_n, Z_{Hm}, C_a, and ρ_a are in millimeters; $(\mathrm{mm}^6 \cdot \mathrm{m}^{-3})$, $(\mathrm{g} \cdot \mathrm{m}^{-3})$, and $(\mathrm{g} \cdot \mathrm{m}^{-3})$, respectively, whereas the shape factor of the ash size distribution in (2), i.e., $\mu^{(c)}$, is unitless. The latter is fixed for each cth class in the current version of VARR. The term f_Z is

$$f_z\left(\mu^{(c)}\right) = \frac{6 \cdot 10^6 \Gamma\left(\mu^{(c)}+7\right)}{\pi\left(\mu^{(c)}+1\right)^3 \Gamma\left(\mu^{(c)}+3\right)} \tag{8}$$

where Γ completes the gamma function, and it holds that $\Gamma(n+1) = n!$ if n is an integer. Once $D_n^{(c)}$ and $\mu^{(c)}$ are known, the parameter $N_n^{(c)}$ of the ash size distribution is derived from [16], as follows:

$$N_n^{(c)} = 10^6 \frac{6\hat{c}_a^{(c)}\left(\mu^{(c)}+1\right)^{\mu^{(c)}+4}}{\pi\rho_a\left(\hat{D}_n^{(c)}\right)^4 \Gamma\left(\mu^{(c)}+4\right)}. \tag{9}$$

By using (7)–(9), the airborne scale-Gamma PSD of the cth ash class can be calculated using (2). The ash mass loading (L_a) is derived from the ash-fall rate, i.e., R_a $(\mathrm{kg} \cdot \mathrm{m}^{-2} \cdot \mathrm{s}^{-1})$, by its integration over a time interval between t_i and t_f in seconds, i.e.,

$$L_a(x,y) = \int_{t_i}^{t_f} R_a^{(c)}(x,y,t)\, dt. \tag{10}$$

Note that R_a is actually known for each radar sampling volume. To obtain a quantity referred close to the ground, a vertical extrapolation from a given altitude up to the ground level was performed. Thus, we carried out an approximate reconstruction of the vertical profile of reflectivity. These reconstructed values of Z_{Hm} are used in (5) to derive R_a. We are implicitly assuming that the radar observations closer to the ground are indicative of ash fall deposited on the ground from the vertical column above a considered position. Indeed, this assumption might lead to an overestimation of L_a.

The erupted mass (M_a) present in the column above the vent can be retrieved by summing up the ash concentration of all radar bins in the (radar visible) column itself V_C, i.e., at a given time step t. Thus

$$M_a(t) = \int_{V_c} C_a^{(c)}(\mathbf{r},t)dV \cong \sum_{i=1}^{N_{VC}} C_a^{(c)}(\mathbf{r_i},t)\Delta V_i \tag{11}$$

where $\mathbf{r}$ is the position vector, N_{VC} is the number of volume bins within the column above the vent, and ΔV_i are the involved radar sampling volumes. The volume V_C can be arbitrarily chosen to include all of the plume or part of it, depending on the calculations one wants to perform.

The mass flow rate (MFR) is a measure of the temporal rate of mass flow through the volcanic vent. The 3-D radar-based ash concentration estimate, given in (5), around the volcanic vent can be used to provide an approximate quantification of MFR. This can be achieved by trying to solve the continuity equation in the discretized spatial and temporal domain of the radar geometry. The mass continuity, adapted to our case states that time variation of the ash mass within a volume, i.e., V_c, above the volcano vent is equal to the net flux, which diverges out from the volume $(\mathbf{J})$, due to the overall contributions flowing out and in, plus the net accretion of the ash mass

inside the volume due to source-minus-sink terms σ. Thus, in formulas, we can write the differential form of the continuity equation as follows:

$$\frac{\partial c_a(\mathbf{r},t)}{\partial t} = -\nabla \cdot \boldsymbol{J}(\mathbf{r},t) + \sigma(\mathbf{r},t). \tag{12}$$

The term $\mathbf{J}$ is a flux rate of ash mass $(\mathrm{g}\cdot\mathrm{m}^{-2}\cdot\mathrm{s}^{-1})$, C_a is in $(\mathrm{g}\cdot\mathrm{m}^{-3})$, and σ is in $(\mathrm{g}\cdot\mathrm{m}^{-3}\cdot\mathrm{s}^{-1})$. The flux $\mathbf{J}$ can be a positive or a negative term indicating an outcoming or incoming flux rate into volume Vc, respectively. We assume that the incoming contribution of $\mathbf{J}$ (labeled as $\mathbf{f}_R$) is referred only to the ash mass rate produced by the volcano activity, whereas the outcoming contributions (labeled as $\mathbf{a}_R$) are those that move out from V_c due to convection and prevailing winds, i.e.,

$$\boldsymbol{J}(\mathbf{r},t) = \boldsymbol{a}_R(\mathbf{r},t) - \boldsymbol{f}_R(\mathbf{r},t). \tag{13}$$

Our unknown is $\mathbf{f}_R$, whereas $\mathbf{a}_R$ can be calculated once the plume advection velocity field $\mathbf{v}$ in $(\mathrm{m}\cdot\mathrm{s}^{-1})$ is estimated, i.e.,

$$\boldsymbol{a}_R(\mathbf{r},t) = C_a(\mathbf{r},t)\boldsymbol{v}(\mathbf{r},t). \tag{14}$$

Note that in (12), we can take into account possible air entrainment into the plume (which would dilute the ash concentration) and the ash flows into the umbrella cloud region due to local turbulent circulation by modulating the source-minus-sink term σ.

By integrating (12) over the eruption columnar volume V_C above the vent and using the divergence theorem, we obtain the integral form of the continuity equation, i.e.,

$$\int_{V_c} \frac{\partial C_a(\mathbf{r},t)}{\partial t} dV = -\oint_{S_C - S_D} \mathbf{n}_0 \cdot \mathbf{a}_R(\mathbf{r},t) dS + \oint_{S_D} \mathbf{n}_0 \cdot \mathbf{f}_R(\mathbf{r},t) dS + \int_{V_C} \sigma(\mathbf{r},t) dV \tag{15}$$

where $\mathbf{n}_0$ is the normal unit vector belonging to the closed surface S_C surrounding the column volume V_C and pointing outward of it, and S_D is the part of S_C closer to the vent and perpendicular to the vertical line above it. A compact formulation of (15) is obtained by substituting (14) in (15) and defining the following quantities:

$$\begin{aligned} D_R(t) &= \int_{V_C} \frac{\partial C_a(\mathbf{r},t)}{\partial t} dV = \frac{\partial M_a(\mathbf{r},t)}{\partial t} \\ A_R(t) &= \oint_{S_C - S_D} \mathbf{n}_0 \cdot \mathbf{a}_R dS = \oint_{S_C - S_D} C_a(\mathbf{r},t)\left[\mathbf{n}_0 \cdot \boldsymbol{v}(\mathbf{r},t)\right] dS \\ F_R(t) &= \oint_{S_D} \mathbf{n}_0 \cdot \mathbf{f}_R(\mathbf{r},t) dS \\ \sum(t) &= \oint_{V_C} \sigma(\mathbf{r},t) dV \end{aligned} \tag{16}$$

where D_R, A_R, F_R, and Σ are the derivative mass rate, the advection rate, the MRF, and the source–sink rate, respectively, all expressed in $(\mathrm{g}\cdot\mathrm{s}^{-1})$. Thus, (15) can be compacted into

$$D_R(t) = -A_R(t) + F_R(t) + \sum(t). \tag{17}$$

Equation (17) makes possible the estimate of MFR by the estimation of D_R, F_R, and Σ. The implementation of (17) is not straightforward in the radar geometry so that some simplifying assumptions are needed. In the following, we describe how we can practically implement (17). First of all, the source–sink term Σ is put to zero since we assume that there are no sources or sinks in the selected volume V_C. At each radar acquisition t_k, MRF is then given by

$$F_R(t_k) = D_R(t_k) + A_R(t_k) \tag{18a}$$

with

$$\begin{cases} D_R(t_k) \cong \sum\limits_{i=1}^{N_{VC}} \frac{\Delta C_{aik}^{(c)}(t_k)}{\Delta t} \Delta V_i \\ A_R(t_k) \cong \sum\limits_{j=1}^{N_{SO}} C_{ajk}^{(c)}(t_k) v_{nj}(t_k) \Delta S_j \end{cases} \tag{18b}$$

where $t_k(\mathrm{s})$ is the radar time sampling of each volume, ΔV_i (m^3) is the ith incremental radar sampling volume with N_{VC} elements, $\Delta \mathrm{S}_j$ (m^2) is the jth incremental outer surface with N_{SO} elements, and v_{nj} $(\mathrm{m}\cdot\mathrm{s}^{-1})$ is the advection velocity component normal to the jth outer surface element. In general, N_{SO} differs from N_{VC}, which is the number of elements in V_C, because A_R takes into account only the contributions transported out from S_C.

If the 3-D vectorial velocity field $\boldsymbol{v}(\mathbf{r},t)$ of the divergent advection rate A_R is negligible or, in any case, difficult to estimate with a good confidence (particularly if Doppler moments are not available from the radar product set), from (18), we can anyway provide an estimate of the MFR. We can basically suppose that positive contributions of D_R (i.e., a mass increment in volume V_C during the time interval Δt) are due to F_R only. On the contrary, negative mass variations in Δt are likely due to a predominant advection term that tends to move out the ash mass from V_C. In formulas, this means

$$\begin{cases} F_{R_{app}}(t_k) \cong D_R^+(t_k) = \sum\limits_{i=1}^{N_C} \Delta V_i \frac{\Delta C_{aik}^{(c)}(t_k)}{\Delta t} \Big|^+ \\ A_{R_{app}}(t_k) \cong D_R^-(t_k) = \sum\limits_{i=1}^{N_C} \Delta V_i \frac{\Delta C_{aik}^{(c)}(t_k)}{\Delta t} \Big|^- \end{cases} \tag{19}$$

where the right-hand-side terms indicate the positive (negative) time derivative of the ash concentration C_a within each radar volume bin ΔV. The subscript "*app*" indicates an approximate solution. The approximate term F_{Rapp} is our retrieval of MFR when the velocity v is not available. The approximation of MFR in (19) is, indeed, an underestimation since we are assuming that the temporal increase of tephra within the column above the volcanic vent is not taking into account the advective outflow, which tends to subtract ash mass from the column. At the same time, the use of (19) underestimates A_R in (18) as the decrease of tephra can be larger if not considering the contribution of the vent source.

The MFR reconstructed from radar scans, directly probing the tephra column above the volcano vent, can be compared with that derived from simplified 1-D volcanic eruption models [7], [21], [25]. In particular, it is well known that MFR can be related to a power of the plume top height H_{top} [26]. Several

analytical formulas have been proposed in the last decades; more recently, a nonlinear model has been derived including both wind and buoyancy local meteorological conditions at a given instant [7]. Thus

$$F_R(t) = a_0 \left[a_1 H_{top}^4(t) + a_2 H_{top}^3(t)\right] \tag{20}$$

where a_0, a_1, and a_2 are coefficients dependent on the gravitational acceleration, air density, buoyancy frequency, top-hat profile radial entrainment coefficient, wind entrainment coefficient, and wind velocity profile [7].

Intercomparisons between (20) and (18) are of interest for validation of the 1-D model and for consistency check of MFR estimates. For a given time step t, the application of (20) relies on 1) knowledge of the atmospheric conditions close to the volcanic vent at least in terms of vertical profiles, derivable from available radiosondes and/or meteorological numerical forecasts, and 2) the estimate of the maximum plume top height H_{top}, which can be provided by the radar itself on the basis of a detection algorithm [17].

IV. Data Intercomparison

The main task of radar retrieval techniques is to quantify physical parameters of volcanic eruptions in real time to facilitate dispersion model initialization and risk mitigation. However, remote sensing techniques need to be first compared and validated with *in situ* direct measurements, if available [18]. This intercomparison between remote estimates and *in situ* data has some inherent problems: 1) The geometry of radar observations is affected by occlusions so that the effective sampling is well above the ground, unless a vertical profile reconstruction is not carried out as already mentioned; 2) radar retrievals are volume-integrated products within bins of few kilometers, whereas ground data are typically surface point measurements. The previous conditions pose a problem of spatial representativeness, which translates into a discrepancy (error), which is coupled with a temporal representativeness discrepancy due to the different time sampling (e.g., every 5 min for radar versus few seconds for ground collectors and months for ash drills). This implies that the error structure of these intercomparisons is affected by these inherent differences, which cannot be all associated to the inaccuracy of the remote sensors and retrieval algorithms.

It is also worth mentioning that hail formation in volcanic columns may influence mass flux estimations based on radar measurements. These changes in effective grain size lead to an increased ash fall and may affect radar reflectivity [1]. From an electromagnetic point of view, hydrometeor signatures at the C-band may be affected by the Mie resonance effects and by mixture and/or coexistence of particles [15], [16]. Due to the difficulty in quantifying these effects, in the VARR approach, these uncertainties are taken into account by increasing the *a priori* standard deviation added to reflectivity forward model simulations [14].

In the following sections, we will first discuss intercomparison results between radar and ground real-time data for the three selected EJn sites. In Section IV-A, this aspect will be carried out in terms of ash mass loading, ash-fall rate, PSD retrieval, and MFR estimation. Then, a further intercomparison of VARR accumulated retrievals with daily tephra production rates based on ground data and model extrapolation will be discussed in Section IV-B.

A. Results for Real-Time Site Measurements

As shown elsewhere, e.g., in [17], the VARR algorithm successfully provided reasonable estimates of the April and May 2010 events in Iceland. Our attention is here concentrated only on the validation sites EJ14, EJ15, and EJ24, which are shown in Fig. 2. The site EJ22 is not considered in the quantitative analysis since it is very far from the Eyjafjallajökull vent (about 20.6 km), and the Keflavík radar poorly intercepts the ash plume at a height of 4 km above the ground (see Fig. 3). However, it is left among the validation sites in Figs. 7–9, to give an evidence of the sensitivity of the radar estimates.

Fig. 7 shows, in terms of PPI (i.e., constant elevation-angle map; see also Figs. 3 and 5), the spatial distribution of VARR-based estimated ash concentration C_a. It is worth noting that the ash mass is relatively confined around the vent and its proximal area due to the C-band radar sensitivity mainly affected by the distance. This means that some fine ash plume is indeed present but poorly revealed by the radar imagery. Estimated ash concentration reaches values up to 8 $\mathrm{g \cdot m^{-3}}$ on May 5 and 6 $\mathrm{g \cdot m^{-3}}$ on May 7, typically with stronger values around the vent.

Analogously to the previous figure, Figs. 8 and 9 show the estimates of ash-fall rate R_a $(\mathrm{kg \cdot m^{-2} \cdot s^{-1}})$ and ash loading $L_a(\mathrm{kg \cdot m^{-2}})$, respectively. Considerations similar to Fig. 7 can be done in terms of tephra spatial distribution with variability of ash column up to 25 $\mathrm{kg \cdot m^{-2}}$ on May 5 and 7: For R_a, we have registered a maximum value of $9 \cdot 10^{-5}$ and $11 \cdot 10^{-5}$ $\mathrm{kg \cdot m^{-2} \cdot s^{-1}}$, respectively, on May 5 and 7.

In Table I, different ground-collected parameters are shown, including accumulation rate $(\mathrm{kg/m^2 s})$ and mass load $(\mathrm{kg/m^2})$, which can be directly compared with those estimated by the radar-based VARR. The latter can provide values of C_a, R_a, and L_a, which have been obtained using the KL velocity model [11] for the whole collection period of EJn experiments. The radar-estimated values of R_a show levels about one order of magnitude higher than the ground-measured accumulation rate for all sites EJ14, EJ15, and EJ24. The estimated values L_a are about one order of magnitude larger than those measured at ground for EJ14 and EJ15, but only three times higher for EJ24. These differences may be due to the lower sensitivity of weather radar to the airborne tephra content close to the ground (and not deposited on the ground yet) as well as to the different temporal sampling and terminal velocity model.

Indeed, the deposited ash depends on the ash-fall terminal velocity v_a. To test the sensitivity of the ash mass estimation to v_a, we have used four different types of power-law regression coefficients, as shown in Fig. 6, for the evaluation of R_a and L_a. Table II shows these results for the three sites EJ14, EJ15, and EJ24. All four different models, extracted from the available literature, have been used (see Fig. 6). The Harris–Rose 1980 parametric model tends to provide lower radar-based estimates, thus reducing the differences with respect to ground

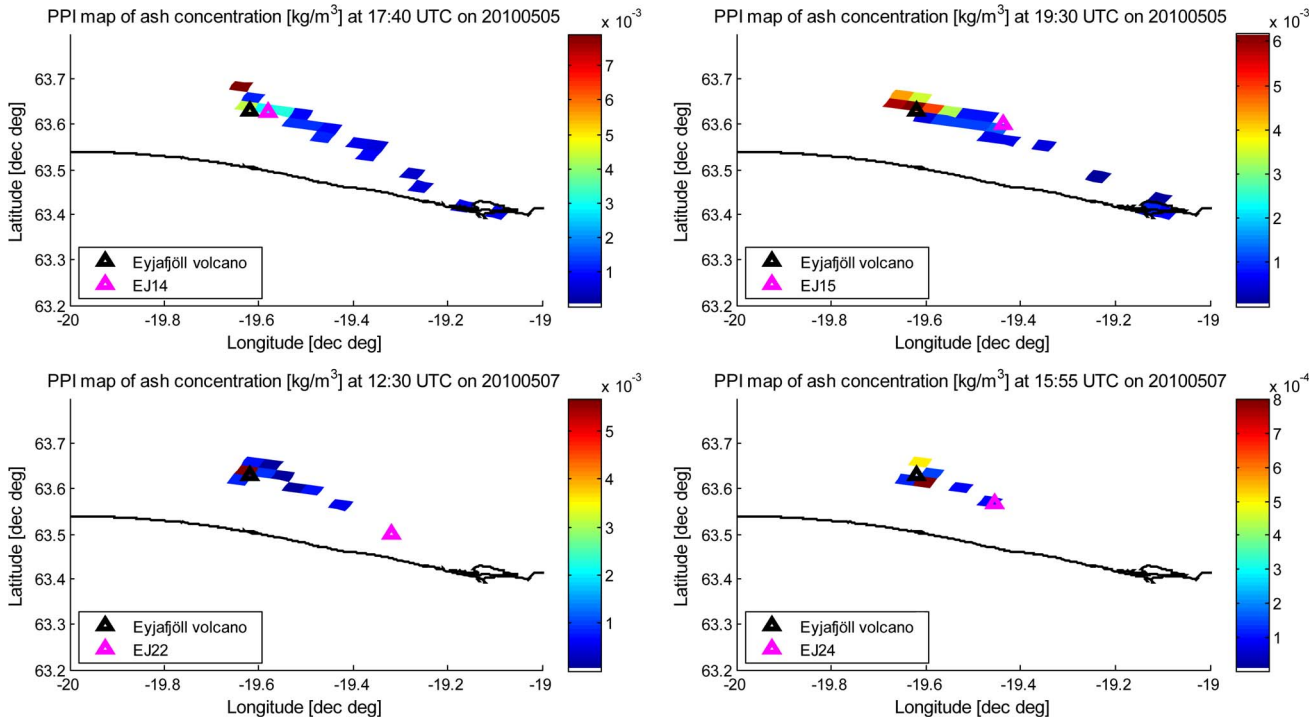

Fig. 7. Radar PPI images of VARR-derived ash concentration C_a, corresponding to RHI and EJ sites of Fig. 4 (EJ14 on the top left, EJ15 on the top right, EJ22 on the bottom left, and EJ24 on the bottom right).

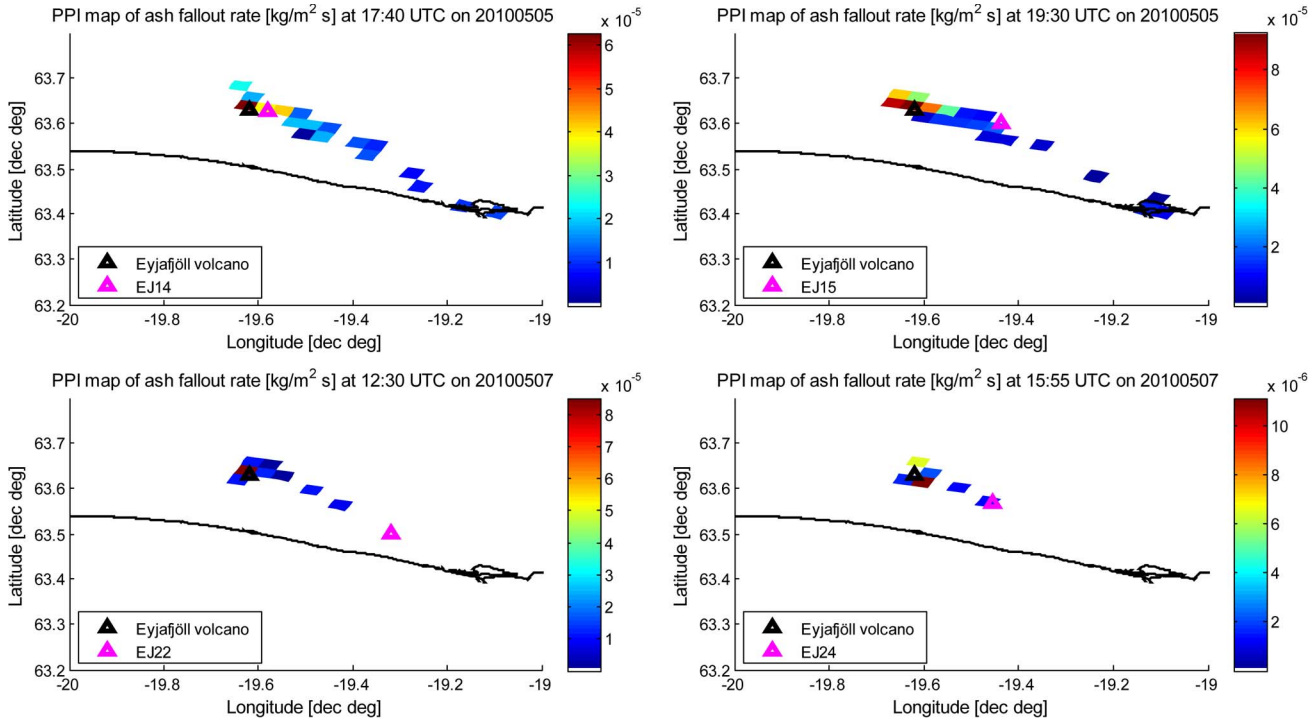

Fig. 8. Radar PPI images of VARR-derived ash-fall rate R_a, corresponding to RHI and EJ sites of Fig. 4 (EJ14 on the top left, EJ15 on the top right, EJ22 on the bottom left, and EJ24 on the bottom right).

measurements. Generally speaking, the terminal velocity parameterization can exhibit a variability of estimates of about 10%–30% with respect to KL ones.

The capability of weather radars to derive microphysical parameters can be exploited by using the technique illustrated in Section III-C. Figs. 10–12 upper plots show the histogram of VARR-based estimates of D_n using (7) and C_a using (5), extracted at and around the sampling sites EJn for the 24-h period of the same. The overall mean diameter, estimated from radar data, is between 0.05 and 0.6 mm for EJ15 and EJ24 sites with some values up to 1 mm for EJ14, whereas from ground data, it is about 1.87 mm for EJ14, 0.62 mm

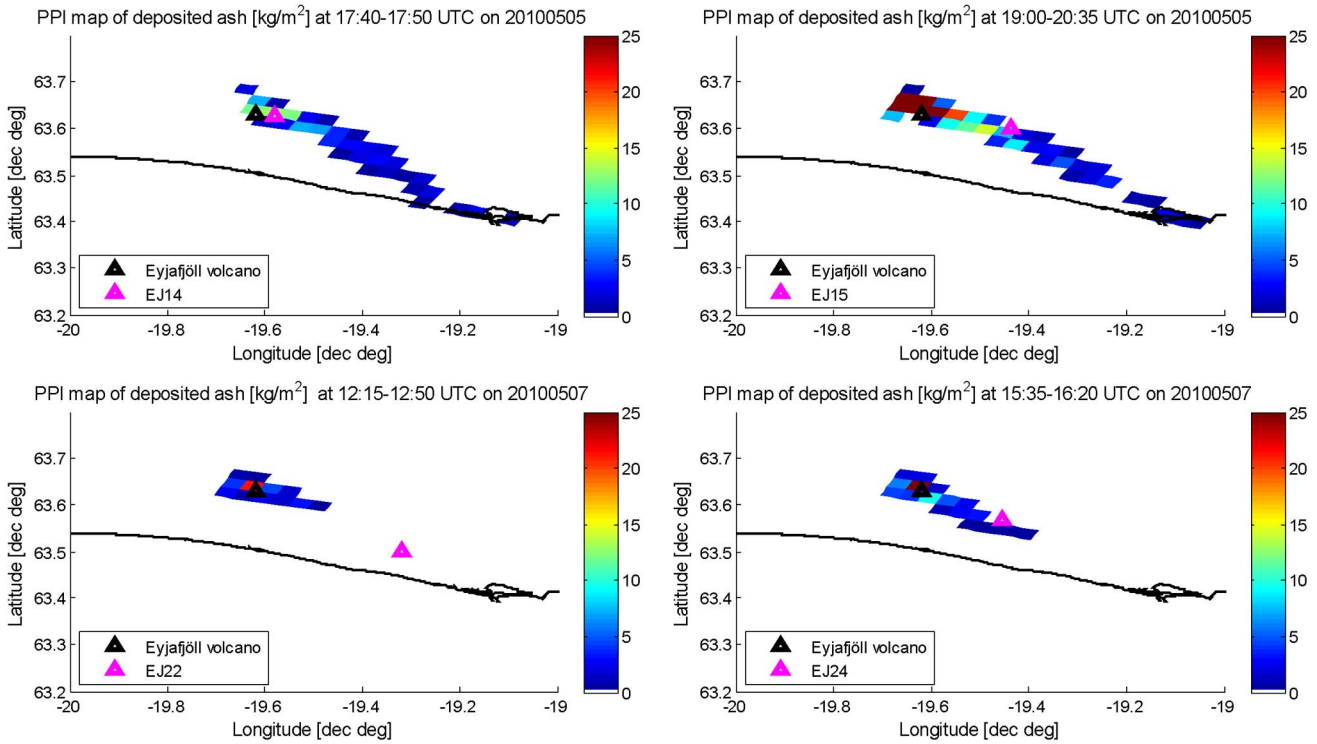

Fig. 9. Radar PPI images of VARR-derived ash loading L_a, corresponding to RHI and EJ sites of Fig. 4 (EJ14 on the top left, EJ15 on the top right, EJ22 on the bottom left, and EJ24 on the bottom right).

TABLE II
SENSITIVITY TO FALLOUT VELOCITY OF VARR-DERIVED ESTIMATES OF ASH-FALL RATE R_a AND DEPOSIT LOADING L_a FOR EJ14, EJ15, AND EJ24 SITES USING FOUR DIFFERENT ASH-FALL VELOCITY MODELS (SEE TEXT FOR DETAILS)

		Velocity-diameter model			
Validation site	**Estimated parameter**	**Kunii & Levienspiel (1969)**	**Wilson (1972)**	**Harris & Rose (1980)**	**Harris & Rose (1982)**
EJ14	R_a [kg/m^2·s]	$1.01\cdot10^{-2}$	$6.87\cdot10^{-3}$	$5.77\cdot10^{-3}$	$8.32\cdot10^{-3}$
	L_a [kg/m^2]	5.78	3.91	3.28	4.74
EJ15	R_a [kg/m^2·s]	$2.97\cdot10^{-3}$	$2.22\cdot10^{-3}$	$1.78\cdot10^{-3}$	$2.51\cdot10^{-3}$
	L_a [kg/m^2]	7.76	5.79	4.65	6.54
EJ24	R_a [kg/m^2·s]	$1.70\cdot10^{-3}$	$1.07\cdot10^{-3}$	$9.67\cdot10^{-4}$	$1.40\cdot10^{-3}$
	L_a [kg/m^2]	1.11	0.70	0.63	0.91

for EJ15, and 0.41 mm for EJ24 (see Table I). The VARR-derived average ash concentration is up to 9 g · m^{-3} with a significant occurrence of samples above 0.1 g · m^{-3} for the closest site EJ14 and only a few samples for the farthest site EJ24.

We can also process radar data to investigate a near "real-time" intercomparison. The same figures, in the lower panels, show the estimated ash PSD $N_a^{(c)}(D)$ via (2), for the ground collection time window and within an area of 5 km × 5 km centered in the EJn site using the first radar elevation angle (i.e., that closer to the ground). Plots of $N_a^{(c)}(D)$ are provided as a function of both diameters (left panel) and ϕ units (right panel). In the lower-right panel, we added the PSD derived by the ground measurements [2] at the selected sites EJn to facilitate ground-to-radar PSD intercomparison.

In Figs. 10–12, we note that the mode of estimated PSD shows an effective diameter D_n of tephra, which varies around 0.04 mm ($\sim 4.6\phi$) for the EJ14, EJ15, and EJ24 sites. These results reveal that for all sites, the VARR-estimated PSD mode, due to airborne ash particles, is smaller than that collected on the ground (general mode within -0.9ϕ and 1.3ϕ; see Table I). The ash class, identified by the VARR algorithm, is generally the coarse ash, whereas a low presence of fine ash (<10%) is detected. The ash population, observed by the radar in the cloud above the selected locations EJ15 and EJ24, exhibits a mode of about 0.03 mm ($\sim 4.7\phi$), which is slightly smaller than that at the closest site EJ14 with a mode of 0.05 mm.

Our conjecture to explain the above results is that a gravitational sedimentation process is taking place. In other words, bigger particles, due to gravity, reach the ground before the smaller particles, which indeed show a longer airborne time. The same trend is clear in the three sites EJ14, EJ15, and EJ24 for a distance from the vent between 2-10 km. For these distance ranges we can then affirm that the airborne particle size is unchanged.

The MFR can be estimated either from radar scans by means of the complete model in (17) or from the approximate relation in (19) or from 1-D analytical eruption models based on the radar-derived plume top height using (20). For these estimations, we have used the radar time sampling $\Delta t = 5$ min, whereas the horizontal section of the columnar volume V_C is set to 5×5 pixels with a pixel size of about 1 km per side, thus having an area of 25 km^2 around the Eyjafjallajökull volcanic.

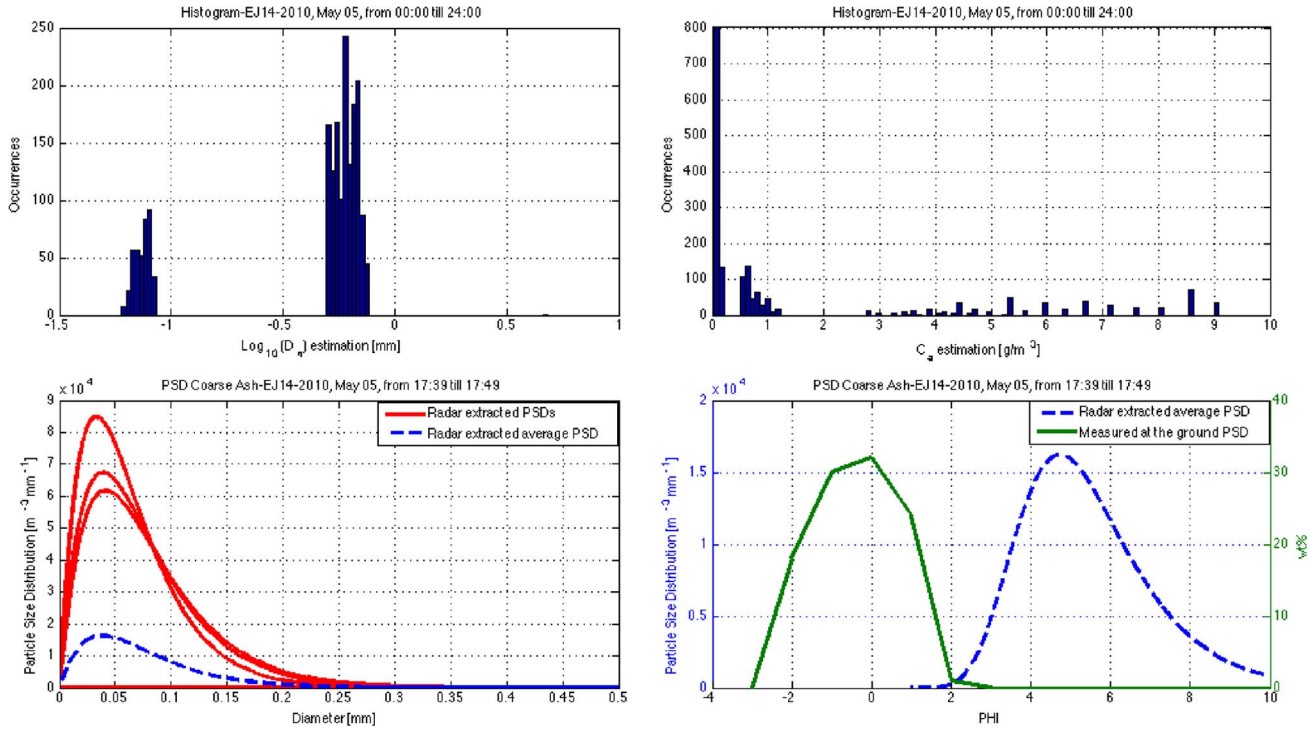

Fig. 10. (Upper panels) Histograms of VARR-derived mean diameter D_n (left) and ash concentration C_a (right) for the identified coarse ash classes, estimated around the site EJ14 for 24 h of May 5, 2010. (Lower panels) VARR-derived average PSD with respect to the particle diameter $D_{\rm n}$ (left) and parameter ϕ (right) for the short ground-collection time interval as reported in Table I and on the plot title. In the left panel, all PSD values, estimated every 5 min, are shown together with the mean PSD for the time interval. On the right panel, the mean VARR-estimated PSD is compared with the corresponding PSD derived from ground-based collection, as shown in Bonadonna *et al.* [2].

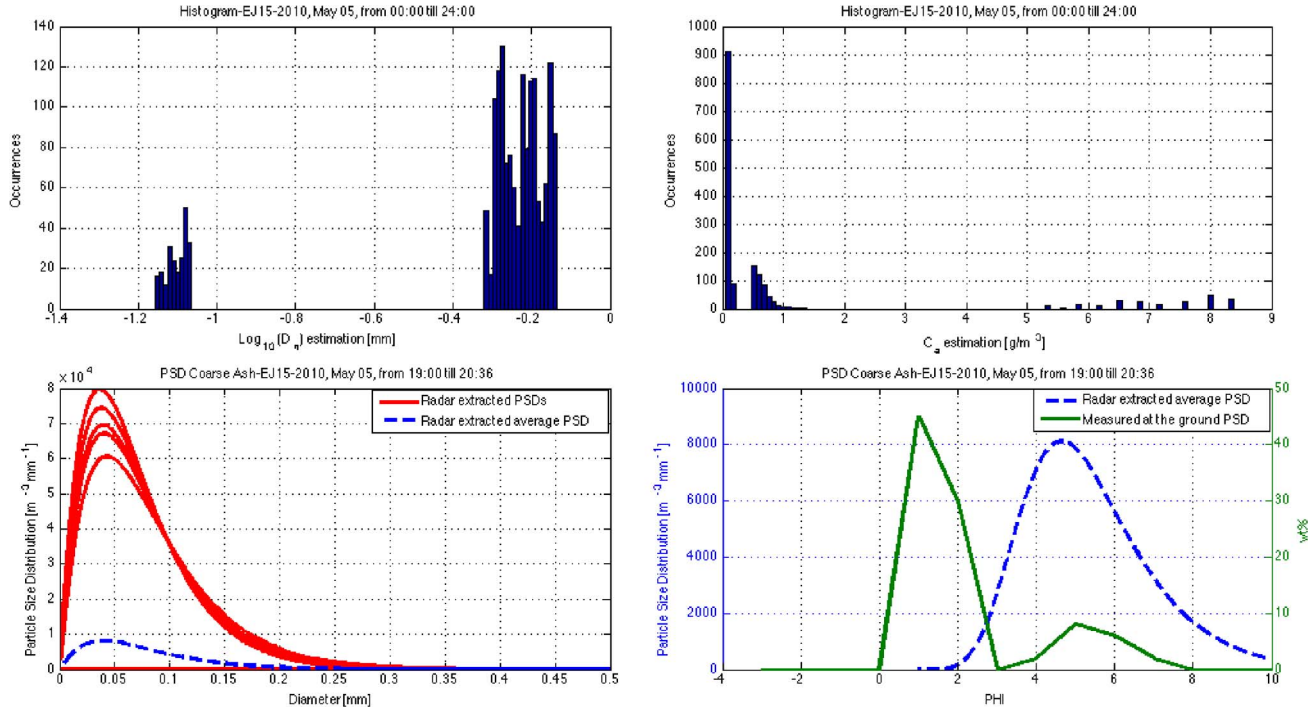

Fig. 11. Same as in Fig. 10, but for the EJ15 site on May 5, 2010.

Fig. 13 (upper left) shows the behavior of the top plume height, above the volcano vent, estimated from the ash concentration threshold on May 5 [17]. The estimated top plume height is between 4 and 8 km, except some peaks above 10 km around 06:00 UTC. The upper-right panel shows the approximate derivative mass rate $F_{Rapp} = D_{\rm R}^{+}$, derived from (19), together with the estimate of the advection rate $A_{Rapp} = D_{\rm R}^{-}$ carried out by inferring the plume advection velocities estimated by the radar data. The latter is not always negligible, as apparent from the advection rate time series. This is particularly true for

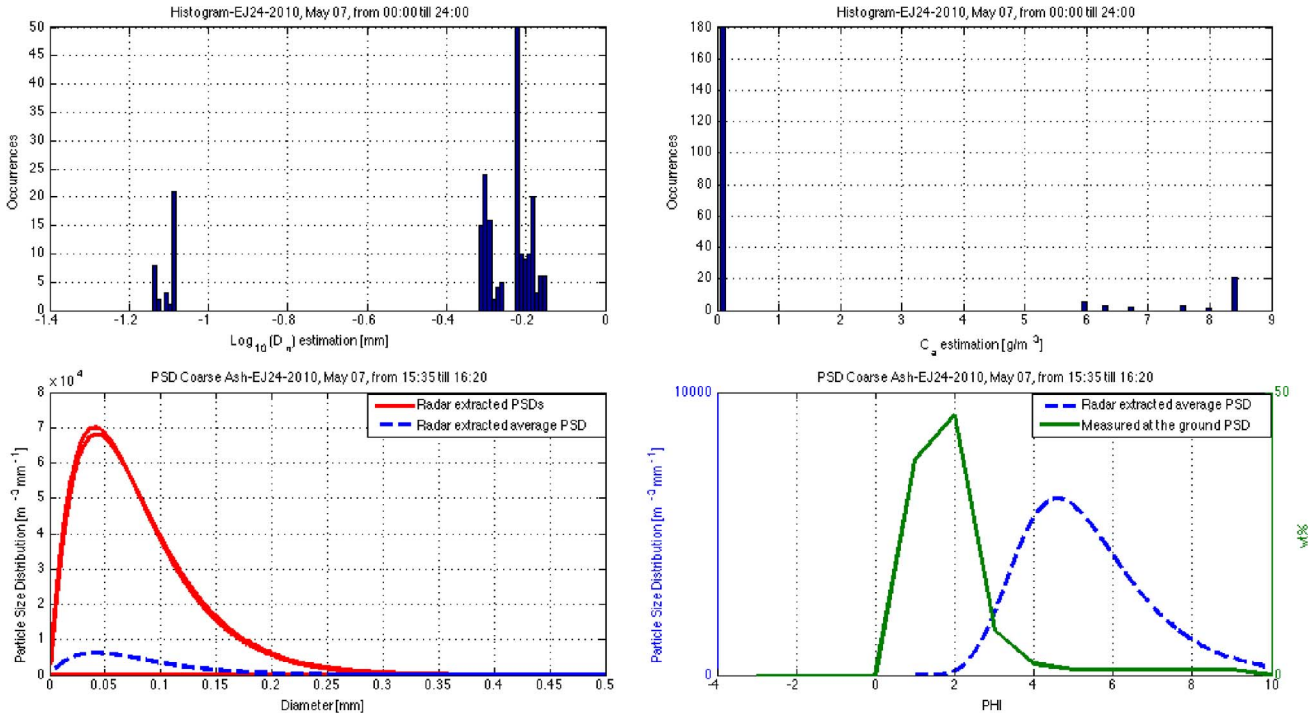

Fig. 12. Same as in Fig. 10, but for the EJ24 site on May 7, 2010.

the Eyjafjallajökull eruption in 2010, where the trophospheric plumes were transported and dispersed by strong winds flowing around 3–6 km.

The left-lower panel of Fig. 13 shows the total radar-based MFR estimations above the volcano vent with respect to the plume top height superimposed to model-based MFR predictions, using the 1-D analytical model of Degruyter–Bonadonna with different wind velocity varying between 0 and 60 m/s [7]. The 1-D model from Mastin *et al.* [21], obtained from plume height only, is considered as well. These MFR models are both derived from radar observations of the plume height and available radiosonde data. The right-lower panel presents the correlation between the total VARR-estimated MFR and model-based MFR derived from [7] for three wind speeds (0, 30, and 60 m/s) to show its variability. VARR-estimated MFR is consistent, in terms of value range, with the Degruyter–Bonadonna MFR predictions. This result is important as it shows that tephra mass rate and advection, estimated from C-band radar measurements available every 5 min, can provide a valuable information for assessing the volcanic eruption activity.

The MFR variability, detected from the weather radar, shows a different behaviour compared with that derived from a 1-D analytical model. The latter is depending on the plume maximum height and on the time interval sampling considered by averaging the plume maximum height. The plume maximum height may not vary so much during the continuous eruption activity as it is sustained by the buoyant plume. By taking into account the ash mass balance in the vent column using radar data, we are indeed looking at the temporal intermittency of the explosive fountain. The oscillations of our MFR estimates are even more exacerbated by the time sampling of the radar, which is on the order of a few minutes, whereas the ash cloud parameters can vary at a scale of a few seconds.

Figs. 14 and 15 show the same results as in Fig. 13, but for May 6 and May 7, 2010. The temporal trend of the VARR-estimated MFR of the Eyjafjallajökull for May 5–7 shows values between 10^4 and 10^6 kg/s, whereas the top plume height ranges between 3 and 7 km, with a mean trend around 4.5 km. The radar-based MFR estimation is coherent with the values obtained by the 1-D eruption model. Note that the advection rate A_R exhibits lower values with respect to those of May 5 (about 1 kg/s) due to the wind transport.

It is worth noting that Figs. 13–15 show almost no correlation between MFR radar retrievals and 1-D-analytical model estimates, but, as mentioned before, the maximum plume height is not necessarily correlated with the intermittent mass eruption rate due to explosive activity. Indeed, knowledge of the height of the plume provides a poor estimate of the ash load in the plume, if the realistic fraction of fine material produced during an eruption is not known, and the temporal influence of atmospheric properties are neglected [37]. This would mean, if confirmed by further analyses, that 1-D analytical models should be taken as reference values to be compared with near real-time estimates from ground-based radar and other instruments.

B. Comparison With Daily Tephra Maps

The previous section has been focused on the capability of radar-based retrievals to capture the microphysical properties of ash fall. Unfortunately, the lack of radar-to-ground data matching has limited the value of this assessment. In this respect, ash loading retrievals can be better handled for routine intercomparisons. Estimates of the Eyjafjallajökull daily

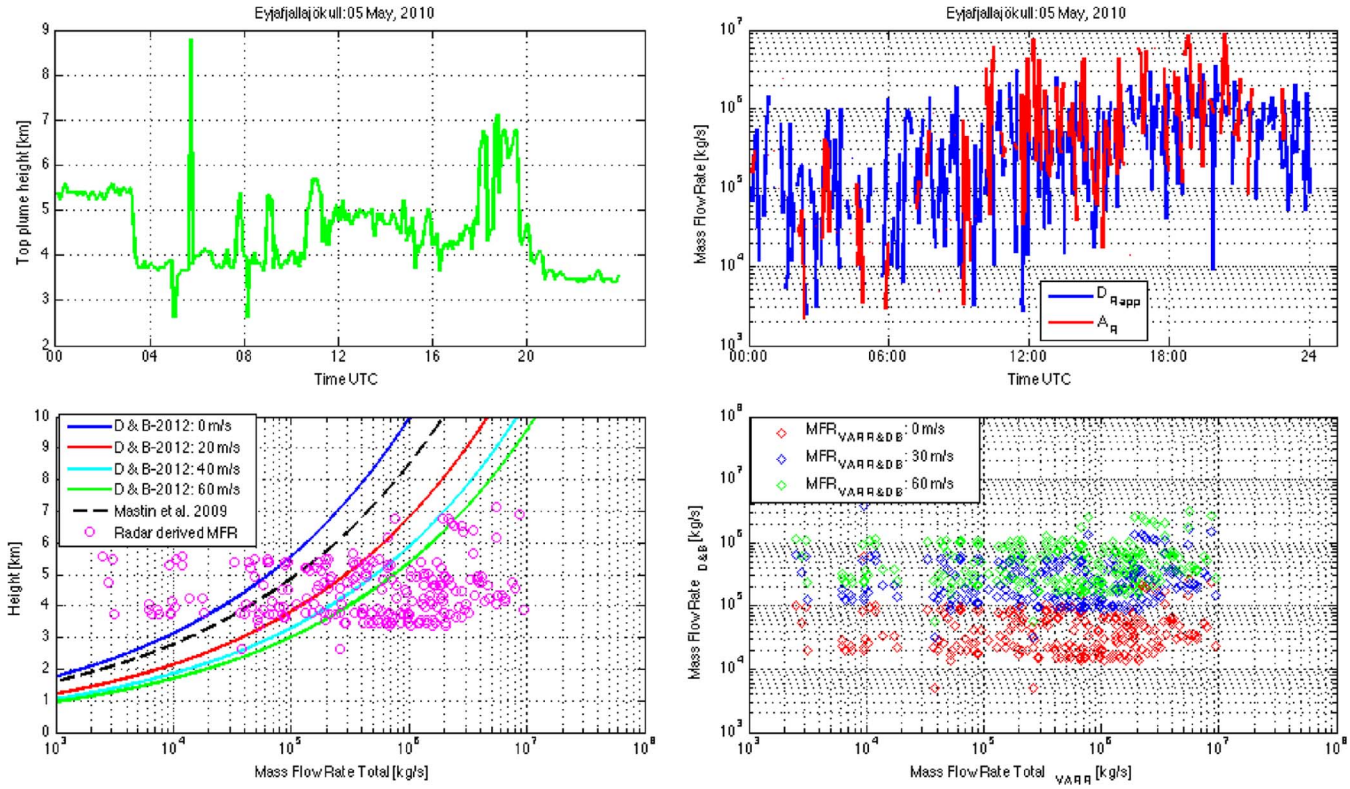

Fig. 13. Radar-based retrievals and intercomparisons from 00:00 until 24:00 UTC on May 5, 2010 during the Eyjafjallajökull volcanic eruption. (Left top) Time trend of the plume height estimated above the vent using the estimated concentration C_a threshold technique within VARR. (Right top) Approximate MFR (F_{Rapp}) using (19) and advection rate term (A_{Rapp}), plotted only when the advection velocity is available, using (18b). (Left bottom) VARR-based estimates of plume top height versus VARR-derived total MFR ($\mathrm{F_R}$ from the union of $\mathrm{A_{Rapp}}$ and $\mathrm{D_{Rapp}}$) and model-based MFR predictions, derived from two 1-D analytical eruption models (specifically, Degruyter and Bonadonna [7] (D & B-2012 in the legend) and Mastin *et al.* [21]) with different wind speeds using (20). (Right bottom) Correlation between VARR-estimated MFR and model-based MFR, deduced from the Degruyter–Bonadonna model for different wind speeds.

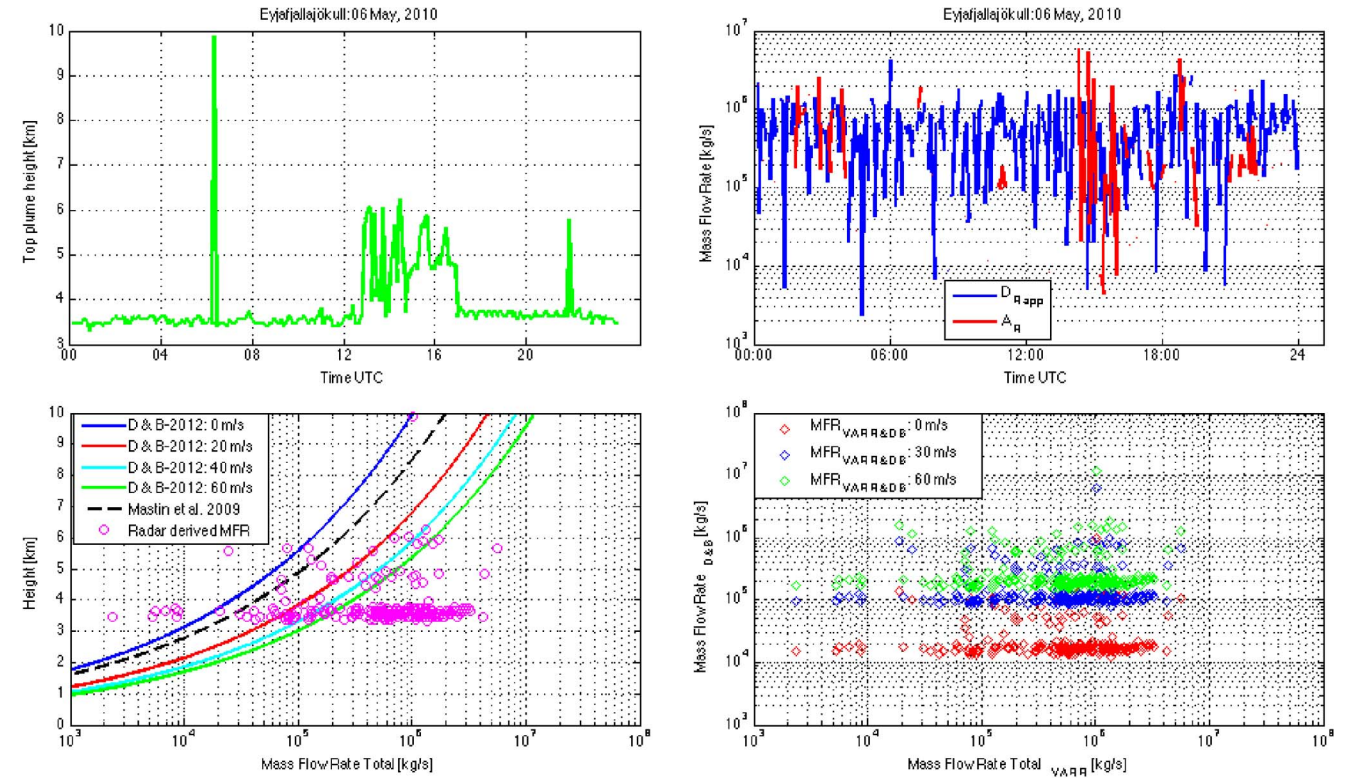

Fig. 14. Same as Fig. 13, but for May 6, 2010.

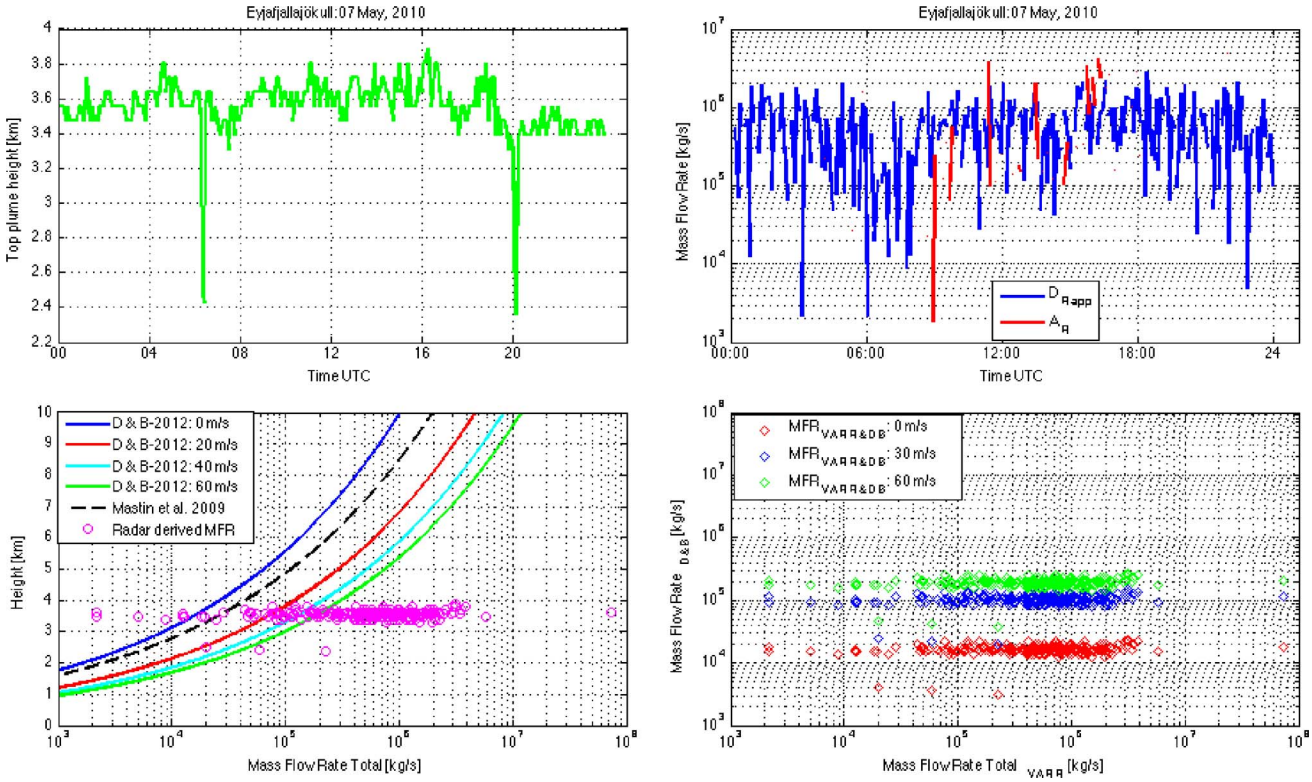

Fig. 15. Same as Fig. 13, but for May 7, 2010.

TABLE III
INTERCOMPARISON BETWEEN ESTIMATED TEPHRA MASS ERUPTED PER DAY BY GUDMUNDSSON *ET AL.* [8], COLUMNS 1–4 WITH CORRESPONDING DAILY TEPHRA ESTIMATED BY MEANS OF C-BAND VARR (FIFTH COLUMN) FOR THE AVAILABLE DAYS OF RADAR OBSERVATIONS, USING THE KL VELOCITY-DIAMETER MODEL

Date	Daily total mass 10^9 [kg/day]	Direction of dispersal	Grain size sample distance [km]	Estimated total Mass (VARR-KL) 10^9 [kg]
14 April	40-50	E	1	34.34 ± 10.9
15 April	5-10	E	58	88.34 ± 26.4
16 April	30-40	E	21	114.46 ± 34.3
17 April	30-40	S	11	33.15 ± 9.9
18 April	05-10	SE	-	4.15 ± 1.2
19 April	1-3	SE	-	1.28 ± 0.4
20 April	<1	SE	-	2.02 ± 0.6
5 May	30-40	SE	30	49.46 ± 14.8
6 May	5-10	E	-	17.20 ± 5.2
7 May	5-10	SE	-	9.24 ± 2.8
8 May	3-5	SE	13	3.43 ± 1,0
9 May	2-5	SE	-	2.37 ± 0.7
10 May	2-5	SE	13	2.53 ± 0.7

tephra production rates, main direction dispersal, and grain size characteristics are listed in Table III, for the period of April 14–May 10 as derived from [8]. The estimated tephra mass, erupted per day and shown in the second column of Table III, is based on the partitioning of tephra and basically refer to inland deposits [21].

The availability of radar volume time series with a time sampling of 5 min can allow a VARR-based estimate of the daily tephra deposits derived from M_a in (11) [18]. The latter can be compared with data in Table III for the time period of April 14–20 and May 5–10, during which radar data were at disposal. The last right column shows the total mass per day (24 h) estimated by integrating the VARR ash concentration rertievals, using the KL terminal velocity model and an uncertainty of 30%, derived from previous validation works [18]. We should, of course, take into account all the limitations due to visibility and sensitivity of radar-derived estimates, but, on the other hand, ground daily tephra loadings are extrapolations of heterogeneous data sets [8].

VARR-based retrieval values of volcanic ash mass, extrapolated at ground for each day, are in a fairly good agreement with values derived from [8], being the values of the same order of magnitude particularly after April 17. This agreement would suggest that the overall daily tephra loading is well captured by VARR radar-based retrievals, notwithstanding its limited sensitivity at a distance of 156 km and partial visibility of the volcanic plume. The major discrepancies are noted on the eruption phase between April 14 and 16, where the radar-based estimates are much higher (between three and five times), which is the most intense eruption phase, as documented by the radar-based retrieval trends [18]. This difference might be explained by considering, on the one hand, that during these initial days of the Eyjafjallajökull eruption, the ground sampling and model extrapolations can be more difficult and less accurate and, on the other hand, that inherent uncertainties affect VARR-based estimates, as discussed in Section II-B.

V. CONCLUSION

The April–May 2010 eruption of the Eyjafjallajökull volcano provided a wide range of *in situ* and remote sensing data whose

combination can highlight important aspects of tephra microphysical processes. Within the VARR methodology, previously introduced, this work has presented a new technique to estimate airborne tephra size distribution and MFR together with a retrieval of the deposited tephra at ground. VARR-based products have been compared with *in situ* campaign measurement data, in terms of size distribution and ash collection near the volcano vent, and multiple-source daily tephra deposits in the plume-affected volcanic area presented.

Retrievals from scanning C-band weather radars are affected by some limitations, which have been previously discussed. Interestingly, the estimated values of fall rate are of the same magnitude order as the values derived from the experimental collected data EJn. The estimated ash loading in the same EJn sites is larger than that collected of a few orders of magnitude, mainly because these radar-derived values are obtained by assuming a georeferenced area of $25\ \mathrm{km}^2$ around the location of each EJn site.

Microwave radars can probe the plume inside, although limiting the sensitivity to coarse and large grains. The VARR-estimated tephra around the Eyjafjallajökull volcano vent in all analyzed cases was classified as coarse ash with a mean diameter around 0.1 mm, according to PSD parameterization here adopted. By comparing the retrieved airborne PSDs with those estimated at ground, tephra accumulation rate appears to be not uniform along the column. VARR-based particle size estimates may suggest that a sorting of airborne particles during the downwind transport is taking place during the ash fall.

The estimate of the volcanic MFR is a crucial goal for eruption dynamics modeling. The MFR, estimated by VARR for the period between May 5 and May 7, 2010, presents a value range that agrees with that shown in 1-D eruption approximate models driven by plume top height.

Future works should be devoted to applying VARR PSD and MFR retrieval algorithms to microwave radar data with higher sensitivity and quality, possibly exploiting shorter distances and polarimetric capability. Radar-derived quantities are indeed of potential interest for ash transport modeling. Specific efforts should be focused on methods for extrapolating radar retrievals from coarser to finer particles, needed to initialize Lagrangian ash dispersion models. Such extrapolation methods might be based on simple PSD shape extension or be aimed at finding scale factors to convert radar-derived quantities into dispersion model parameters.

ACKNOWLEDGMENT

The authors would like to thank B. Pálmason, H. Pétursson, and S. Karlsdóttir (IMO, Iceland) for providing C-band radar data and useful suggestions on data processing. They would also like to thank W. Degruyter for the comments and suggestions that helped improve the manuscript.

REFERENCES

[1] Þ. Arason, S. B. Þorláksdóttir, G. S. Sigurðsson, R. F. Yeo, and T. Thorsteinsson, "Properties of ash-infused hail during the Grímsvötn 2011 eruption and implications for radar detection of volcanic columns," vol. 15, EGU2013-4797, 2013.

[2] C. Bonadonna *et al.*, "Tephra sedimentation during the 2010 Eyjafjallajökull eruption (Iceland) from deposit, radar, and satellite observations," *J. Geophys. Res.*, vol. 116, no. B12, pp. 202–345, 2011.

[3] C. Bonadonna and J. C. Phillips, "Sedimentation from strong volcanic plumes," *J. Geophys. Res.*, vol. 108, no. B7, 2340, 2003.

[4] C. Bonadonna and B. F. Houghton, "Total grain-size distribution and volume of tephra fall deposits," *Bull. Volcanol.*, vol. 67, pp. 441–456, 2005.

[5] C. Bonadonna and A. Costa, "Estimating the volume of tephra deposits: A new simple strategy," *Geology*, vol. 40, pp. 415–418, 2012.

[6] M. I. Bursik *et al.*, "Estimation and propagation of volcanic source parameter uncertainty in an ash transport and dispersal model application to the Eyjafjallajokull plume of 14–16 April 2010," *Bull. Volcanol.*, vol. 74, no. 10, 2321–2338, Dec. 2012.

[7] W. Degruyter and C. Bonadonna, "Improving on mass flow rate estimates of volcanic eruptions," *Geophys. Res. Lett.*, vol. 39, no. 16, 2012, Art. ID. L16308.

[8] M. T. Gudmundsson *et al.*, "Ash generation and distribution from the April–May 2010 eruption of Eyjafjallajökull, Iceland," *Nature Sci. Rep.*, vol. 2, 572, Jul. 2012.

[9] D. L. Inman, "Measures for describing the size distribution of sediments," *J. Sedimentary Petrology*, vol. 22, no. 3, pp. 125–145, 1952.

[10] D. M. Harris and W. I. Rose, "Estimating particle sizes, concentrations, and total mass of ash in volcanic clouds using weather radar," *J. Geophys. Res.*, vol. 88, no. C15, pp. 10 969–10 983, Dec. 1983.

[11] D. Kunii and O. Levenspiel, *Fluidization Engineering*. New York, NY, USA: Wiley, 1969.

[12] C. Lacasse *et al.*, "Weather radar observations of the Hekla 2000 eruption cloud," *Iceland Bull Volcanol*, vol. 66, no. 5, pp. 457–473, Dec. 2004.

[13] F. S. Marzano, G. Vulpiani, and W. I. Rose, "Microphysical characterization of microwave radar reflectivity due to volcanic ash clouds," *IEEE Trans. Geosci. Remote Sens.*, vol. 44, no. 2, pp. 313–327, Feb. 2006.

[14] F. S. Marzano, S. Barbieri, G. Vulpiani, and W. I. Rose, "Volcanic ash cloud retrieval by ground-based microwave weather radar," *IEEE Trans. Geosci. Remote Sens.*, vol. 44, no. 11, pp. 3235–3246, Nov. 2006.

[15] F. S. Marzano, S. Marchiotto, C. Textor, and D. Schneider, "Model-based weather radar remote sensing of explosive volcanic ash eruption," *IEEE Trans. Geosci. Remote Sens.*, vol. 48, no. 10, pp. 3591–3607, Oct. 2010.

[16] F. S. Marzano, S. Barbieri, E. Picciotti, and S. Karlsdóttir, "Monitoring sub-glacial volcanic eruption using C-band radar imagery," *IEEE Trans. Geosci. Remote Sens.*, vol. 48, no. 1, pp. 403–414, Jan. 2010.

[17] F. S. Marzano, M. Lamantea, M. Montopoli, S. Di Fabio, and E. Picciotti, "The Eyjafjallajökull explosive volcanic eruption from a microwave weather radar perspective," *Atmos. Chem. Phys.*, vol. 11, 9503–9518, 2011.

[18] F. S. Marzano, M. Lamantea, M. Montopoli, B. Oddsson, and M. T. Gudmundsson, "Validating sub-glacial volcanic eruption using ground-based C-band radar imagery," *IEEE Trans. Geosci. Remote Sens.*, vol. 50, no. 4, pp. 1266–1282, Apr. 2012.

[19] F. S. Marzano, E. Picciotti, G. Vulpiani, and M. Montopoli, "Synthetic signatures of volcanic ash cloud particles from X-band dual-polarization radar," *IEEE Trans. Geosci. Remote Sens.*, vol. 50, no. 1, pp. 193–211, Jan. 2012.

[20] F. S. Marzano, D. Scaranari, and G. Vulpiani, "Supervised fuzzy-logic classification of hydrometeors using C-band weather radars," *IEEE Trans. Geosci. Remote Sens.*, vol. 45, no. 11, pp. 3784–3799, Nov. 2007.

[21] L. G. Mastin *et al.*, "A multidisciplinary effort to assign realistic source parameters to models of volcanic ash-cloud transport and dispersion during eruptions," *J. Volcanol. Geothermal Res.*, vol. 186, no. 1/2, pp. 10–21, 2009.

[22] G. N. Petersen, "A short meteorological overwiew of the Eyjafjallajökull eruption 14 April–23 May 2010," *Weather*, vol. 65, no. 8, pp. 203–207, Aug. 2010.

[23] S. Pouget, M. Bursik, P. Webley, J. Dehn, and M. Pavolonis, "Estimation of eruption source parameters from Umbrella cloud or downwind plume growth rate," *J. Volcanol. Geothermal Res.*, vol. 258, pp. 100–112, May 2013.

[24] H. Sauvageot, *Radar Meteorology*. Boston, MA, USA: Artech House, 1992.

[25] R. Sparks, "The dimensions and dynamics of volcanic eruption columns," *Bull. Volcanol.*, vol. 48, no. 1, pp. 3–15, Feb. 1986.

[26] R. S. J. Sparks *et al.*, *Volcanic Plumes*. New York, NY, USA: Wiley, 1997.

[27] J. Taddeucci *et al.*, "Aggregation-dominated ash settling from the Eyjafjallajökull volcanic cloud illuminated by field and laboratory high-speed imaging," *Geology*, vol. 39, pp. 891–894, Aug. 2011.

[28] T. Yu, W. I. Rose, and A. J. Prata, "Atmospheric correction for satellite based volcanic ash mapping and retrievals using split-window IR data from GOES and AVHRR," *J. Geophys. Res.*, vol. 107, no. D16, pp. 4311–4316, 2002.
[29] L. Wilson, "Explosive volcanic eruptions—II: The atmospheric trajectories of pyroclasts," *Geophys. J. R. Astron. Soc.*, vol. 30, no. 4, pp. 381–392, Dec. 1972.
[30] G. P. L. Walker, "Explosive volcanic eruptions—A new classification scheme," *Geol. Rundschau*, vol. 62, no. 2, pp. 432–4461973.
[31] C. Zehner, Ed. "Monitoring volcanic ash from space," in *Proc. ESA-EUMETSAT Workshop 14 Apr. –23 May 2010 Eruption Eyjafjoll Volcano*, Frascati, Italy, May 26–27, 2010, pp. 1–110.
[32] D. J. Schneider and R. P. Hoblitt, "Doppler weather radar observations of the 2009 eruption of Redoubt volcano, Alaska," *J. Volcanol. Geothemal Res.*, vol. 259, pp. 133–144, Jun. 2013.
[33] M. J. Woodhouse, A. J. Hogg, J. C. Phillips, and R. S. J. Sparks, "Interaction between volcanic plumes and wind during the 2010 Eyjafjallajökull eruption, Iceland," *J. Geophys. Res. Solid Earth*, vol. 118, no. 1, pp. 92–109, Jan. 2013.
[34] L. Wilson, "Explosive volcanic eruptions—II: The atmospheric trajectories of pyroclasts," *Geophys. J. R. Astron. Soc.*, vol. 30, no. 2, pp. 381–392, 1972.
[35] M. Montopoli, G. Vulpiani, D. Cimini, E. Picciotti, and F. S. Marzano, "Interpretation of observed microwave signatures from ground dual polarization radar and space multi-frequency radiometer for the 2011 Grímsvötn volcanic eruption," *Atmos. Meas. Techn.*, vol. 7, no. 2, pp. 537–552, 2014.
[36] C. Textor *et al.*, "Volcanic particle aggregation in explosive eruption columns. Part II: Numerical experiments," *J. Volcanol. Geothermal Res.*, vol. 150, no. 4, pp. 399–394, Feb. 2005.
[37] E. Kaminski *et al.*, "Estimation of ash injection in the atmosphere by basaltic volcanic plumes: The case of the Eyjafjallajökull 2010 eruption," *J. Geophys. Res.*, vol. 116, Sep. 2011 Art. ID. B00C02.

Luigi Mereu received the B.Sc. and M.Sc. degrees in telecommunication engineering from Sapienza University of Rome, Rome, Italy, in 2007 and 2012, respectively.

In 2012, he joined the Department of Information Engineering, Sapienza University of Rome and the CETEMPS Center of Excellence, University of L'Aquila, L'Aquila, Italy, to cooperate on radar remote sensing of volcanic ash clouds within the ICT Ph.D. program. He is involved within the FUTUREVOLC European project that started in 2012.

Mr. Mereu received the IEEE GRS South Italy award for Best Master Thesis in remote sensing in 2012.

Frank S. Marzano (S'89–M'99–SM'03) received the Laurea degree (*cum laude*) in electrical engineering and the Ph.D. degree in applied electromagnetics from Sapienza University of Rome, Rome, Italy, in 1988 and 1993, respectively.

In 1992, he was a Visiting Scientist with Florida State University, Tallahassee, FL, USA. In 1993, he collaborated with the Institute of Atmospheric Physics, National Council of Research (CNR), Rome. From 1994 to 1996, he was a Postdoctoral Researcher with the Italian Space Agency, Rome. After being a Lecturer with the University of Perugia, Perugia, Italy, in 1997, he joined the Department of Electrical Engineering, University of L'Aquila, L'Aquila, Italy, as an Assistant Professor teaching courses on electromagnetic fields. In 1999, he was a Visiting Scientist with the Naval Research Laboratory, Monterey, CA, USA. In 2002, he got the qualification to Associate Professorship and has cofounded the Center of Excellence on Remote Sensing and Hydro-Meteorological Modeling (CETEMPS), University of L'Aquila, L'Aquila, Italy. In 2005, he finally joined the Department of Information Engineering, Electronics and Telecommunications, Sapienza University of Rome, where he currently teaches courses on antennas, propagation, and remote sensing. Since 2007, he has been the Vice Director of CETEMPS, where he became a Director in 2013. He has published more than 110 papers on refereed international journals, more than 30 contributions to international book chapters, and more than 230 extended abstract on international and national congress proceedings. He was the Editor of two books. His current research concerns passive and active remote sensing of the atmosphere from ground-based, airborne, and spaceborne platforms and electromagnetic propagation studies.

Dr. Marzano has been acting as an Associate Editor of the IEEE GEOSCIENCE REMOTE SENSING LETTERS since January 2004. In 2005 and 2007, he was a Guest Coeditor of the MicroRad04 and MicroRad06 Special Issues for the IEEE TRANSACTIONS ON GEOSCIENCE REMOTE SENSING. Since January 2011, he has been an Associate Editor of the journal *EGU Atmospheric Measurements Techniques*. He is a Fellow of the U.K. Royal Meteorological Society and a member of the MWI-ICI Science Advisory Group of EuMetSat and PMM Science Team of NASA.

Mario Montopoli received the Laurea degree in electronic engineering from the University of L'Aquila, L'Aquila, Italy, in 2004 and the Ph.D. degree in radar meteorology, under a joint program, from the University of Basilicata, Potenza, Italy, and Sapienza University of Rome, Rome, Italy, in 2008.

In 2005, he joined the CETEMPS Center of Excellence, University of L'Aquila, as a Research Scientist on ground-based radar meteorology and microwave remote sensing. In 2006, he was a Research Assistant with the Department of Electrical Engineering and Information, University of L'Aquila. From October 2011 to 2013, he was with the Department of Geography, University of Cambridge, Cambridge, U.K., under the Marie Curie FP7 European program. He is currently with the Department of Information Engineering, Sapienza University of Rome and a EuMetSat Visiting Scientist with the H-SAF facility.

Costanza Bonadonna received the B.S. degree in geology from the University of Pisa, Pisa, Italy, and the Ph.D. degree from the University of Bristol, Bristol, U.K.

She was then awarded the position of SOEST Young Investigator at the University of Hawaii, Honolulu, HI, USA, for two years and was later appointed the position of Assistant Professor at the University of South Florida, Tampa, FL, USA. She is now an Associate Professor with the Section of Earth Sciences of the Faculty of Sciences, University of Geneva, Geneva, Switzerland, and the Head of the CERG-C Program for the Assessment and Management of Geological and Climate related risk. She has devoted most of her research to modeling sedimentation from volcanic plumes, exploring new methodologies for the characterization of tephra-fall deposits, and developing probabilistic analyses for the assessment of tephra-fall hazards. She is now also involved in several multidisciplinary projects for the quantification of risk.

Professor Bonadonna was a recipient of the President's Award of the Geological Society of London (2001), the IAVCEI Outstanding Recent Graduate (2004), the Outstanding Woman in Science Award of the Geological Society of America (2004), and the USF Outstanding Faculty Research Achievement Award (2005).

Retrieval of Tephra Size Spectra and Mass Flow Rate From C-Band Radar During the 2010 Eyjafjallajökull Eruption, Iceland

Luigi Mereu, Frank S. Marzano, *Senior Member, IEEE*, Mario Montopoli, and Costanza Bonadonna

***Abstract*—The eruption of the Eyjafjallajökull volcano in April–May 2010 was continuously monitored by the Keflavík C-band weather radar. The Keflavík radar is located at a distance of about 156 km from the volcano vent, and it has sensitivity of about −5 dBZ at 2-km range resolution over the volcanic area. The time series of radar volume data, which was available every 5 min, is quantitatively analyzed by using the Volcanic Ash Radar Retrieval (VARR) technique. The latter is a physically based methodology that is applied to estimate ash-fall rate and mass concentration within each radar volume. The VARR methodology is here extended, with respect to the previous formulation, to provide an approximate estimate of both mean particle diameter and airborne tephra particle size distribution under some assumptions. Deposited tephra at ground is also extrapolated together with an estimate of the magma mass flow rate (MFR) at the volcano vent, derived from the implementation of the mass continuity equation in the radar reference system. The VARR-based retrievals are compared with those derived from a direct tephra sampling at the ground, experimentally carried out in terms of ash grain size and loading during the Eyjafjallajökull eruption activity on May 5–7, 2010. VARR-based particle diameter estimates may suggest that a sorting of airborne particles during the downwind transport is taking place together with aggregation processes during the ash fall. VARR-derived daily ash mass loadings in the period between April 14 and May 10 are also evaluated with respect to integrated ground and model-based data in the Eyjafjallajökull area. VARR-retrieved MFRs are finally compared with corresponding values obtained from analytical 1-D eruption models, using radar-estimated plume height and radio-sounding wind fields. A fairly good agreement is obtained, thus opening the exploitation of weather radar retrievals for volcanic eruption quantitative studies and ash dispersion model initialization.**

***Index Terms*—Radar data, tephra, volcanic eruption.**

Manuscript received June 21, 2014; revised December 22, 2014 and March 8, 2015; accepted April 8, 2015. This work was supported in part by the Marie Curie Fellowship within the call FP7-POPLE-2010-IEF under Grant 273666 and in part by the FP7 project FUTUREVOLC "A European volcanological supersite in Iceland: A monitoring system and network for the future" under Grant 308377. The work of C. Bonadonna was supported by a Fond National Suisse project (200020-125024).

L. Mereu, F. S. Marzano, and M. Montopoli are with the Dipartimento di Ingegneria dell'Informazione (DIET), Sapienza Università di Roma, 00184 Rome, Italy, and also with the CETEMPS Center of Excellence, Università dell'Aquila, 67100 L'Aquila, Italy (e-mail: mereu@diet.uniroma1.it; marzano@diet.uniroma1.it; frank.marzano@uniroma1.it; montopoli@diet.uniroma1.it).

C. Bonadonna is with the Section des Sciences de la Terre et de l'Environnement, Université de Genève, 1205 Genève, Switzerland (e-mail: Costanza.Bonadonna@unige.ch).

Color versions of one or more of the figures in this paper are available online at http://ieeexplore.ieee.org.

Digital Object Identifier 10.1109/TGRS.2015.2427032

I. Introduction

THE explosive eruption at the summit of subglacial Eyjafjallajökull volcano in 2010 was of modest size, but ash was widely dispersed over Iceland and Europe [31]. The Eyjafjallajökull pulsating explosive activity started on April 14 and ended on May 22 with a volcanic eruption index of about 3, which was estimated on the basis of the maximum volume discharge, and a total tephra volume of about 0.01–0.1 km^3 [8], [30]. The combination of prolonged and sustained ejection of volcanic ash and persistent northwesterly winds resulted in the dispersal of the volcanic cloud over a large part of Europe [2], [22].

Tephra dispersal from an explosive eruption is a function of multiple factors, including magma mass flow rate (MFR), degree of magma fragmentation, vent geometry, plume height, particle size distribution (PSD), wind direction, and its velocity [4], [25], [26]. Volcanologists are used to characterizing the volume and explosivity of the volcanic eruptions through the analysis of tephra distribution. This is because tephra deposits retain a large amount of important information related to the dynamics and physical parameters of the associated volcanic eruptions [29]. One of the most important geophysical parameters, derivable from the analysis of tephra deposits, is the erupted mass, which is essential for the source characterization and assessment of the associated hazards [5]. MFR can then be derived by dividing the erupted mass by the eruption duration (if known) or based on empirical and analytical relations with plume height (e.g., [7], [21], and [33]).

By combining data from ground surveys and remote sensing measurements, it is possible to gain more insights into tephra dispersal [6]. In particular, multispectral visible and infrared observations from both low-Earth orbit and geosynchronous Earth orbit satellites can provide estimates of dispersed fine ash, particularly over the ocean at hundreds of kilometers far away from the vent [31]. However, contamination by water clouds, water vapor variability, and low sensitivity to particles larger than 10 microns are still open issues for quantitative retrieval [28].

Microwave radars can be exploited to extract tephra spatial–temporal distribution in proximity of the volcano vent [10], [12], [16]. Radar technology is well established and can nowadays provide fast 3-D scanning antennas together with Doppler and dual polarization capabilities [19], [32]. The sensitivity of microwave radar measurements depends on the distance between the radar antenna and the target, the transmitter central wavelength, receiver minimum detachable power, and the

resolution volume [24]. Previous studies have shown that coarse ash grain sizes larger than 100 microns can be detected by C-band radars at few hundreds of kilometers with a spatial resolution of a few kilometers [19]. The quantitative interpretation of the detected ash signal was investigated in [13] and [14], where the Volcanic Ash Radar Retrieval (VARR) physically based technique was introduced.

The aim of this paper is to analyze C-band radar data for the Eyjafjallajökull eruption in April–May 2010 to estimate the airborne tephra characteristics and to compare the radar-based retrievals with those obtained from direct tephra sampling at ground carried out during the Eyjafjallajökull volcanic activity [2], [8]. These ground-based measurements were taken by using conventional *a posteriori* techniques: 1) studying stratigraphic sections and collecting ground samples of the tephra deposit to estimate ash loading in a given set of points [8]); and 2) collecting tephra using dedicated ash trays together with mechanical sieving and laser diffraction for estimating accumulation rate and ash size distribution in a given set of locations [2]. Although satellite-based ash loading estimates are available, the latter cannot be considered *in situ* data and, among other problems, are affected by an inherent saturation in the areas close to the vent, thus limiting the sensitivity to finer ash particles (smaller than about 10 μm) [27].

The radar data we used are those of the Keflavík C-band weather radar with time and range spatial sampling of 5 min and 2 km, respectively, located at a distance of about 156 km from the volcano vent and operated by the Icelandic Meteorological Office (IMO) [17]. The VARR technique has been applied to give an estimation of the tephra particle category, ash-fall rate, and mass concentration together with the airborne PSD, as already applied in a previous detailed intercomparison for the Grimsvötn volcanic eruption observed in 2004 [18]. The objective of this work is to assess the VARR estimates for the 2010 Eyjafjallajökull eruption by providing a further analysis of PSD parametric retrieval close to the eruption source and to provide an evaluation of the MFR from radar-based measurements above the volcanic vent.

This paper is organized as follows. Section II provides an overview of the available data in terms of ground deposits and radar measurements. VARR is briefly summarized in Section III, where an extension to the estimate of PSD, mean diameter, and MFR is proposed. Section IV is dedicated to the intercomparison of available ash measurements at ground in terms of PSD, MFR, and ash loading. Conclusions are drawn in Section V.

II. Available Data

During an explosive volcanic eruption, a mixture of ash and gas (so-called volcanic plume) rises into the atmosphere, first due to momentum and then to buoyancy. If the speed of the surrounding wind is larger to the vertical plume speed, the volcanic plume is bent downwind and starts spreading horizontally when it reaches the neutral buoyancy level [26].

The 2010 eruption of the Icelandic Eyjafjallajökull volcano was characterized by a long-lasting bent-over plume that injected a large amount of ash into the atmosphere [23]. The downwind plume was observed from several satellites, which followed its transport as it crossed the European airspace. The ash reached a maximal altitude of 10 km above sea level due to the strong wind modulating the plume elevation and advecting it eastward [2], [6], [22].

Fig. 1. Ash plume of the Eyjafjallajökull volcano and cloud seen during an observation flight on May 13, 2010. The eruption plume is gray and heading southeast. The height is mainly 6 km but has reached up to ∼9 km. Wind is calm over the eruption site and unstable air south of it, which does affect the height of the ash cloud. Ash fall has been reported since six o'clock this morning from various farms in the vicinity; the ash is somewhat finer today than yesterday. These observations are based on a status report issued collectively by the IMO and the Institute of Earth Sciences at 16:00 UTC. Flight over Eyjafjallajökull 13th May 2010, 19:45 UTC. Credits: Photo by Árni Sigurðsson, http://en.vedur.is/earthquakes-and-volcanism/articles/nr/1884.

The ash plume development in time is typically characterized by a lowering of the cloud top with increasing distance from the volcano, as shown in Fig. 1. The latter shows the ash plume about 30 km southwestward with respect to the Eyjafjallajökull vent, pictured during an observation flight on May 13, 2010 at 19:45 UTC. The plume height at that time was between 5 and 7 km with the plume top hitting a stable layer in the atmosphere. The ash cloud drifted away in spatially stable long waves.

When volcanic plumes develop in strong wind fields, their MFR cannot be determined based only on plume height as their height is significantly affected by entrainment due to wind shear [7], [33]. Direct observations and experimental studies have shown that most particles with a diameter of less than 125 μm fall as aggregates of various types, according to the amount of liquid involved [25]. Particle aggregation has been also observed during the 2010 Eyjafjallajökull eruption [2], [27]. In the following sections, the *in situ* specifications and the radar retrieval methods for the 2010 Eyjafjallajökull events are summarized.

A. In Situ Measurements

Two sets of ash-fall measurements are here considered: 1) proximal sampling, where the tephra samples are collected up to 56 km from the vent [2]; and 2) distal sampling, where the tephra samples are collected by a systematic survey within a wide area comprising Iceland and the North Atlantic [8].

Proximal samplings are described by Bonadonna *et al.* in [2]. Three sampling methodologies are followed: 1) collecting tephra in dedicated trays to determine PSD and accumulation

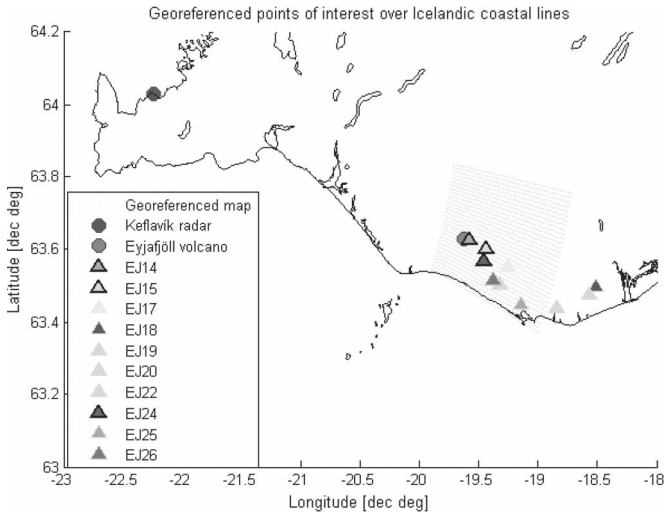

Fig. 2. Ground reference sampling sites are coded as "EJn" for the nth site and indicated by symbols (Δ). Black lines highlight the ground sites used in this study (EJ14, EJ15, and EJ24). Also the site EJ22 was considered in this study, although not providing useful data for our analysis. The georeferenced Keflavík radar grid points, within the ground reference area of experimental sites, are superimposed by cyan dots ($\cdot$). The Eyjafjallajökull volcano and the Keflavík radar location are indicated by (•) and (•), respectively.

rate; 2) collecting volcanic particles and aggregates while they were falling to characterize their properties in terms of size, shape, and surface features; and 3) carrying out vertically pointing X-band Doppler radar measurements of near-surface settling velocities (using the PLUDIX instrument).

Both eruptive and atmospheric conditions were relatively constant during the whole sampling period (i.e. 4-8 May 2010), allowing the direct tephra sampling in ten locations, close to the vent, distributed between 2 and 56 km from it in the east and southeast sectors. Fig. 2 shows the relative positions of the ten experimental sites (hereinafter named "EJn" with n as the site number) with respect to the volcano and the Keflavík radar location. Only three out of ten experimental sites are considered in this study because of their temporal matching with the radar acquisitions and because of their visibility to the lowest radar rays that were not blocked by the surrounding topography.

Table I lists, for each of the three considered experimental sites, the location coordinates, the collection time, and some of the tephra deposit features. In particular, the tephra deposit features [2]. The tephra accumulation over 30 minutes and accumulation rateat the locations within $\sim$ 21km from the vent vary between 0.01 and 1.26 kg $\cdot$ m^{-2} and between $\sim 5 \cdot 10^{-6}$ and $\sim 7 \cdot 10^{-4}$ kg $\cdot$ m$^{-2} \cdot$ s^{-1}, respectively [2]. The highest tephra accumulation rates were recorded close to the vent. Beyond 20 km, accumulation rates were found to range between about 10^{-2} and 10^{-4} kg $\cdot$ m$^{-2} \cdot$ s^{-1}.

In contrast to the proximal sampling data set we just discussed, the data set collected in distal area is referred to as a systematic survey within a wide area comprising Iceland, the Atlantic Ocean, and the European continental regions. Distal sampling was carried out combining data from ground surveys and remote sensing tools, as described by Gudmundsson *et al.* in [8]. As already mentioned, the combination of prolonged and sustained ejection of volcanic ash and persistent northwesterly winds resulted in significant particle dispersion over a large part of Europe, although concentrations were everywhere quite low.

TABLE I
SUMMARY OF COLLECTION AND DEPOSIT CHARACTERISTICS OF ALL SAMPLES ANALYZED, EXTRACTED FROM [2], FOR THE LISTED SITES (EJ14, EJ15, AND EJ24) DURING A SPECIFIC TIME INTERVAL. THE LAST THREE ROWS ARE REFERRED TO ESTIMATES OF TOTAL ASH CONCENTRATION C_a, SURFACE DEPOSIT LOADING L_a, AND FALL RATE R_a FOR THE CORRESPONDING SITE AND INTERVAL AS DERIVED FROM C-BAND VARR ALGORITHM, USING THE KL VELOCITY-DIAMETER MODEL. ($\phi = -\log_2$ D, WHERE D IS THE PARTICLE DIAMETER IN MILLIMETERS)

		Measuring sites		
Features	**Units**	**Sample EJ14**	**Sample EJ15**	**Sample EJ24**
Longitude	[decimal deg]	-19.5811	-19.4376	-19.4536
Latitude	[deg]	63.62738	63.60145	63.56872
Elevation [m]	[m]	1414	835	521
Distance from vent	[km]	2	9.6	10.7
Collection date	[dd/mm/yyyy]	05/05/2010	05/05/2010	07/05/2010
Collection time	[hh/mm]	17:39-17:49	19:00-20:36	15:35-16:20
Total mass/area	[kg/m^2]	0.42	0.68	0.29
Accumulation rate	[kg/m^{2}s]	$6.98 \cdot 10^{-4}$	$1.19 \cdot 10^{-4}$	$1.07 \cdot 10^{-4}$
Median particle diameter	[mm (ϕ)]	1.87 (-0.9)	0.62 (0.7)	0.41 (1.3)
30-min mass/area	[kg/m^2]	1.26	0.21	0.19
***Average* C_a (VARR-KL)**	[kg/m^3]	$2.08 \cdot 10^{-3}$	$6.02 \cdot 10^{-4}$	$3.71 \cdot 10^{-4}$
***Average* L_a (VARR-KL)**	[kg/m^2]	5.78	7.76	1.11
***Average* R_a (VARR-KL)**	[kg/(m$^2 \cdot$ s)]	$1.01 \cdot 10^{-2}$	$2.97 \cdot 10^{-3}$	$1.70 \cdot 10^{-3}$

Field observations in the region within 10 km from the vent in the summers of 2010 and 2011 and individual grain size analyses indicate that during the first period, the produced tephra was coarser with a reduced percentage of very fine ash. During the second period of analysis, the tephra was sampled in a systematic manner with a number of traps around the volcano. The results in this second period, in terms of grain size and during the most intense explosive phase of April 2010 at distance of 10–15 km from the vent, indicate that about 35%–50% of the ash was finer than 63 μm, whereas 10%–30% was finer than 30 μm [8].

B. Weather Radar Observations

Meteorological microwave radars can be used to quantitatively estimate the geophysical properties of a volcanic ash cloud, as successfully demonstrated in the last decade [12], [14], [18]. Under the assumption of Rayleigh scattering, the copolar horizontally polarized reflectivity factor Z_H (mm$^6 \cdot$ m^{-3}), very often expressed in decibels (dBZ) and hereinafter also referred to as reflectivity, is related to the size distribution of ash particle polydispersion by [24]

$$Z_H(r,\theta,\varphi) = \int_{D_1}^{D_2} D^6 N_a(D) dD \qquad (1)$$

where D(mm) is the equivolume spherical particle diameter, and $N_a(D)$ is the PSD (m$^{-3} \cdot$ mm^{-1}) with D_1 and D_2 as the expected minimum and maximum particle diameter. The quantity ϕ is defined as $\phi = -\log_2 D$, and it is usually preferred to D in geology.

The Rayleigh approximation (i.e., wavelength $\gg D$) used to derive (1) is not always valid, particularly at wavelengths shorter than the C-band (i.e.,. wavelength less than 5 cm). In these cases, the particle Mie backscattering effects need to be taken into consideration depending on the ash cloud formation and the radar wavelength [13], [15]. However, an equivalent Rayleigh reflectivity Z_H is usually defined. It is a function

of the radar-received power, and it has sensitivity to ash size and concentration, which mainly depends on the transmitted wavelength, receiver minimum detectable signal, range (the received power is inversely proportional to square range), and antenna beamwidth [24].

Previous numerical analyses have shown that intense concentration of fine ash (about 5 g/m^3 of average diameter of 0.01 mm) cannot be detected by a C-band radar [14]. This means that the Keflavík radar measurements can be used to detect light to intense concentration of coarse ash and any lapilli distribution, i.e., particles with average diameters larger than 0.1 and 1 mm, respectively. Thus, microwave radar signatures refer to near-source plume depending on the sedimentation and settling of coarse ash and lapilli. Indeed, fine ash may represent few percentage of the total tephra and can be transported far from the volcano vent [26]. Moreover, the radar observation geometry inevitably produces occluded regions at longer ranges and in the presence of obstacles.

The sampling size along the radial directions (Δr) is proportional to the pulse duration (order of microseconds), whereas its transverse spacing quadratically increases with the target range (r). Thus, for a given antenna elevation angle, the radar sampling volume (ΔV) increases with distance from the radar as $\Delta V \approx (\pi/4) \cdot r^2 \cdot \Delta\theta \cdot \Delta\varphi \cdot \Delta r$. This has a dual-range effect: 1) to increase the probability of intercepting undesired ground targets by the radar sampling volumes; and 2) to have the sampling volumes not uniformly filled producing an ambiguous reduction of Z_H [24]. For example, for the Keflavík radar, at a distance of 155 km from the radar, the transverse section of the sampling volume, i.e., ΔV, is about 4.2 km^3 (i.e., 2 km in range and 2.1 km in azimuth). Another aspect of ash detection is the issue related to the discrimination between ash and hydrometeors and the identification of ash-water aggregates. The former can be theoretically tackled investigating the time evolution of the radar acquisitions, whereas the latter seems, at the current knowledge, beyond the capabilities of single-polarization weather radar, and it should be treated as an ambiguity (uncertainty) affecting the qualitative and quantitative interpretation of the radar imagery of ash clouds [18], [19].

The main specifications of the C-band (5.6 GHz) weather radar in Keflavík are: 5-min time sampling; antenna elevation angles: 0.5°, 0.9°, 1.3°, 2.4°, 3.5°, 4.5°, 6.0°, 8.0°, 10.0°, and 15.0°; azimuth spacing: 0.86°; range spacing 2 km (after a radial averaging) minimum detectable reflectivity signal: -5 dBZ (after radial averaging), at the Eyjafjallajökull position. The radar system is operated by IMO, and a detailed description is found in [12] and [16]. The Eyjafjallajökull eruption was observed by Keflavík radar, 155 km northwest far away from the Eyjafjallajökull volcano from 00:10 UTC on May 5, 2010 until 23:55 UTC on May 10, 2010. The complete radar data set consists of a total of 3730 polar volumes in spherical coordinates, where each volume consists of a matrix having 420 rows (azimuth angles) and 120 columns (range bins).

Being aware of the previous *caveats* when quantitatively interpreting radar data, the three sampling locations, which are identified as EJ14, EJ15, and EJ24, respectively, 2, 9.6, and 10.7 km away from the volcano vent have been analyzed (see Table I and Fig. 2). These sites are those where the beam occlusion effects are almost negligible, and the lowest radar bin is relatively close to the surface. As a matter of fact, by increasing the distance of the EJn site with respect to the Eyjafjallajökull volcano, the radar sampling altitude considerably increases, as shown in Fig. 3. The minimum altitude between the top of the Eyjafjallajökull volcano and the lowest radar ray is 2.5 km when considering radar ray bending in a standard atmosphere [24].

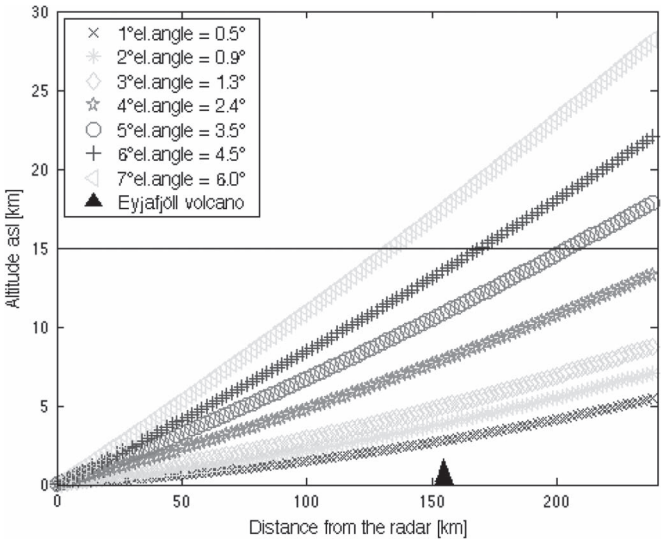

Fig. 3. Altitude of the radar antenna boresight beam simulated within a standard atmosphere for different radar elevation angles, as listed in the figure's legend. The position of the Eyjafjallajökull volcano is shown by a black triangle, whereas the Keflavík radar is set in the origin of the figure.

In the case of the 2010 Eyjafjallajökull event, the observed temporal sequence of radar imagery indicates a distinct ash feature erupted from the volcano vent, which can be effectively detected, as already documented in [17]. An example of the radar vertical profiles [range height indicator (RHI)] of Z_H is shown in Fig. 4 during four instants of the volcanic activity on May 5, as specified in each panel title. The position of the ground sampling sites EJn is also highlighted in each panel by a red box. From this figure, we can derive an average horizontal and vertical extension of the plume on the order of 10 and 6 km, respectively. For the reasons mentioned above, this is a partial three-dimension perspective of the ongoing event. In the same figure, we can note the absence of the radar-detected ash plume in correspondence of EJ22 and EJ24 sites. The latter sites clearly show a measured signature at ground; this discrepancy may probably be due to the radar beam partial occlusion and also to the selected azimuth direction.

To complete the radar standpoint, Fig. 5 shows the ground projection [called the plan position indicator (PPI)] of the radar reflectivity Z_H conical sampled area at the lowest antenna elevation angle. These maps are georeferenced and are enlarged around the volcano vent within an area of about 110 km^2. They clearly show the predominant downwind plume southeast direction with the progressive attenuation of the reflectivity as the end of the sequence is approaching. Fig. 5 confirms that the ash plume is not detected above the site EJ22 at 20.6 km from the vent, but it is present above the site EJ24.

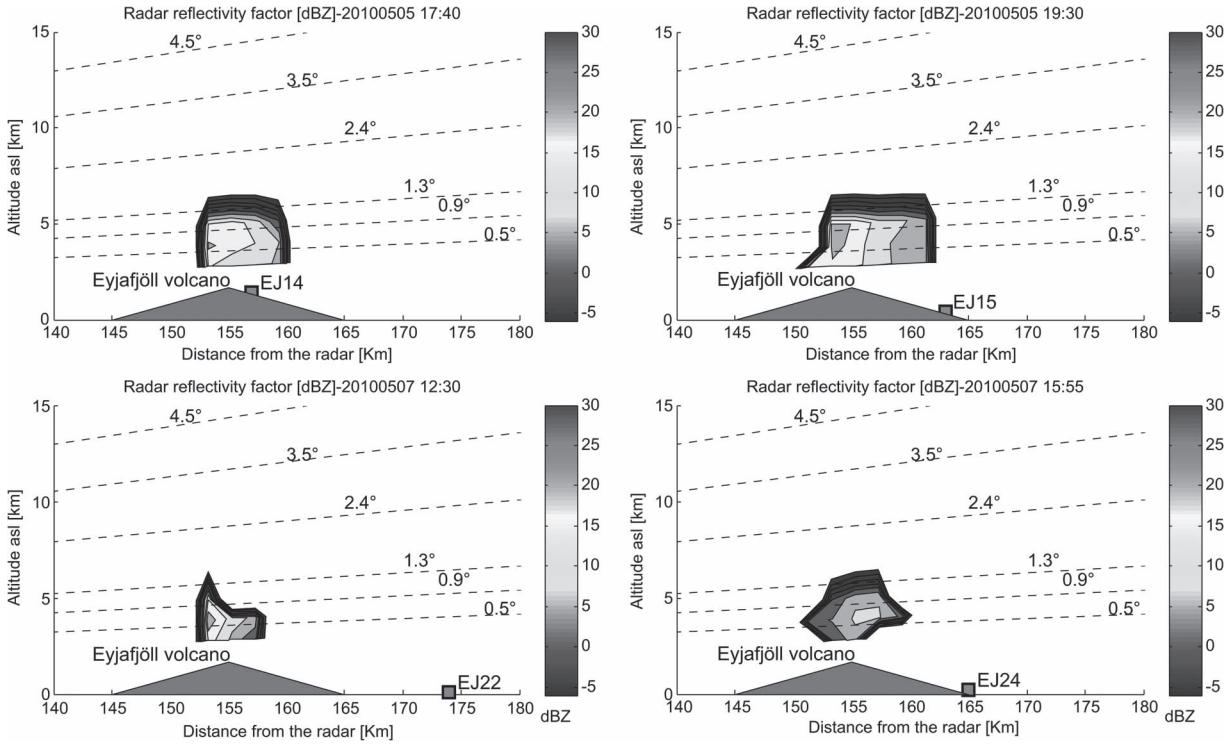

Fig. 4. Radar RHI images of radar reflectivity Z_{H} along the radar-EJn line of sight at 17:40 UTC on May 5, 2010 (EJ14), at 19:30 UTC on May 5, 2010 (EJ15), at 12:30 UTC on May 7, 2010 (EJ22), and at 15:55 UTC on 72010 (EJ24). See Fig. 1 and Table I for details on the EJn sites.

III. VARR

In the following sections, quantitative definitions and a physical parameterization of volcanic ash clouds will be briefly introduced, together with some radar reflectivity modeling issues (details can be found in [13] and [14]). Note that we will limit our attention to the single-polarization amplitude radar observables due to the characteristics of the Keflavík radar, although polarimetric signatures can be included as well when they are available [19], [35].

A. Tephra Particle Parameterization

From (1), which describes the radar reflectivity factor under the Rayleigh assumption, it is clear as it includes the information on the ash particle size and its distribution. In particular, the weighted integrals of the ash size distribution, i.e., N_a, is able to explain all quantities of our interest: ash mass concentration (C_a), ash-fall rate (R_a), and number-weighted mean diameter (D_n). When N_a assumes a form of Gamma or Weibull distribution, the weighted integrals are easily calculated in a closed form as moments of N_a of k-th order [13]. Thus, among others, it is convenient choosing some of these distribution shapes. In addition, past studies have also demonstrated, using experimental data, that their assumption is a reasonable choice [9], [13], [15].

In this paper, the ash particle distribution, i.e., N_a $(\mathrm{mm}^{-1}\mathrm{m}^{-3})$, is assumed to behave as a scaled gamma, which assumes the following form:

$$N_a(D) = N_n \left(\frac{D}{D_n}\right)^{\mu} e^{-(\mu+1)\left(\frac{D}{D_n}\right)} \tag{2}$$

where D_n, N_n, and μ are the number-weighted mean diameter in millimeters, the intercept parameter in $(\mathrm{mm}^{-1}\mathrm{m}^{-3})$, and the unitless shape factor, respectively. Thus, from (2), the ash mass concentration and the ash-fall rate, respectively, indicated by C_a in $(\mathrm{g}\cdot\mathrm{m}^{-3})$ and R_a in $(\mathrm{kg}\cdot\mathrm{m}^{-2}\cdot\mathrm{h}^{-1})$, can be expressed by

$$C_a = 10^{-9}\int_{D_1}^{D_2} m_a(D)N_a(D)dD = \frac{\pi}{6}\rho_a E_3 \tag{3}$$

$$R_a = 3.6\cdot 10^{-9}\int_{D_1}^{D_2} v_a(D)m_a(D)N_a(D)dD = \frac{\pi}{6}v_a\rho_a E_{(3+b_v)}. \tag{4}$$

In (3) and (4), $m_a = \rho_a(\pi/6)\cdot D^3$ is the ash mass of the particle's equivalent sphere, and ρ_a is the ash density in $(\mathrm{g}\cdot\mathrm{m}^{-3})$. In (4), the particle's terminal velocity (v_a) in $(\mathrm{m}\cdot\mathrm{s}^{-1})$ is assumed to follow a power law as $v_a(D) = a_v D^{bv}$ with a_v and b_v empirical coefficients. The coefficients are chosen from a regression analysis of past experiments of previous eruptions (see [2], [10], [11], and [34]). Four different models have been extracted from those proposed in the literature: 1) Wilson's model (1972) [34], which refers to ash plume heights between 5 and 10 km above the ground; 2) Harris and Rose's models, respectively, of 1980 (Mt. St. Helens; May 18, 1980) and 1982 (Mt. St. Helens; March 19, 1982) [10]; and 3) Kunii and Levenspiel's (KL) model (1969), considering an ash density of $1500\cdot\mathrm{kg}\cdot\mathrm{m}^{-3}$ [3], [11] (see Section III-B). The methods in 1) and 2) are derived from a parametric regression analysis [14], whereas the KL model is physically based and depends

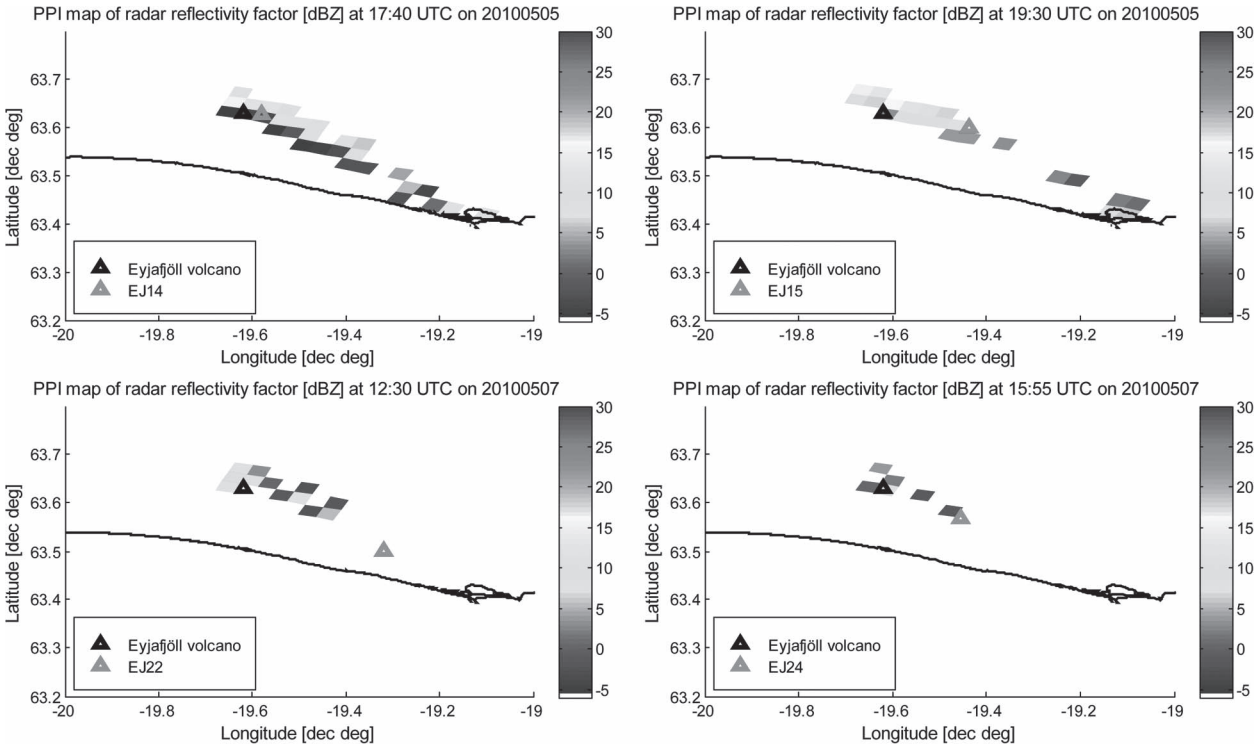

Fig. 5. Radar PPI images of radar reflectivity Z_H, corresponding to RHI and EJ sites of Fig. 4 (EJ14 on the top left, EJ15 on the top right, EJ22 on the bottom left, and EJ24 on the bottom right).

on ambient parameters so that it is taken as a reference in this work.

Fig. 6 shows the modeled curves for $v_a(D)$ for various sets of a_v and b_v parameters, as listed in the legend. The velocity-diameter models may significantly differ for larger diameters, even doubling the velocity itself for a given particle size. In this paper, we have used, as a primary choice, the Kunii–Levenspiel (KL) model parameters, described in [11] and applied to the 2010 Eyjafjallajökull event. It is worth noting that one of the main issues in considering the particle's terminal fall velocity is that the airborne ash-fall velocity cannot be directly measured so that we can take the literature models as a set of possible plume scenarios to take into account the fall velocity uncertainty.

B. VARR Methodology

The VARR attempts to extract some quantitative information from radar data of volcanic clouds, making use of forward model electromagnetic simulations of the radar signal as a function of various possible ash scenarios. The VARR methodology is extensively described in detail in previous works by Marzano *et al.* [14]–[16]. In this paper, we give the elements useful for the VARR implementation without going into the details of the algorithms. VARR outputs, in its default configuration, are estimates of the ash mass concentration C_a $(\mathrm{g}\cdot\mathrm{m}^{-3})$, and the ash-fall rate, R_a $(\mathrm{kg}\cdot\mathrm{m}^{-2}\cdot\mathrm{h}^{-1})$. These quantities are related to the measured radar reflectivity Z_{Hm} $(\mathrm{mm}^6\cdot\mathrm{m}^{-3})$ through power law coefficients c_c, d_c, a_c, and b_c as follows:

$$\begin{cases}\hat{C}_a^{(c)} = a_c Z_{H_m}^{b_c} \\ \hat{R}_a^{(c)} = c_c Z_{H_m}^{d_c}\end{cases} \tag{5}$$

where the symbol "c" is used as the apex, and the subscript in (5) indicates a particular ash scenario also called ash class.

The ash classes are fixed in VARR and stored as lookup tables. They basically include parameter variations of the ash size distribution, N_a, in (2), i.e., D_n, N_n and μ in a prescribed and consistent way. From $N_a(D)$, Z_H, C_a, and R_a are calculated using (1), (3), and (4). Thus, we identified $N_c = 12$ classes of ash scenarios (3 size by 3 mass concentration classes). In each class, D_n and N_n follow a Gaussian random distribution, whereas μ is fixed. The defined classes are labeled as fine, coarse ash, and lapilli further partitioned into light, moderate, and intense mass concentration regimes. Thus, for each of the aforementioned classes, we have average values of particle diameters $\langle D_n\rangle$ equal to 0.01, 0.1, and 1.0 mm for fine, coarse, and lapilli ash classes, respectively, with a standard deviation $\sigma_{Dn} = 0.2\langle D_n\rangle$ and ash mass concentration with mean values $\langle C_a\rangle$ equal to 0.1, 1, and 5 $\mathrm{g}\cdot\mathrm{m}^{-3}$ for light, moderate, and intense concentration regimes, respectively, and a standard deviation $\sigma_{\mathrm{Ca}} = 0.5\langle C_a\rangle$.

The ash density ρ_a is assumed equal to an average value of $1500\cdot\mathrm{kg}\cdot\mathrm{m}^{-3}$, according to the ash particle andesitic density model of Bonadonna and Phillips [3] considering a particle diameter of 0.1 mm, and the PSD shape parameter μ has been set to 0.9, 1.1, and 1.4 for fine ash, coarse ash, and lapilli particles, respectively. Note that the choice of the ash density is consistent with Eyajafjallajokull data and the goal of estimating airborne PSD from radar observations [2], [3].

The ash classes are identified as minimizing the distance between the radar measured quantities (i.e., the radar reflectivity, Z_H, in our case) and the expected radar signatures of

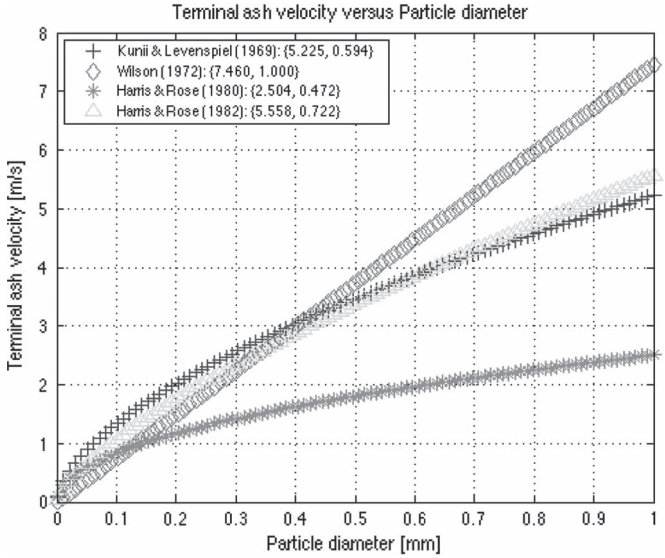

Fig. 6. Parameterized power law models ($v_a(D) = a_v \mathrm{D}^{b_v}$) for the ash terminal velocity [2], [10], [11], [34]. The values a_v and b_v for each model are listed in the panel's legend.

ash for each class. In VARR, this is performed in a probabilistic framework using the maximum *a posteriori* probability criterion. Each ash class is characterized by some members in terms of radar variables, which are distributed with a Gaussian probability density distribution. Thus, the minimization process to assign a class "cth" to the measured reflectivity factor ZHm requires the maximization of the conditional probability $p(c|ZHm)$. It can be demonstrated that this reduces to the minimization of a quadratic form characterized by 1) $m_Z^{(c)}$ and $\sigma_Z^{(c)}$, which are the mean and standard deviation of the simulated reflectivity for class "c," and 2) $p(c)$, which is the *a priori* probability of existence of class c.

C. Estimate of Ash PSD, Loading, and MFR

Here, we wish to extend the VARR outputs including the estimation of the mean diameter, mass loading, and MFR. Within the usual approximation of Rayleigh backscattering and assuming the scaled gamma distribution for N_a as in (2), it can be easily demonstrated as Z_H in (1) can be expressed as

$$Z_{H_m}^{(c)} = f_z(\mu^c)\frac{D_n^3}{\rho_a}\hat{C}_a^{(c)} \tag{6}$$

which yields

$$D_n = \sqrt[3]{\frac{\rho_a Z_{H_m}^{(c)}}{\hat{c}_a^{(c)} f_z\left(\mu^{(c)}\right)}}. \tag{7}$$

In (6) and (7), D_n, Z_{Hm}, C_a, and ρ_a are in millimeters; $(\mathrm{mm}^6 \cdot \mathrm{m}^{-3})$, $(\mathrm{g} \cdot \mathrm{m}^{-3})$, and $(\mathrm{g} \cdot \mathrm{m}^{-3})$, respectively, whereas the shape factor of the ash size distribution in (2), i.e., $\mu^{(c)}$, is unitless. The latter is fixed for each cth class in the current version of VARR. The term f_Z is

$$f_z\left(\mu^{(c)}\right) = \frac{6 \cdot 10^6 \Gamma\left(\mu^{(c)}+7\right)}{\pi\left(\mu^{(c)}+1\right)^3 \Gamma\left(\mu^{(c)}+3\right)} \tag{8}$$

where Γ completes the gamma function, and it holds that $\Gamma(n+1) = n!$ if n is an integer. Once $D_n^{(c)}$ and $\mu^{(c)}$ are known, the parameter $N_n^{(c)}$ of the ash size distribution is derived from [16], as follows:

$$N_n^{(c)} = 10^6 \frac{6\hat{c}_a^{(c)}\left(\mu^{(c)}+1\right)^{\mu^{(c)}+4}}{\pi\rho_a\left(\hat{D}_n^{(c)}\right)^4 \Gamma\left(\mu^{(c)}+4\right)}. \tag{9}$$

By using (7)–(9), the airborne scale-Gamma PSD of the cth ash class can be calculated using (2). The ash mass loading (L_a) is derived from the ash-fall rate, i.e., R_a $(\mathrm{kg} \cdot \mathrm{m}^{-2} \cdot \mathrm{s}^{-1})$, by its integration over a time interval between t_i and t_f in seconds, i.e.,

$$L_a(x,y) = \int_{t_i}^{t_f} R_a^{(c)}(x,y,t)\,dt. \tag{10}$$

Note that R_a is actually known for each radar sampling volume. To obtain a quantity referred close to the ground, a vertical extrapolation from a given altitude up to the ground level was performed. Thus, we carried out an approximate reconstruction of the vertical profile of reflectivity. These reconstructed values of Z_{Hm} are used in (5) to derive R_a. We are implicitly assuming that the radar observations closer to the ground are indicative of ash fall deposited on the ground from the vertical column above a considered position. Indeed, this assumption might lead to an overestimation of L_a.

The erupted mass (M_a) present in the column above the vent can be retrieved by summing up the ash concentration of all radar bins in the (radar visible) column itself V_C, i.e., at a given time step t. Thus

$$M_a(t) = \int_{V_c} C_a^{(c)}(\mathbf{r},t)dV \cong \sum_{i=1}^{N_{VC}} C_a^{(c)}(\mathbf{r_i},t)\Delta V_i \tag{11}$$

where $\mathbf{r}$ is the position vector, N_{VC} is the number of volume bins within the column above the vent, and ΔV_i are the involved radar sampling volumes. The volume V_C can be arbitrarily chosen to include all of the plume or part of it, depending on the calculations one wants to perform.

The mass flow rate (MFR) is a measure of the temporal rate of mass flow through the volcanic vent. The 3-D radar-based ash concentration estimate, given in (5), around the volcanic vent can be used to provide an approximate quantification of MFR. This can be achieved by trying to solve the continuity equation in the discretized spatial and temporal domain of the radar geometry. The mass continuity, adapted to our case states that time variation of the ash mass within a volume, i.e., V_c, above the volcano vent is equal to the net flux, which diverges out from the volume $(\mathbf{J})$, due to the overall contributions flowing out and in, plus the net accretion of the ash mass

inside the volume due to source-minus-sink terms σ. Thus, in formulas, we can write the differential form of the continuity equation as follows:

$$\frac{\partial c_a(\mathbf{r},t)}{\partial t} = -\nabla \cdot \boldsymbol{J}(\mathbf{r},t) + \sigma(\mathbf{r},t). \tag{12}$$

The term $\mathbf{J}$ is a flux rate of ash mass $(\mathrm{g}\cdot\mathrm{m}^{-2}\cdot\mathrm{s}^{-1})$, C_a is in $(\mathrm{g}\cdot\mathrm{m}^{-3})$, and σ is in $(\mathrm{g}\cdot\mathrm{m}^{-3}\cdot\mathrm{s}^{-1})$. The flux $\mathbf{J}$ can be a positive or a negative term indicating an outcoming or incoming flux rate into volume Vc, respectively. We assume that the incoming contribution of $\mathbf{J}$ (labeled as $\mathbf{f}_R$) is referred only to the ash mass rate produced by the volcano activity, whereas the outcoming contributions (labeled as $\mathbf{a}_R$) are those that move out from V_c due to convection and prevailing winds, i.e.,

$$\boldsymbol{J}(\mathbf{r},t) = \boldsymbol{a}_R(\mathbf{r},t) - \boldsymbol{f}_R(\mathbf{r},t). \tag{13}$$

Our unknown is $\mathbf{f}_R$, whereas $\mathbf{a}_R$ can be calculated once the plume advection velocity field $\mathbf{v}$ in $(\mathrm{m}\cdot\mathrm{s}^{-1})$ is estimated, i.e.,

$$\boldsymbol{a}_R(\mathbf{r},t) = C_a(\mathbf{r},t)\boldsymbol{v}(\mathbf{r},t). \tag{14}$$

Note that in (12), we can take into account possible air entrainment into the plume (which would dilute the ash concentration) and the ash flows into the umbrella cloud region due to local turbulent circulation by modulating the source-minus-sink term σ.

By integrating (12) over the eruption columnar volume V_C above the vent and using the divergence theorem, we obtain the integral form of the continuity equation, i.e.,

$$\int_{V_c} \frac{\partial C_a(\mathbf{r},t)}{\partial t} dV = -\oint_{S_C - S_D} \mathbf{n}_0 \cdot \mathbf{a}_R(\mathbf{r},t) dS + \oint_{S_D} \mathbf{n}_0 \cdot \mathbf{f}_R(\mathbf{r},t) dS + \int_{V_C} \sigma(\mathbf{r},t) dV \tag{15}$$

where $\mathbf{n}_0$ is the normal unit vector belonging to the closed surface S_C surrounding the column volume V_C and pointing outward of it, and S_D is the part of S_C closer to the vent and perpendicular to the vertical line above it. A compact formulation of (15) is obtained by substituting (14) in (15) and defining the following quantities:

$$\begin{aligned} D_R(t) &= \int_{V_C} \frac{\partial C_a(\mathbf{r},t)}{\partial t} dV = \frac{\partial M_a(\mathbf{r},t)}{\partial t} \\ A_R(t) &= \oint_{S_C - S_D} \mathbf{n}_0 \cdot \mathbf{a}_R dS = \oint_{S_C - S_D} C_a(\mathbf{r},t)\left[\mathbf{n}_0 \cdot \boldsymbol{v}(\mathbf{r},t)\right] dS \\ F_R(t) &= \oint_{S_D} \mathbf{n}_0 \cdot \mathbf{f}_R(\mathbf{r},t) dS \\ \sum(t) &= \oint_{V_C} \sigma(\mathbf{r},t) dV \end{aligned} \tag{16}$$

where D_R, A_R, F_R, and Σ are the derivative mass rate, the advection rate, the MRF, and the source–sink rate, respectively, all expressed in $(\mathrm{g}\cdot\mathrm{s}^{-1})$. Thus, (15) can be compacted into

$$D_R(t) = -A_R(t) + F_R(t) + \sum(t). \tag{17}$$

Equation (17) makes possible the estimate of MFR by the estimation of D_R, F_R, and Σ. The implementation of (17) is not straightforward in the radar geometry so that some simplifying assumptions are needed. In the following, we describe how we can practically implement (17). First of all, the source–sink term Σ is put to zero since we assume that there are no sources or sinks in the selected volume V_C. At each radar acquisition t_k, MRF is then given by

$$F_R(t_k) = D_R(t_k) + A_R(t_k) \tag{18a}$$

with

$$\begin{cases} D_R(t_k) \cong \sum\limits_{i=1}^{N_{VC}} \frac{\Delta C_{aik}^{(c)}(t_k)}{\Delta t} \Delta V_i \\ A_R(t_k) \cong \sum\limits_{j=1}^{N_{SO}} C_{ajk}^{(c)}(t_k) v_{nj}(t_k) \Delta S_j \end{cases} \tag{18b}$$

where $t_k(\mathrm{s})$ is the radar time sampling of each volume, ΔV_i (m^3) is the ith incremental radar sampling volume with N_{VC} elements, $\Delta \mathrm{S}_j$ (m^2) is the jth incremental outer surface with N_{SO} elements, and v_{nj} $(\mathrm{m}\cdot\mathrm{s}^{-1})$ is the advection velocity component normal to the jth outer surface element. In general, N_{SO} differs from N_{VC}, which is the number of elements in V_C, because A_R takes into account only the contributions transported out from S_C.

If the 3-D vectorial velocity field $\boldsymbol{v}(\mathbf{r},t)$ of the divergent advection rate A_R is negligible or, in any case, difficult to estimate with a good confidence (particularly if Doppler moments are not available from the radar product set), from (18), we can anyway provide an estimate of the MFR. We can basically suppose that positive contributions of D_R (i.e., a mass increment in volume V_C during the time interval Δt) are due to F_R only. On the contrary, negative mass variations in Δt are likely due to a predominant advection term that tends to move out the ash mass from V_C. In formulas, this means

$$\begin{cases} F_{R_{app}}(t_k) \cong D_R^+(t_k) = \sum\limits_{i=1}^{N_C} \Delta V_i \frac{\Delta C_{aik}^{(c)}(t_k)}{\Delta t} \Big|^+ \\ A_{R_{app}}(t_k) \cong D_R^-(t_k) = \sum\limits_{i=1}^{N_C} \Delta V_i \frac{\Delta C_{aik}^{(c)}(t_k)}{\Delta t} \Big|^- \end{cases} \tag{19}$$

where the right-hand-side terms indicate the positive (negative) time derivative of the ash concentration C_a within each radar volume bin ΔV. The subscript "*app*" indicates an approximate solution. The approximate term F_{Rapp} is our retrieval of MFR when the velocity v is not available. The approximation of MFR in (19) is, indeed, an underestimation since we are assuming that the temporal increase of tephra within the column above the volcanic vent is not taking into account the advective outflow, which tends to subtract ash mass from the column. At the same time, the use of (19) underestimates A_R in (18) as the decrease of tephra can be larger if not considering the contribution of the vent source.

The MFR reconstructed from radar scans, directly probing the tephra column above the volcano vent, can be compared with that derived from simplified 1-D volcanic eruption models [7], [21], [25]. In particular, it is well known that MFR can be related to a power of the plume top height H_{top} [26]. Several

analytical formulas have been proposed in the last decades; more recently, a nonlinear model has been derived including both wind and buoyancy local meteorological conditions at a given instant [7]. Thus

$$F_R(t) = a_0 \left[a_1 H_{top}^4(t) + a_2 H_{top}^3(t) \right] \tag{20}$$

where a_0, a_1, and a_2 are coefficients dependent on the gravitational acceleration, air density, buoyancy frequency, top-hat profile radial entrainment coefficient, wind entrainment coefficient, and wind velocity profile [7].

Intercomparisons between (20) and (18) are of interest for validation of the 1-D model and for consistency check of MFR estimates. For a given time step t, the application of (20) relies on 1) knowledge of the atmospheric conditions close to the volcanic vent at least in terms of vertical profiles, derivable from available radiosondes and/or meteorological numerical forecasts, and 2) the estimate of the maximum plume top height H_{top}, which can be provided by the radar itself on the basis of a detection algorithm [17].

IV. Data Intercomparison

The main task of radar retrieval techniques is to quantify physical parameters of volcanic eruptions in real time to facilitate dispersion model initialization and risk mitigation. However, remote sensing techniques need to be first compared and validated with *in situ* direct measurements, if available [18]. This intercomparison between remote estimates and *in situ* data has some inherent problems: 1) The geometry of radar observations is affected by occlusions so that the effective sampling is well above the ground, unless a vertical profile reconstruction is not carried out as already mentioned; 2) radar retrievals are volume-integrated products within bins of few kilometers, whereas ground data are typically surface point measurements. The previous conditions pose a problem of spatial representativeness, which translates into a discrepancy (error), which is coupled with a temporal representativeness discrepancy due to the different time sampling (e.g., every 5 min for radar versus few seconds for ground collectors and months for ash drills). This implies that the error structure of these intercomparisons is affected by these inherent differences, which cannot be all associated to the inaccuracy of the remote sensors and retrieval algorithms.

It is also worth mentioning that hail formation in volcanic columns may influence mass flux estimations based on radar measurements. These changes in effective grain size lead to an increased ash fall and may affect radar reflectivity [1]. From an electromagnetic point of view, hydrometeor signatures at the C-band may be affected by the Mie resonance effects and by mixture and/or coexistence of particles [15], [16]. Due to the difficulty in quantifying these effects, in the VARR approach, these uncertainties are taken into account by increasing the *a priori* standard deviation added to reflectivity forward model simulations [14].

In the following sections, we will first discuss intercomparison results between radar and ground real-time data for the three selected EJn sites. In Section IV-A, this aspect will be carried out in terms of ash mass loading, ash-fall rate, PSD retrieval, and MFR estimation. Then, a further intercomparison of VARR accumulated retrievals with daily tephra production rates based on ground data and model extrapolation will be discussed in Section IV-B.

A. Results for Real-Time Site Measurements

As shown elsewhere, e.g., in [17], the VARR algorithm successfully provided reasonable estimates of the April and May 2010 events in Iceland. Our attention is here concentrated only on the validation sites EJ14, EJ15, and EJ24, which are shown in Fig. 2. The site EJ22 is not considered in the quantitative analysis since it is very far from the Eyjafjallajökull vent (about 20.6 km), and the Keflavík radar poorly intercepts the ash plume at a height of 4 km above the ground (see Fig. 3). However, it is left among the validation sites in Figs. 7–9, to give an evidence of the sensitivity of the radar estimates.

Fig. 7 shows, in terms of PPI (i.e., constant elevation-angle map; see also Figs. 3 and 5), the spatial distribution of VARR-based estimated ash concentration C_a. It is worth noting that the ash mass is relatively confined around the vent and its proximal area due to the C-band radar sensitivity mainly affected by the distance. This means that some fine ash plume is indeed present but poorly revealed by the radar imagery. Estimated ash concentration reaches values up to 8 $\mathrm{g \cdot m^{-3}}$ on May 5 and 6 $\mathrm{g \cdot m^{-3}}$ on May 7, typically with stronger values around the vent.

Analogously to the previous figure, Figs. 8 and 9 show the estimates of ash-fall rate R_a $(\mathrm{kg \cdot m^{-2} \cdot s^{-1}})$ and ash loading $L_a(\mathrm{kg \cdot m^{-2}})$, respectively. Considerations similar to Fig. 7 can be done in terms of tephra spatial distribution with variability of ash column up to 25 $\mathrm{kg \cdot m^{-2}}$ on May 5 and 7: For R_a, we have registered a maximum value of $9 \cdot 10^{-5}$ and $11 \cdot 10^{-5}$ $\mathrm{kg \cdot m^{-2} \cdot s^{-1}}$, respectively, on May 5 and 7.

In Table I, different ground-collected parameters are shown, including accumulation rate $(\mathrm{kg/m^2 s})$ and mass load $(\mathrm{kg/m^2})$, which can be directly compared with those estimated by the radar-based VARR. The latter can provide values of C_a, R_a, and L_a, which have been obtained using the KL velocity model [11] for the whole collection period of EJn experiments. The radar-estimated values of R_a show levels about one order of magnitude higher than the ground-measured accumulation rate for all sites EJ14, EJ15, and EJ24. The estimated values L_a are about one order of magnitude larger than those measured at ground for EJ14 and EJ15, but only three times higher for EJ24. These differences may be due to the lower sensitivity of weather radar to the airborne tephra content close to the ground (and not deposited on the ground yet) as well as to the different temporal sampling and terminal velocity model.

Indeed, the deposited ash depends on the ash-fall terminal velocity v_a. To test the sensitivity of the ash mass estimation to v_a, we have used four different types of power-law regression coefficients, as shown in Fig. 6, for the evaluation of R_a and L_a. Table II shows these results for the three sites EJ14, EJ15, and EJ24. All four different models, extracted from the available literature, have been used (see Fig. 6). The Harris–Rose 1980 parametric model tends to provide lower radar-based estimates, thus reducing the differences with respect to ground

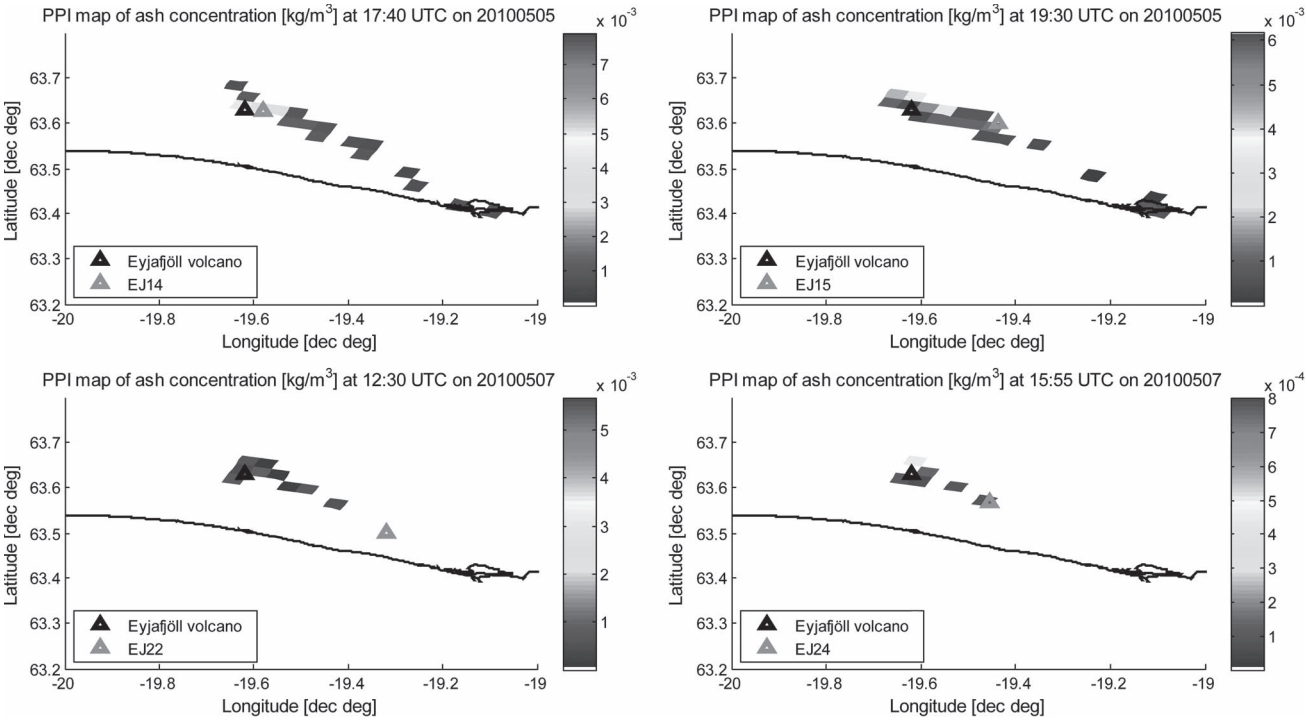

Fig. 7. Radar PPI images of VARR-derived ash concentration C_a, corresponding to RHI and EJ sites of Fig. 4 (EJ14 on the top left, EJ15 on the top right, EJ22 on the bottom left, and EJ24 on the bottom right).

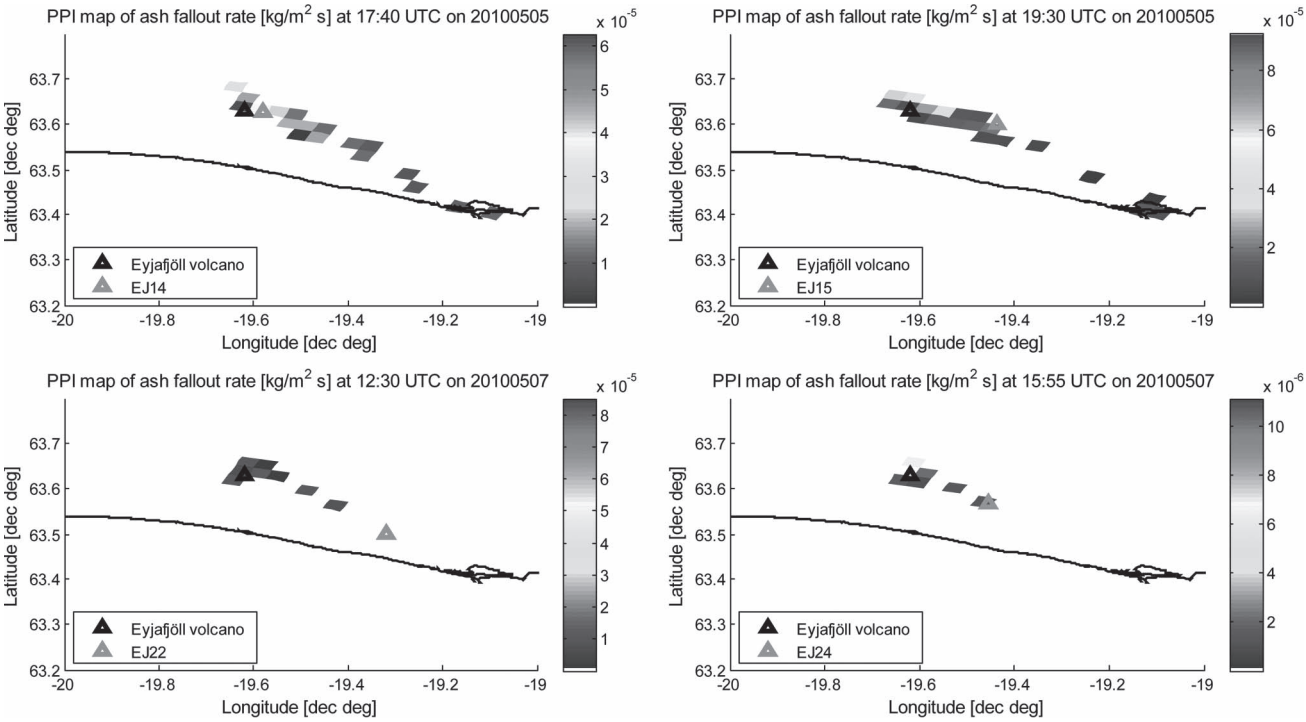

Fig. 8. Radar PPI images of VARR-derived ash-fall rate R_a, corresponding to RHI and EJ sites of Fig. 4 (EJ14 on the top left, EJ15 on the top right, EJ22 on the bottom left, and EJ24 on the bottom right).

measurements. Generally speaking, the terminal velocity parameterization can exhibit a variability of estimates of about 10%–30% with respect to KL ones.

The capability of weather radars to derive microphysical parameters can be exploited by using the technique illustrated in Section III-C. Figs. 10–12 upper plots show the histogram of VARR-based estimates of D_n using (7) and C_a using (5), extracted at and around the sampling sites EJn for the 24-h period of the same. The overall mean diameter, estimated from radar data, is between 0.05 and 0.6 mm for EJ15 and EJ24 sites with some values up to 1 mm for EJ14, whereas from ground data, it is about 1.87 mm for EJ14, 0.62 mm

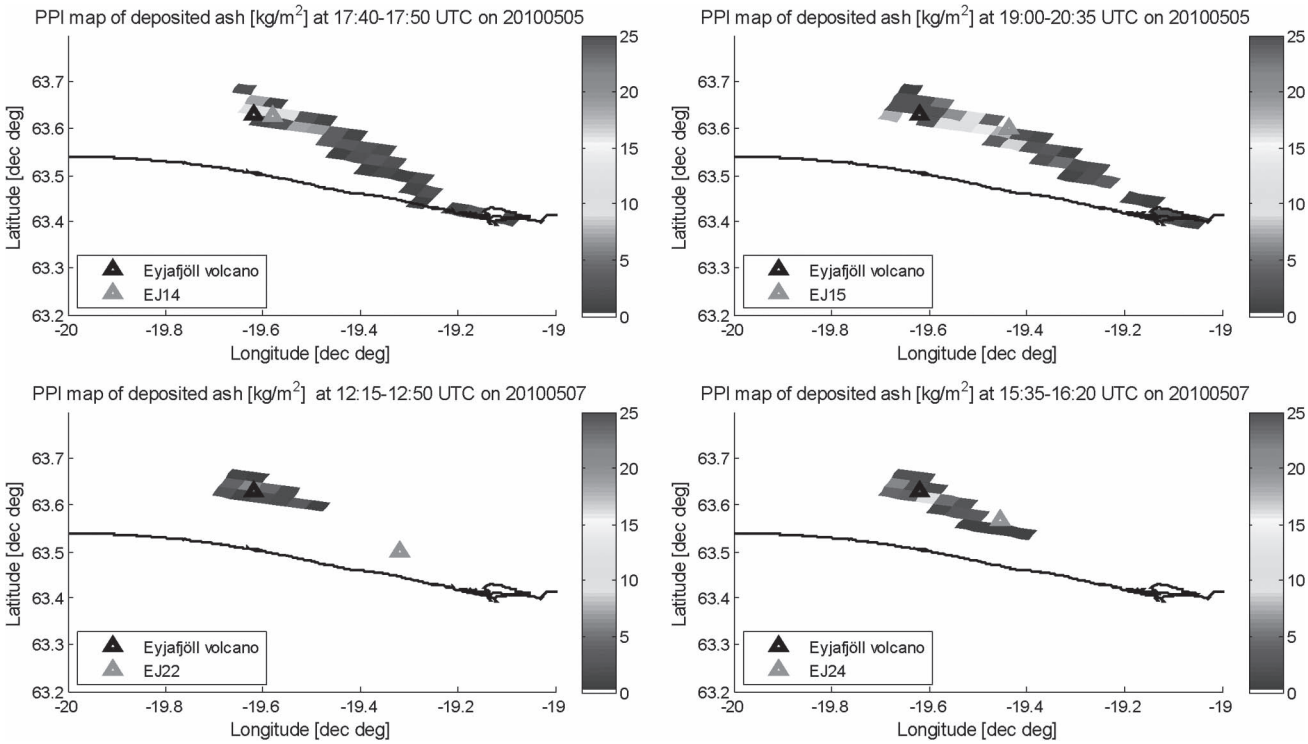

Fig. 9. Radar PPI images of VARR-derived ash loading L_a, corresponding to RHI and EJ sites of Fig. 4 (EJ14 on the top left, EJ15 on the top right, EJ22 on the bottom left, and EJ24 on the bottom right).

TABLE II
SENSITIVITY TO FALLOUT VELOCITY OF VARR-DERIVED ESTIMATES OF ASH-FALL RATE R_a AND DEPOSIT LOADING L_{aS} FOR EJ14, EJ15, AND EJ24 SITES USING FOUR DIFFERENT ASH-FALL VELOCITY MODELS (SEE TEXT FOR DETAILS)

		Velocity-diameter model			
Validation site	**Estimated parameter**	**Kunii & Levienspiel (1969)**	**Wilson (1972)**	**Harris & Rose (1980)**	**Harris & Rose (1982)**
EJ14	R_a [kg/m^2·s]	$1.01\cdot10^{-2}$	$6.87\cdot10^{-3}$	$5.77\cdot10^{-3}$	$8.32\cdot10^{-3}$
	L_a [kg/m^2]	5.78	3.91	3.28	4.74
EJ15	R_a [kg/m^2·s]	$2.97\cdot10^{-3}$	$2.22\cdot10^{-3}$	$1.78\cdot10^{-3}$	$2.51\cdot10^{-3}$
	L_a [kg/m^2]	7.76	5.79	4.65	6.54
EJ24	R_a [kg/m^2·s]	$1.70\cdot10^{-3}$	$1.07\cdot10^{-3}$	$9.67\cdot10^{-4}$	$1.40\cdot10^{-3}$
	L_a [kg/m^2]	1.11	0.70	0.63	0.91

for EJ15, and 0.41 mm for EJ24 (see Table I). The VARR-derived average ash concentration is up to 9 g $\cdot$ m^{-3} with a significant occurrence of samples above 0.1 g $\cdot$ m^{-3} for the closest site EJ14 and only a few samples for the farthest site EJ24.

We can also process radar data to investigate a near "real-time" intercomparison. The same figures, in the lower panels, show the estimated ash PSD $N_a^{(c)}(D)$ via (2), for the ground collection time window and within an area of 5 km $\times$ 5 km centered in the EJn site using the first radar elevation angle (i.e., that closer to the ground). Plots of $N_a^{(c)}(D)$ are provided as a function of both diameters (left panel) and ϕ units (right panel). In the lower-right panel, we added the PSD derived by the ground measurements [2] at the selected sites EJn to facilitate ground-to-radar PSD intercomparison.

In Figs. 10–12, we note that the mode of estimated PSD shows an effective diameter D_n of tephra, which varies around 0.04 mm ($\sim 4.6\phi$) for the EJ14, EJ15, and EJ24 sites. These results reveal that for all sites, the VARR-estimated PSD mode, due to airborne ash particles, is smaller than that collected on the ground (general mode within -0.9ϕ and 1.3ϕ; see Table I). The ash class, identified by the VARR algorithm, is generally the coarse ash, whereas a low presence of fine ash (<10%) is detected. The ash population, observed by the radar in the cloud above the selected locations EJ15 and EJ24, exhibits a mode of about 0.03 mm ($\sim 4.7\phi$), which is slightly smaller than that at the closest site EJ14 with a mode of 0.05 mm.

Our conjecture to explain the above results is that a gravitational sedimentation process is taking place. In other words, bigger particles, due to gravity, reach the ground before the smaller particles, which indeed show a longer airborne time. The same trend is clear in the three sites EJ14, EJ15, and EJ24 for a distance from the vent between 2-10 km. For these distance ranges we can then affirm that the airborne particle size is unchanged.

The MFR can be estimated either from radar scans by means of the complete model in (17) or from the approximate relation in (19) or from 1-D analytical eruption models based on the radar-derived plume top height using (20). For these estimations, we have used the radar time sampling $\Delta t = 5$ min, whereas the horizontal section of the columnar volume V_C is set to 5×5 pixels with a pixel size of about 1 km per side, thus having an area of 25 km^2 around the Eyjafjallajökull volcanic.

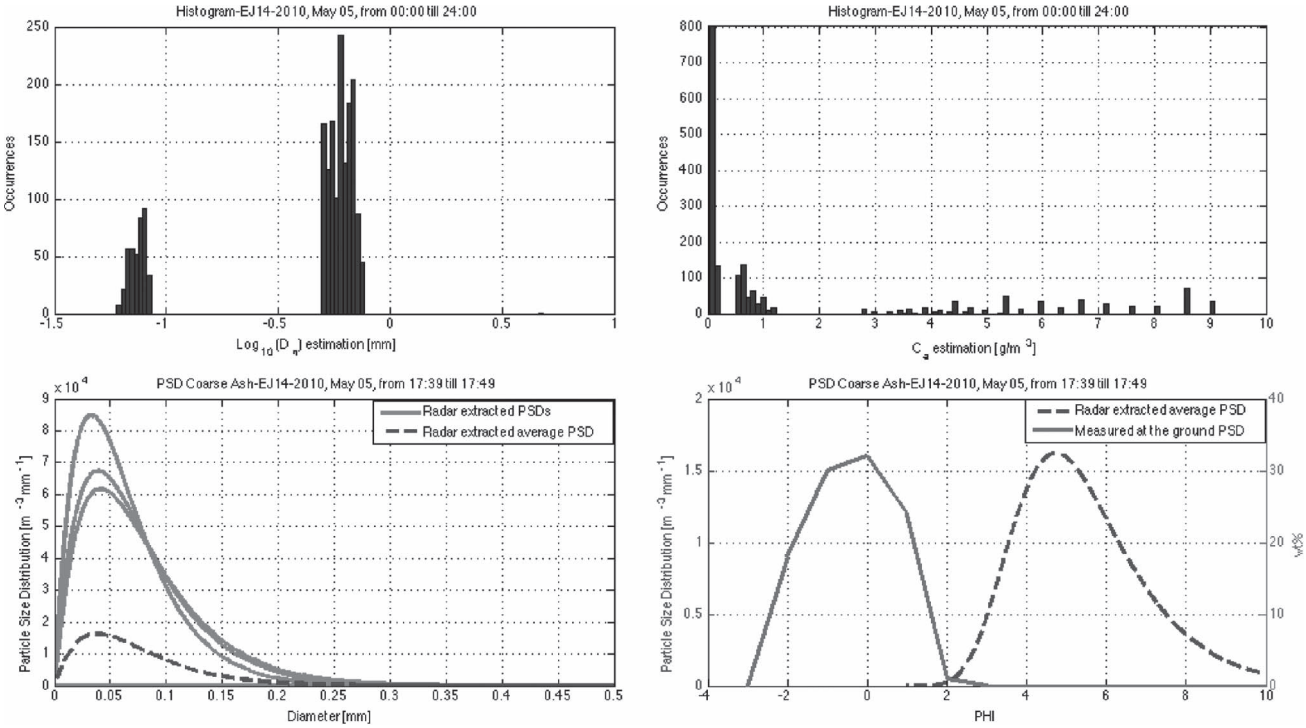

Fig. 10. (Upper panels) Histograms of VARR-derived mean diameter D_n (left) and ash concentration C_a (right) for the identified coarse ash classes, estimated around the site EJ14 for 24 h of May 5, 2010. (Lower panels) VARR-derived average PSD with respect to the particle diameter $D_{\rm n}$ (left) and parameter ϕ (right) for the short ground-collection time interval as reported in Table I and on the plot title. In the left panel, all PSD values, estimated every 5 min, are shown together with the mean PSD for the time interval. On the right panel, the mean VARR-estimated PSD is compared with the corresponding PSD derived from ground-based collection, as shown in Bonadonna *et al.* [2].

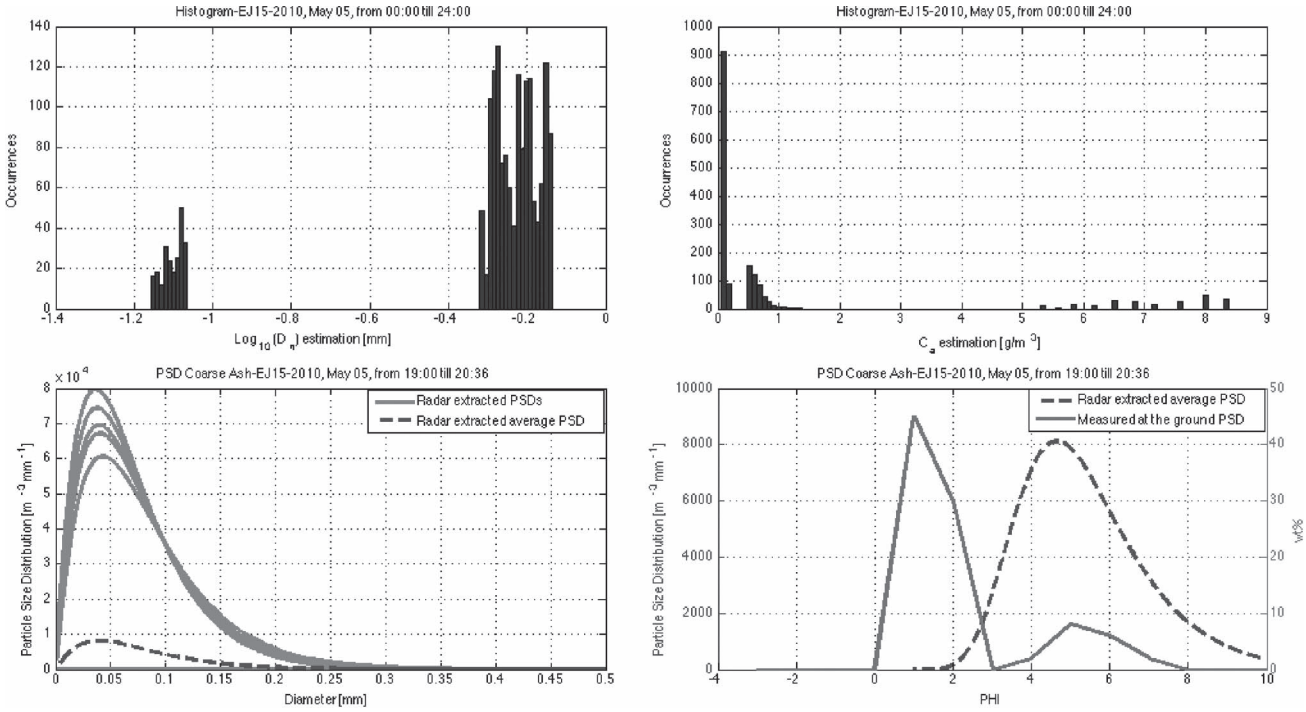

Fig. 11. Same as in Fig. 10, but for the EJ15 site on May 5, 2010.

Fig. 13 (upper left) shows the behavior of the top plume height, above the volcano vent, estimated from the ash concentration threshold on May 5 [17]. The estimated top plume height is between 4 and 8 km, except some peaks above 10 km around 06:00 UTC. The upper-right panel shows the approximate derivative mass rate $F_{Rapp} = D_{\rm R}^{+}$, derived from (19), together with the estimate of the advection rate $A_{Rapp} = D_{\rm R}^{-}$ carried out by inferring the plume advection velocities estimated by the radar data. The latter is not always negligible, as apparent from the advection rate time series. This is particularly true for

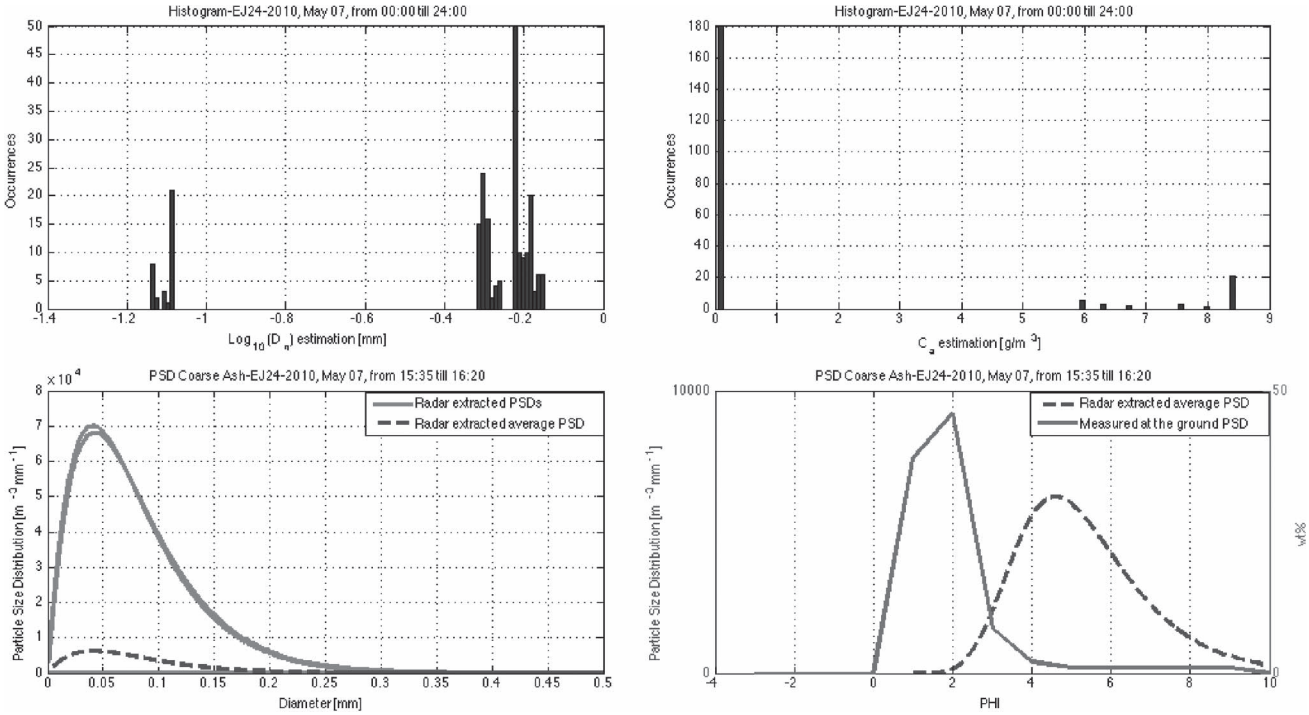

Fig. 12. Same as in Fig. 10, but for the EJ24 site on May 7, 2010.

the Eyjafjallajökull eruption in 2010, where the trophospheric plumes were transported and dispersed by strong winds flowing around 3–6 km.

The left-lower panel of Fig. 13 shows the total radar-based MFR estimations above the volcano vent with respect to the plume top height superimposed to model-based MFR predictions, using the 1-D analytical model of Degruyter–Bonadonna with different wind velocity varying between 0 and 60 m/s [7]. The 1-D model from Mastin *et al.* [21], obtained from plume height only, is considered as well. These MFR models are both derived from radar observations of the plume height and available radiosonde data. The right-lower panel presents the correlation between the total VARR-estimated MFR and model-based MFR derived from [7] for three wind speeds (0, 30, and 60 m/s) to show its variability. VARR-estimated MFR is consistent, in terms of value range, with the Degruyter–Bonadonna MFR predictions. This result is important as it shows that tephra mass rate and advection, estimated from C-band radar measurements available every 5 min, can provide a valuable information for assessing the volcanic eruption activity.

The MFR variability, detected from the weather radar, shows a different behaviour compared with that derived from a 1-D analytical model. The latter is depending on the plume maximum height and on the time interval sampling considered by averaging the plume maximum height. The plume maximum height may not vary so much during the continuous eruption activity as it is sustained by the buoyant plume. By taking into account the ash mass balance in the vent column using radar data, we are indeed looking at the temporal intermittency of the explosive fountain. The oscillations of our MFR estimates are even more exacerbated by the time sampling of the radar, which is on the order of a few minutes, whereas the ash cloud parameters can vary at a scale of a few seconds.

Figs. 14 and 15 show the same results as in Fig. 13, but for May 6 and May 7, 2010. The temporal trend of the VARR-estimated MFR of the Eyjafjallajökull for May 5–7 shows values between 10^4 and 10^6 kg/s, whereas the top plume height ranges between 3 and 7 km, with a mean trend around 4.5 km. The radar-based MFR estimation is coherent with the values obtained by the 1-D eruption model. Note that the advection rate A_R exhibits lower values with respect to those of May 5 (about 1 kg/s) due to the wind transport.

It is worth noting that Figs. 13–15 show almost no correlation between MFR radar retrievals and 1-D-analytical model estimates, but, as mentioned before, the maximum plume height is not necessarily correlated with the intermittent mass eruption rate due to explosive activity. Indeed, knowledge of the height of the plume provides a poor estimate of the ash load in the plume, if the realistic fraction of fine material produced during an eruption is not known, and the temporal influence of atmospheric properties are neglected [37]. This would mean, if confirmed by further analyses, that 1-D analytical models should be taken as reference values to be compared with near real-time estimates from ground-based radar and other instruments.

B. Comparison With Daily Tephra Maps

The previous section has been focused on the capability of radar-based retrievals to capture the microphysical properties of ash fall. Unfortunately, the lack of radar-to-ground data matching has limited the value of this assessment. In this respect, ash loading retrievals can be better handled for routine intercomparisons. Estimates of the Eyjafjallajökull daily

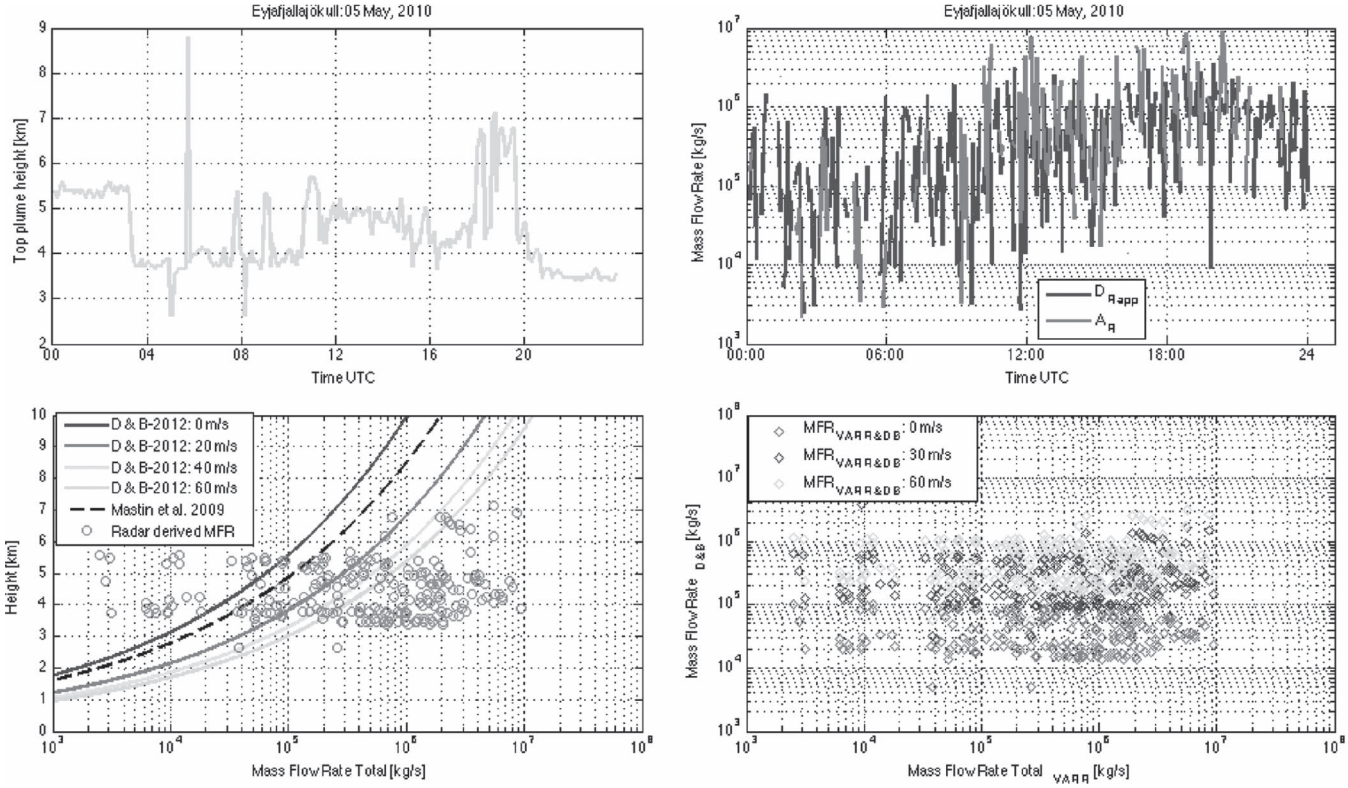

Fig. 13. Radar-based retrievals and intercomparisons from 00:00 until 24:00 UTC on May 5, 2010 during the Eyjafjallajökull volcanic eruption. (Left top) Time trend of the plume height estimated above the vent using the estimated concentration C_a threshold technique within VARR. (Right top) Approximate MFR (F_{Rapp}) using (19) and advection rate term (A_{Rapp}), plotted only when the advection velocity is available, using (18b). (Left bottom) VARR-based estimates of plume top height versus VARR-derived total MFR ($\mathrm{F_R}$ from the union of $\mathrm{A_{Rapp}}$ and $\mathrm{D_{Rapp}}$) and model-based MFR predictions, derived from two 1-D analytical eruption models (specifically, Degruyter and Bonadonna [7] (D & B-2012 in the legend) and Mastin *et al.* [21]) with different wind speeds using (20). (Right bottom) Correlation between VARR-estimated MFR and model-based MFR, deduced from the Degruyter–Bonadonna model for different wind speeds.

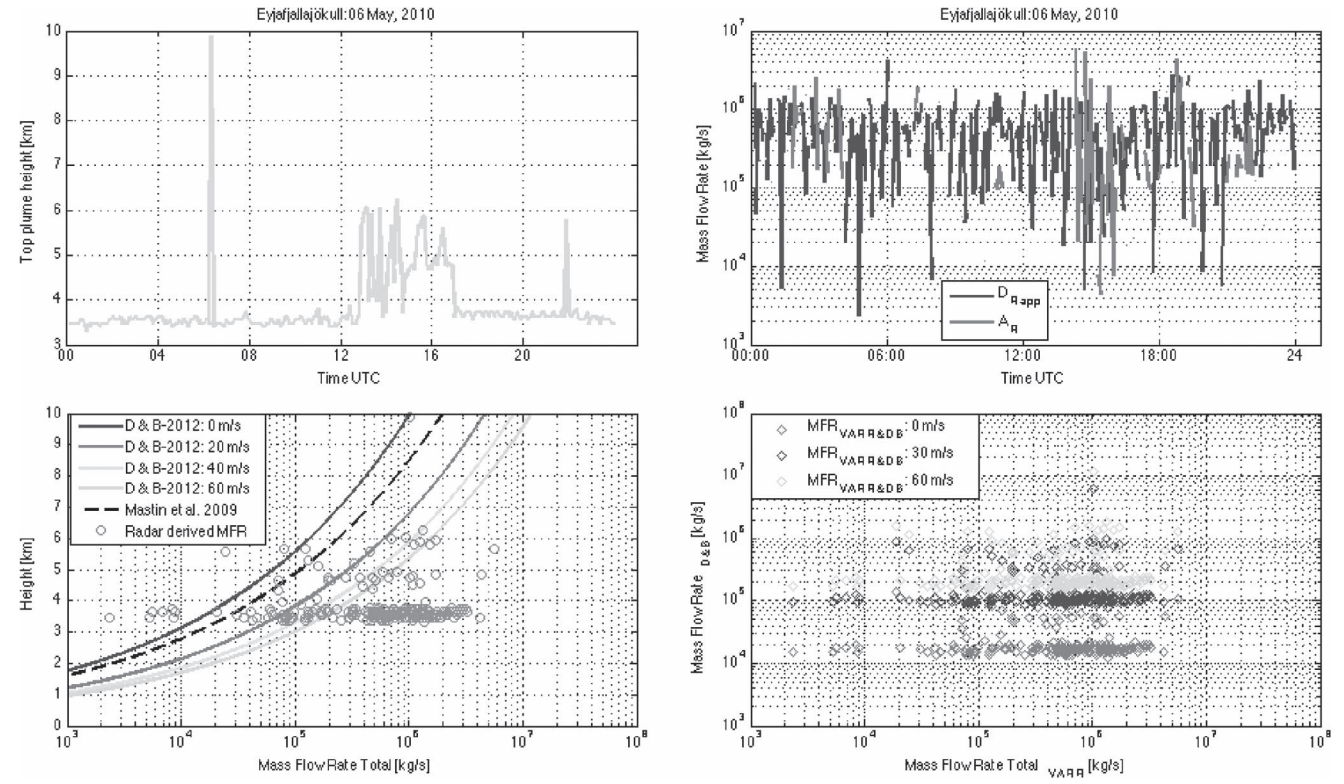

Fig. 14. Same as Fig. 13, but for May 6, 2010.

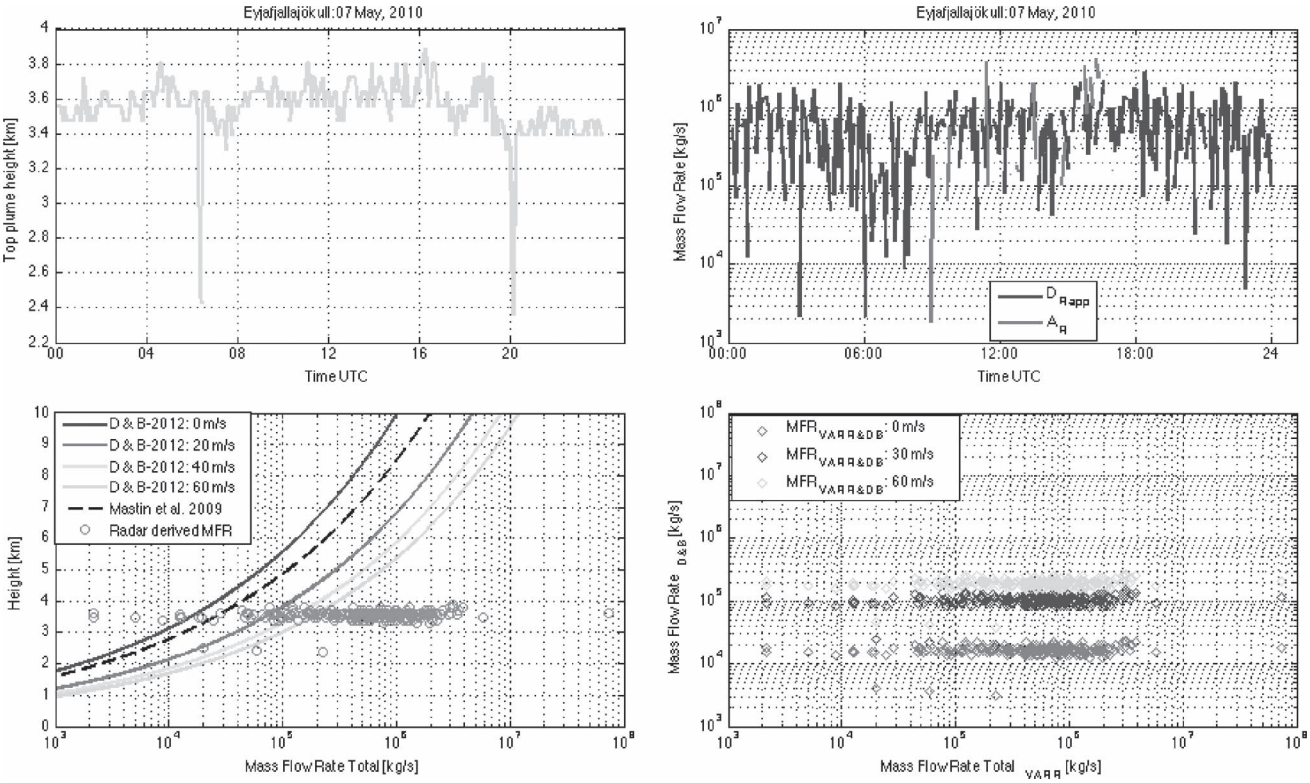

Fig. 15. Same as Fig. 13, but for May 7, 2010.

TABLE III
INTERCOMPARISON BETWEEN ESTIMATED TEPHRA MASS ERUPTED PER DAY BY GUDMUNDSSON *ET AL.* [8], COLUMNS 1–4 WITH CORRESPONDING DAILY TEPHRA ESTIMATED BY MEANS OF C-BAND VARR (FIFTH COLUMN) FOR THE AVAILABLE DAYS OF RADAR OBSERVATIONS, USING THE KL VELOCITY-DIAMETER MODEL

Date	Daily total mass 10^9 [kg/day]	Direction of dispersal	Grain size sample distance [km]	Estimated total Mass (VARR-KL) 10^9 [kg]
14 April	40-50	E	1	34.34 ± 10.9
15 April	5-10	E	58	88.34 ± 26.4
16 April	30-40	E	21	114.46 ± 34.3
17 April	30-40	S	11	33.15 ± 9.9
18 April	05-10	SE	-	4.15 ± 1.2
19 April	1-3	SE	-	1.28 ± 0.4
20 April	<1	SE	-	2.02 ± 0.6
5 May	30-40	SE	30	49.46 ± 14.8
6 May	5-10	E	-	17.20 ± 5.2
7 May	5-10	SE	-	9.24 ± 2.8
8 May	3-5	SE	13	3.43 ± 1,0
9 May	2-5	SE	-	2.37 ± 0.7
10 May	2-5	SE	13	2.53 ± 0.7

tephra production rates, main direction dispersal, and grain size characteristics are listed in Table III, for the period of April 14–May 10 as derived from [8]. The estimated tephra mass, erupted per day and shown in the second column of Table III, is based on the partitioning of tephra and basically refer to inland deposits [21].

The availability of radar volume time series with a time sampling of 5 min can allow a VARR-based estimate of the daily tephra deposits derived from M_a in (11) [18]. The latter can be compared with data in Table III for the time period of April 14–20 and May 5–10, during which radar data were at disposal. The last right column shows the total mass per day (24 h) estimated by integrating the VARR ash concentration rertievals, using the KL terminal velocity model and an uncertainty of 30%, derived from previous validation works [18]. We should, of course, take into account all the limitations due to visibility and sensitivity of radar-derived estimates, but, on the other hand, ground daily tephra loadings are extrapolations of heterogeneous data sets [8].

VARR-based retrieval values of volcanic ash mass, extrapolated at ground for each day, are in a fairly good agreement with values derived from [8], being the values of the same order of magnitude particularly after April 17. This agreement would suggest that the overall daily tephra loading is well captured by VARR radar-based retrievals, notwithstanding its limited sensitivity at a distance of 156 km and partial visibility of the volcanic plume. The major discrepancies are noted on the eruption phase between April 14 and 16, where the radar-based estimates are much higher (between three and five times), which is the most intense eruption phase, as documented by the radar-based retrieval trends [18]. This difference might be explained by considering, on the one hand, that during these initial days of the Eyjafjallajökull eruption, the ground sampling and model extrapolations can be more difficult and less accurate and, on the other hand, that inherent uncertainties affect VARR-based estimates, as discussed in Section II-B.

V. CONCLUSION

The April–May 2010 eruption of the Eyjafjallajökull volcano provided a wide range of *in situ* and remote sensing data whose

combination can highlight important aspects of tephra microphysical processes. Within the VARR methodology, previously introduced, this work has presented a new technique to estimate airborne tephra size distribution and MFR together with a retrieval of the deposited tephra at ground. VARR-based products have been compared with *in situ* campaign measurement data, in terms of size distribution and ash collection near the volcano vent, and multiple-source daily tephra deposits in the plume-affected volcanic area presented.

Retrievals from scanning C-band weather radars are affected by some limitations, which have been previously discussed. Interestingly, the estimated values of fall rate are of the same magnitude order as the values derived from the experimental collected data EJn. The estimated ash loading in the same EJn sites is larger than that collected of a few orders of magnitude, mainly because these radar-derived values are obtained by assuming a georeferenced area of $25\ \mathrm{km}^2$ around the location of each EJn site.

Microwave radars can probe the plume inside, although limiting the sensitivity to coarse and large grains. The VARR-estimated tephra around the Eyjafjallajökull volcano vent in all analyzed cases was classified as coarse ash with a mean diameter around 0.1 mm, according to PSD parameterization here adopted. By comparing the retrieved airborne PSDs with those estimated at ground, tephra accumulation rate appears to be not uniform along the column. VARR-based particle size estimates may suggest that a sorting of airborne particles during the downwind transport is taking place during the ash fall.

The estimate of the volcanic MFR is a crucial goal for eruption dynamics modeling. The MFR, estimated by VARR for the period between May 5 and May 7, 2010, presents a value range that agrees with that shown in 1-D eruption approximate models driven by plume top height.

Future works should be devoted to applying VARR PSD and MFR retrieval algorithms to microwave radar data with higher sensitivity and quality, possibly exploiting shorter distances and polarimetric capability. Radar-derived quantities are indeed of potential interest for ash transport modeling. Specific efforts should be focused on methods for extrapolating radar retrievals from coarser to finer particles, needed to initialize Lagrangian ash dispersion models. Such extrapolation methods might be based on simple PSD shape extension or be aimed at finding scale factors to convert radar-derived quantities into dispersion model parameters.

ACKNOWLEDGMENT

The authors would like to thank B. Pálmason, H. Pétursson, and S. Karlsdóttir (IMO, Iceland) for providing C-band radar data and useful suggestions on data processing. They would also like to thank W. Degruyter for the comments and suggestions that helped improve the manuscript.

REFERENCES

[1] Þ. Arason, S. B. Þorláksdóttir, G. S. Sigurðsson, R. F. Yeo, and T. Thorsteinsson, "Properties of ash-infused hail during the Grímsvötn 2011 eruption and implications for radar detection of volcanic columns," vol. 15, EGU2013-4797, 2013.

[2] C. Bonadonna *et al.*, "Tephra sedimentation during the 2010 Eyjafjallajökull eruption (Iceland) from deposit, radar, and satellite observations," *J. Geophys. Res.*, vol. 116, no. B12, pp. 202–345, 2011.

[3] C. Bonadonna and J. C. Phillips, "Sedimentation from strong volcanic plumes," *J. Geophys. Res.*, vol. 108, no. B7, 2340, 2003.

[4] C. Bonadonna and B. F. Houghton, "Total grain-size distribution and volume of tephra fall deposits," *Bull. Volcanol.*, vol. 67, pp. 441–456, 2005.

[5] C. Bonadonna and A. Costa, "Estimating the volume of tephra deposits: A new simple strategy," *Geology*, vol. 40, pp. 415–418, 2012.

[6] M. I. Bursik *et al.*, "Estimation and propagation of volcanic source parameter uncertainty in an ash transport and dispersal model application to the Eyjafjallajokull plume of 14–16 April 2010," *Bull. Volcanol.*, vol. 74, no. 10, 2321–2338, Dec. 2012.

[7] W. Degruyter and C. Bonadonna, "Improving on mass flow rate estimates of volcanic eruptions," *Geophys. Res. Lett.*, vol. 39, no. 16, 2012, Art. ID. L16308.

[8] M. T. Gudmundsson *et al.*, "Ash generation and distribution from the April–May 2010 eruption of Eyjafjallajökull, Iceland," *Nature Sci. Rep.*, vol. 2, 572, Jul. 2012.

[9] D. L. Inman, "Measures for describing the size distribution of sediments," *J. Sedimentary Petrology*, vol. 22, no. 3, pp. 125–145, 1952.

[10] D. M. Harris and W. I. Rose, "Estimating particle sizes, concentrations, and total mass of ash in volcanic clouds using weather radar," *J. Geophys. Res.*, vol. 88, no. C15, pp. 10 969–10 983, Dec. 1983.

[11] D. Kunii and O. Levenspiel, *Fluidization Engineering*. New York, NY, USA: Wiley, 1969.

[12] C. Lacasse *et al.*, "Weather radar observations of the Hekla 2000 eruption cloud," *Iceland Bull Volcanol*, vol. 66, no. 5, pp. 457–473, Dec. 2004.

[13] F. S. Marzano, G. Vulpiani, and W. I. Rose, "Microphysical characterization of microwave radar reflectivity due to volcanic ash clouds," *IEEE Trans. Geosci. Remote Sens.*, vol. 44, no. 2, pp. 313–327, Feb. 2006.

[14] F. S. Marzano, S. Barbieri, G. Vulpiani, and W. I. Rose, "Volcanic ash cloud retrieval by ground-based microwave weather radar," *IEEE Trans. Geosci. Remote Sens.*, vol. 44, no. 11, pp. 3235–3246, Nov. 2006.

[15] F. S. Marzano, S. Marchiotto, C. Textor, and D. Schneider, "Model-based weather radar remote sensing of explosive volcanic ash eruption," *IEEE Trans. Geosci. Remote Sens.*, vol. 48, no. 10, pp. 3591–3607, Oct. 2010.

[16] F. S. Marzano, S. Barbieri, E. Picciotti, and S. Karlsdóttir, "Monitoring sub-glacial volcanic eruption using C-band radar imagery," *IEEE Trans. Geosci. Remote Sens.*, vol. 48, no. 1, pp. 403–414, Jan. 2010.

[17] F. S. Marzano, M. Lamantea, M. Montopoli, S. Di Fabio, and E. Picciotti, "The Eyjafjallajökull explosive volcanic eruption from a microwave weather radar perspective," *Atmos. Chem. Phys.*, vol. 11, 9503–9518, 2011.

[18] F. S. Marzano, M. Lamantea, M. Montopoli, B. Oddsson, and M. T. Gudmundsson, "Validating sub-glacial volcanic eruption using ground-based C-band radar imagery," *IEEE Trans. Geosci. Remote Sens.*, vol. 50, no. 4, pp. 1266–1282, Apr. 2012.

[19] F. S. Marzano, E. Picciotti, G. Vulpiani, and M. Montopoli, "Synthetic signatures of volcanic ash cloud particles from X-band dual-polarization radar," *IEEE Trans. Geosci. Remote Sens.*, vol. 50, no. 1, pp. 193–211, Jan. 2012.

[20] F. S. Marzano, D. Scaranari, and G. Vulpiani, "Supervised fuzzy-logic classification of hydrometeors using C-band weather radars," *IEEE Trans. Geosci. Remote Sens.*, vol. 45, no. 11, pp. 3784–3799, Nov. 2007.

[21] L. G. Mastin *et al.*, "A multidisciplinary effort to assign realistic source parameters to models of volcanic ash-cloud transport and dispersion during eruptions," *J. Volcanol. Geothermal Res.*, vol. 186, no. 1/2, pp. 10–21, 2009.

[22] G. N. Petersen, "A short meteorological overwiew of the Eyjafjallajökull eruption 14 April–23 May 2010," *Weather*, vol. 65, no. 8, pp. 203–207, Aug. 2010.

[23] S. Pouget, M. Bursik, P. Webley, J. Dehn, and M. Pavolonis, "Estimation of eruption source parameters from Umbrella cloud or downwind plume growth rate," *J. Volcanol. Geothermal Res.*, vol. 258, pp. 100–112, May 2013.

[24] H. Sauvageot, *Radar Meteorology*. Boston, MA, USA: Artech House, 1992.

[25] R. Sparks, "The dimensions and dynamics of volcanic eruption columns," *Bull. Volcanol.*, vol. 48, no. 1, pp. 3–15, Feb. 1986.

[26] R. S. J. Sparks *et al.*, *Volcanic Plumes*. New York, NY, USA: Wiley, 1997.

[27] J. Taddeucci *et al.*, "Aggregation-dominated ash settling from the Eyjafjallajökull volcanic cloud illuminated by field and laboratory high-speed imaging," *Geology*, vol. 39, pp. 891–894, Aug. 2011.

[28] T. Yu, W. I. Rose, and A. J. Prata, "Atmospheric correction for satellite based volcanic ash mapping and retrievals using split-window IR data from GOES and AVHRR," *J. Geophys. Res.*, vol. 107, no. D16, pp. 4311–4316, 2002.
[29] L. Wilson, "Explosive volcanic eruptions—II: The atmospheric trajectories of pyroclasts," *Geophys. J. R. Astron. Soc.*, vol. 30, no. 4, pp. 381–392, Dec. 1972.
[30] G. P. L. Walker, "Explosive volcanic eruptions—A new classification scheme," *Geol. Rundschau*, vol. 62, no. 2, pp. 432–4461973.
[31] C. Zehner, Ed. "Monitoring volcanic ash from space," in *Proc. ESA-EUMETSAT Workshop 14 Apr. –23 May 2010 Eruption Eyjafjoll Volcano*, Frascati, Italy, May 26–27, 2010, pp. 1–110.
[32] D. J. Schneider and R. P. Hoblitt, "Doppler weather radar observations of the 2009 eruption of Redoubt volcano, Alaska," *J. Volcanol. Geothemal Res.*, vol. 259, pp. 133–144, Jun. 2013.
[33] M. J. Woodhouse, A. J. Hogg, J. C. Phillips, and R. S. J. Sparks, "Interaction between volcanic plumes and wind during the 2010 Eyjafjallajökull eruption, Iceland," *J. Geophys. Res. Solid Earth*, vol. 118, no. 1, pp. 92–109, Jan. 2013.
[34] L. Wilson, "Explosive volcanic eruptions—II: The atmospheric trajectories of pyroclasts," *Geophys. J. R. Astron. Soc.*, vol. 30, no. 2, pp. 381–392, 1972.
[35] M. Montopoli, G. Vulpiani, D. Cimini, E. Picciotti, and F. S. Marzano, "Interpretation of observed microwave signatures from ground dual polarization radar and space multi-frequency radiometer for the 2011 Grímsvötn volcanic eruption," *Atmos. Meas. Techn.*, vol. 7, no. 2, pp. 537–552, 2014.
[36] C. Textor *et al.*, "Volcanic particle aggregation in explosive eruption columns. Part II: Numerical experiments," *J. Volcanol. Geothermal Res.*, vol. 150, no. 4, pp. 399–394, Feb. 2005.
[37] E. Kaminski *et al.*, "Estimation of ash injection in the atmosphere by basaltic volcanic plumes: The case of the Eyjafjallajökull 2010 eruption," *J. Geophys. Res.*, vol. 116, Sep. 2011 Art. ID. B00C02.

Luigi Mereu received the B.Sc. and M.Sc. degrees in telecommunication engineering from Sapienza University of Rome, Rome, Italy, in 2007 and 2012, respectively.

In 2012, he joined the Department of Information Engineering, Sapienza University of Rome and the CETEMPS Center of Excellence, University of L'Aquila, L'Aquila, Italy, to cooperate on radar remote sensing of volcanic ash clouds within the ICT Ph.D. program. He is involved within the FUTUREVOLC European project that started in 2012.

Mr. Mereu received the IEEE GRS South Italy award for Best Master Thesis in remote sensing in 2012.

Frank S. Marzano (S'89–M'99–SM'03) received the Laurea degree (*cum laude*) in electrical engineering and the Ph.D. degree in applied electromagnetics from Sapienza University of Rome, Rome, Italy, in 1988 and 1993, respectively.

In 1992, he was a Visiting Scientist with Florida State University, Tallahassee, FL, USA. In 1993, he collaborated with the Institute of Atmospheric Physics, National Council of Research (CNR), Rome. From 1994 to 1996, he was a Postdoctoral Researcher with the Italian Space Agency, Rome. After being a Lecturer with the University of Perugia, Perugia, Italy, in 1997, he joined the Department of Electrical Engineering, University of L'Aquila, L'Aquila, Italy, as an Assistant Professor teaching courses on electromagnetic fields. In 1999, he was a Visiting Scientist with the Naval Research Laboratory, Monterey, CA, USA. In 2002, he got the qualification to Associate Professorship and has cofounded the Center of Excellence on Remote Sensing and Hydro-Meteorological Modeling (CETEMPS), University of L'Aquila, L'Aquila, Italy. In 2005, he finally joined the Department of Information Engineering, Electronics and Telecommunications, Sapienza University of Rome, where he currently teaches courses on antennas, propagation, and remote sensing. Since 2007, he has been the Vice Director of CETEMPS, where he became a Director in 2013. He has published more than 110 papers on refereed international journals, more than 30 contributions to international book chapters, and more than 230 extended abstract on international and national congress proceedings. He was the Editor of two books. His current research concerns passive and active remote sensing of the atmosphere from ground-based, airborne, and spaceborne platforms and electromagnetic propagation studies.

Dr. Marzano has been acting as an Associate Editor of the IEEE GEOSCIENCE REMOTE SENSING LETTERS since January 2004. In 2005 and 2007, he was a Guest Coeditor of the MicroRad04 and MicroRad06 Special Issues for the IEEE TRANSACTIONS ON GEOSCIENCE REMOTE SENSING. Since January 2011, he has been an Associate Editor of the journal *EGU Atmospheric Measurements Techniques*. He is a Fellow of the U.K. Royal Meteorological Society and a member of the MWI-ICI Science Advisory Group of EuMetSat and PMM Science Team of NASA.

Mario Montopoli received the Laurea degree in electronic engineering from the University of L'Aquila, L'Aquila, Italy, in 2004 and the Ph.D. degree in radar meteorology, under a joint program, from the University of Basilicata, Potenza, Italy, and Sapienza University of Rome, Rome, Italy, in 2008.

In 2005, he joined the CETEMPS Center of Excellence, University of L'Aquila, as a Research Scientist on ground-based radar meteorology and microwave remote sensing. In 2006, he was a Research Assistant with the Department of Electrical Engineering and Information, University of L'Aquila. From October 2011 to 2013, he was with the Department of Geography, University of Cambridge, Cambridge, U.K., under the Marie Curie FP7 European program. He is currently with the Department of Information Engineering, Sapienza University of Rome and a EuMetSat Visiting Scientist with the H-SAF facility.

Costanza Bonadonna received the B.S. degree in geology from the University of Pisa, Pisa, Italy, and the Ph.D. degree from the University of Bristol, Bristol, U.K.

She was then awarded the position of SOEST Young Investigator at the University of Hawaii, Honolulu, HI, USA, for two years and was later appointed the position of Assistant Professor at the University of South Florida, Tampa, FL, USA. She is now an Associate Professor with the Section of Earth Sciences of the Faculty of Sciences, University of Geneva, Geneva, Switzerland, and the Head of the CERG-C Program for the Assessment and Management of Geological and Climate related risk. She has devoted most of her research to modeling sedimentation from volcanic plumes, exploring new methodologies for the characterization of tephra-fall deposits, and developing probabilistic analyses for the assessment of tephra-fall hazards. She is now also involved in several multidisciplinary projects for the quantification of risk.

Professor Bonadonna was a recipient of the President's Award of the Geological Society of London (2001), the IAVCEI Outstanding Recent Graduate (2004), the Outstanding Woman in Science Award of the Geological Society of America (2004), and the USF Outstanding Faculty Research Achievement Award (2005).